

662.6622
LIU
TESIS/PETROLEO

SIMULATION OF UNDERGROUND LIQUEFACTION
OF LIGNITE

A Dissertation

by

TUAN-CHI LIU

Submitted to the Graduate College of
Texas A&M University
in partial fulfillment of the requirement for the degree of
DOCTOR OF PHILOSOPHY

May 1980

Major Subject: Chemical Engineering

• • •

1. The first part of the document is a list of names and addresses of the members of the committee. The names are listed in alphabetical order, and the addresses are listed below each name. The list includes names such as Mr. J. B. Smith, Mr. J. C. Jones, and Mr. A. D. Brown.

2. The second part of the document is a list of the names and addresses of the members of the committee who were present at the meeting. The names are listed in alphabetical order, and the addresses are listed below each name. The list includes names such as Mr. J. B. Smith, Mr. J. C. Jones, and Mr. A. D. Brown.

3. The third part of the document is a list of the names and addresses of the members of the committee who were absent from the meeting. The names are listed in alphabetical order, and the addresses are listed below each name. The list includes names such as Mr. J. B. Smith, Mr. J. C. Jones, and Mr. A. D. Brown.

4. The fourth part of the document is a list of the names and addresses of the members of the committee who were present at the meeting. The names are listed in alphabetical order, and the addresses are listed below each name. The list includes names such as Mr. J. B. Smith, Mr. J. C. Jones, and Mr. A. D. Brown.


SIMULATION OF UNDERGROUND LIQUEFACTION
OF LIGNITE

A Dissertation

by

TUAN-CHI LIU


Approved as to style and content by:



(Chairman of Committee)



(Member)



(Member)



(Member)



(Head of Department)

May 1980

ACKNOWLEDGEMENTS

The author wishes to express his sincere appreciation to Dr. R. G. Anthony, Chairman of the author's Graduate Committee, for his consistent interest, help and encouragement throughout the development of all phases of the work.

The author would also like to thank Dr. R. R. Davison, Dr. K. R. Hall of the Chemical Engineering Department, and Dr. L. A. Hale of the Mechanical Engineering Department, for their guidance and for serving as members of the author's Graduate Committee. Dr. C. V. Philip also assisted in many ways during the course of the work.

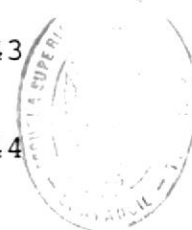
The financial support of Dow Chemical Company, The Texas Engineering Experiment Station, The Center for Energy and Mineral Resources, and the Department of Chemical Engineering is greatly appreciated. The lignite was furnished by Alcoa and Dow Chemical Company. The SRC recycled solvent was furnished by Catalytic, Incorporated.

Finally, I would like to express my sincere gratitude to my parents for their support and encouragement during my years at Texas A&M University.

VI.	KINETIC MODELING	85
	Equilibrium Conversion	85
	Rate Equation	87
	Results and Discussion of Kinetic Models	89
VII.	MATHEMATICAL SIMULATION OF THE TUBULAR REACTOR CONTINUOUS EXTRACTION UNIT	98
	Tubular Reactor Temperature Profile	98
	Tubular Reactor Concentration Profile	108
VIII.	MATHEMATICAL SIMULATION OF UNDERGROUND LIQUEFACTION	130
	Model Description	130
	Mathematical Formulation	131
	Numerical Method	139
	Results and Discussion	157
IX.	CONCLUSIONS AND RECOMMENDATIONS	161
	LITERATURE CITED	165
	APPENDIX A	169
	APPENDIX B	175
	APPENDIX C	183
	APPENDIX D	184
	APPENDIX E	190
	VITA	195

LIST OF FIGURES

FIGURE		PAGE
1.	Single borehole concept of solvent mining	4
2.	Two borehole concept of solvent mining	5
3.	Coal structure (Wiser 1975)	9
4.	Gas chromatogram of creosote oil	19
5.	Mini-reactor	22
6.	Laboratory unit for simulation of underground liquefaction	23
7.	Tubular reactor	25
8.	Mini-reactor experimental procedure	29
9.	Mini-reactor pressure curve	30
10.	Gas sampling and volume measurement	32
11.	The effect of pressure on lignite conversion	42
12.	The effect of pressure on the conversion of lignite to gas	43
13.	The effect of temperature on lignite conversion	44
14.	The effect of temperature on the conversion of lignite to gas	45
15.	The effect of time on lignite conversion - tetralin	47
16.	The effect of time on lignite conversion - SRC recycled solvent	48
17.	The effect of time on lignite conversion - creosote oil	49



FACULTAD DE ING.
CIENCIAS DE LA TIERRA

LIST OF FIGURES (continued)

FIGURE		PAGE
33.	Gas composition of tubular reactor Run No. 6 - minor components	77
34.	Gas composition of tubular reactor Run No. 9 - major components	78
35.	Gas composition of tubular reactor Run No. 9 - minor components	79
36.	Concentration of lignite-derived liquid analyzed by GPC	81
37.	Correlation of lignite-derived liquid concentration	83
38.	Scatter plot of lignite conversion	95
39.	Scatter plot of lignite converted to gas	96
40.	Tubular reactor temperature profile	109
41.	Sections of a continuous flow reactor ...	112
42.	Error caused by boundary condition approximation	115
43.	Liquid product concentration at the sample port ($z=2L$)	121
44.	Concentration distribution	123
45.	Tubular reactor conversion profile	126
46.	Tubular reactor gas production rate	127
47.	Lignite recovery	129
48.	Model for underground liquefaction	132
49.	Computation field of underground liquefaction	140
50.	Computation field of underground liquefaction in grid coordinates	142

LIST OF FIGURES (continued)

FIGURE		PAGE
51.	Temperature profile of the lignite seam at $r=0$ for a solvent feed temperature of 400°C	158
52.	Temperature profile in the radial direction, $z=L/6$ (i.e. 4.2 m from the injection borehole)	159
53.	Temperature profile at $r=0$, (i.e., at center of seam)	160

CHAPTER I
INTRODUCTION

As the demand for energy continuously rises, crude oil alone is not enough to meet the requirement in the near future. The limited supply of petroleum along with its skyrocketing price encourages the effort to seek alternative energy sources. Coal, a traditional fuel, is once again brought into attention because of its abundance.

However, the current strip mining technique can only recover the coal resources at depths of less than 60 meters. The deep basin coal, which accounts for more than 90% of the coal resources, is either uneconomical or unsafe to recover by strip mining. Alternative recovery methods are in situ liquefaction or gasification.

With the information gained from the other in situ operations and the above-ground coal liquefaction, underground coal liquefaction is considered as a possible means to recover deep basin coal. Compared with underground coal gasification, underground coal liquefaction has many advantages which are:

1. The recovered product has a much higher energy density per unit volume, therefore, it should be economical to transport long distances.
2. Underground liquefaction operates at much lower

This thesis follows the style and format of the AIChE Journal.

temperature, hence a higher thermal efficiency should be attainable.

3. The recovered coal slurry can be processed with the existing equipment for crude oil to produce a wide range of products which could be used as transportation fuels and chemical feedstocks.
4. It is easier to control the extent of the recovery because the reaction can be controlled by temperature alone.
5. There is less restriction on the thickness of the coal seam because of the higher thermal efficiency.



CHAPTER II LITERATURE SURVEY

Underground Operations

In situ processes have been used successfully in the recovery of sulfur, copper, uranium, and salt. Generally speaking, there are two modes of operation for in **situ** processes, the single borehole (Figure 1) and the multi-borehole (Figure 2) processes.

In the single-borehole process, usually involving a double-pipe, the injection of the solvent and the recovery of the product are both through the same borehole.

When a multi-borehole process is used, the producing boreholes are different from the injecting boreholes. A problem associated with the multi-borehole process is the permeability. Permeability allows the solvent to flow through the seam. For underground liquefaction, hot solvent flows through the lignite-derived liquid to the production borehole. This dissertation does not address the problems which might be encountered in establishing permeability. The assumption was made that the formation can in some manner be rubblized. The solvent flow would then be similar to flow through a packed bed reactor.

Underground Gasification

A significant number of field tests have been conducted to recover coal by in situ gasification in the USSR.

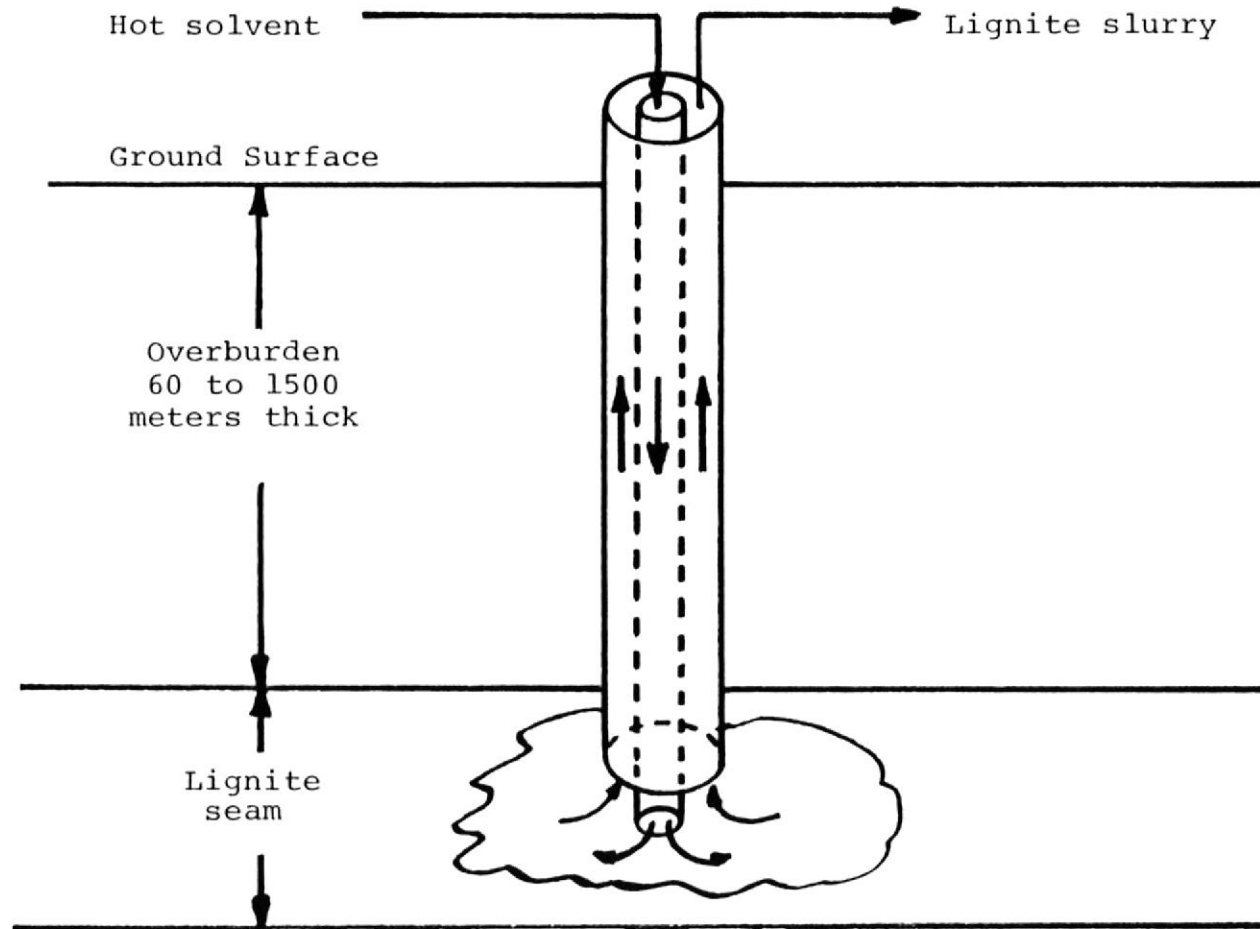


Figure 1. Single borehole Concept of Solvent Mining.

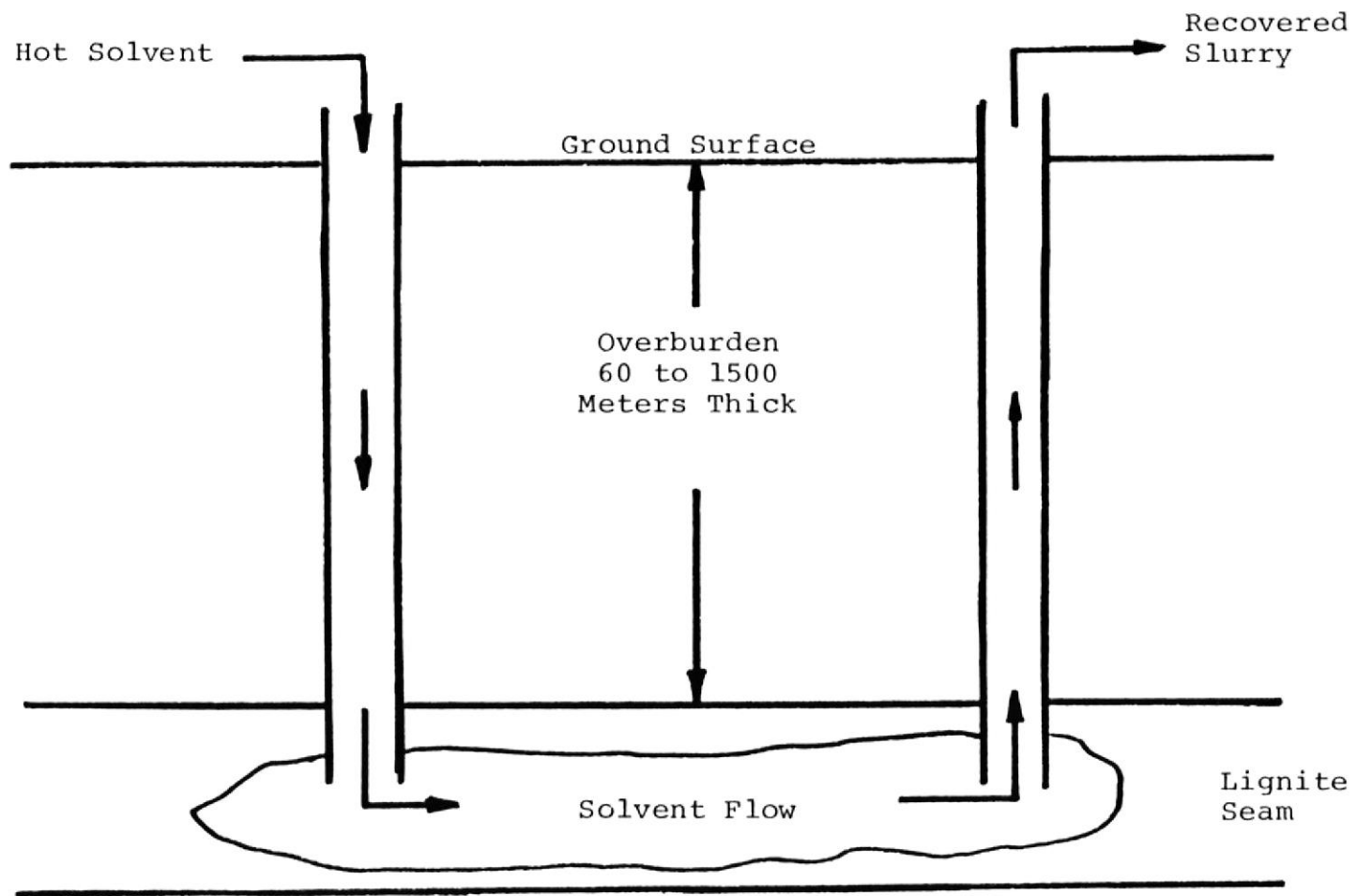


Figure 2. Two borehole Concept of Solvent Mining

Knowledge has been gained also from several field tests operated in the U.S. (Gregg and Edger 1978). Most of these use the multi-borehole concept. Air is injected into one borehole and partially oxidizes the coal seam. The product gases which contain N_2 , O_2 , CO , CH_4 , CO_2 , H_2 , and H_2O are recovered from the other boreholes.

Coal Liquefaction

The conversion of coal into liquid fuel was pioneered by the Germans during World War II. Four liquefaction techniques developed recently seem to have potential for commercialization. Solvent Refined Coal Process, pursued by both the Southern Co. and Gulf Oil Co., liquefies the coal by dissolving it in a solvent under heat and pressure; then hydrogen is added to the resulting hot liquid. In this process, ash and sulfur are separated from the hot liquid. The hot liquid can be cooled to produce relatively ashless and low-sulfur solid, suitable for burning under a boiler. Southern's SRC-I process produces clean solid coal. The hot liquid can, by pursuing Gulf's SRC-II process, be further hydrogenated to produce a product which remains as liquid at room temperature. Increased consumption of hydrogen in general produces lighter products and more liquid product. Exxon Donor Solvent Process: Exxon's method uses solvent pre-hydrogenated or solvent capable of donating hydrogen. Then coal and the donor

BIBLIOTECA

FACULTAD DE ING.
EN CIENCIAS DE LA TIERRA

solvent are brought under heat and pressure to produce liquid product. Compared to the SRC-II process, the hydrogen is added to the solvent in a separate reactor. Both have similar liquid product. H-coal was developed by Hydrocarbon Research Inc. in the early 1960's; this process differs from the others by use of a catalyst to increase the rate of liquefaction. None of these technologies have moved beyond pilot plant operation.

Coal Structure

There is a general concensus that coal originates primarily from plants that decompose and then transform into humic acid. The humic acid is then transformed sequentially into peat, lignite, subbituminous coal, bituminous coal and finally to anthracite. With these transformations, the carbon content increases and the oxygen content decreases. As a result, the heating value increases.

Some of the most stable structure of the original plants may survive this evolution. Cellulose and lignin constitute the majority of the plant components (Francis 1961). Given et al. (1977) have shown that certain components of coal can be related to the structure of lignin.

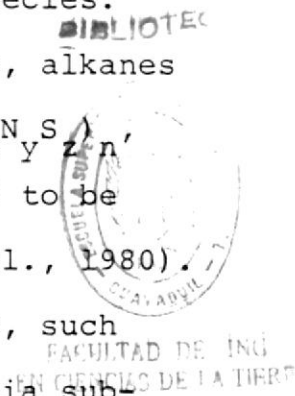
Friedel and Queiser (1959) using ultraviolet techniques concluded that coal could not be polyaromatic and contained large amounts of aliphatic structure. Given and Peover (1960), in characterizing coal extracts by polarographic reduction

concluded that low rank coals were greater than 20% aromatic and high rank coal were greater than 50% aromatic.

A number of researchers have attempted to derive a representative structure of coal. Given (1960) presented a structure consistent with highly substituted aromatics, which are not highly condensed, with functionalities which are known to be present in coal. A more recent model was presented by Wiser (1975) and is shown in Figure 3. The significance of this figure is the location of a number of relative bonds indicated by arrows which can account for the rapid breakup of coal into smaller radical fragments. In the presences of hydrogen donor solvents, the radicals catch the hydrogen and appear as stable species.

From the analysis of Texas lignite-derived products, alkanes (ranging from CH_4 to $\text{C}_{44}\text{H}_{90}$), asphaltenes ($\text{C}_{14}\text{H}_{15}\text{O}_x\text{N}_y\text{S}_z$), alkylated phenols and alkylated aromatics were found to be the predominant species in the liquid (Anthony et al., 1980).

Similar results were found for other types of coals, such as Western Kentucky subbituminous coal, West Virginia subbituminous coal, Utah subbituminous coal and North Dakota lignite. The skeletal structure of any coal, therefore, should be composed of small alkylated ring structures (benzene, indan, and naphthalene) connected by weak ether linkages. The rings may have additional functional groups such as methyl, carboxylic, hydroxy, methoxy, amino and



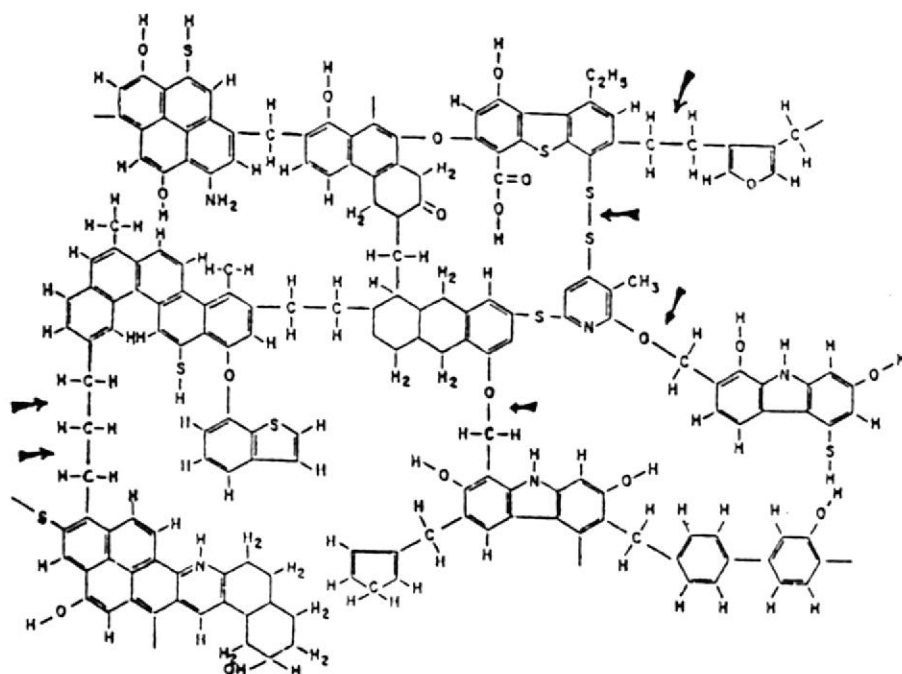


Figure 3. Coal structure (Wiser 1975).

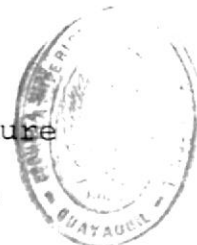
sulfhydryl groups. The straight chain alkanes may be present as caged molecules or may be attached randomly to the main skeletal ring structure via ether or ester linkage. This model is different from Wiser's model in two ways (Anthony et al. 1980):

1. There is little evidence for highly condensed aromatic rings in coal or the coal-derived liquid. The predominate aromatic species are mono- and diaromatic rings. This structure is also supported by Whitehurst (1977).
2. The aliphatic linkages between rings are not likely to exist.

Solvents

Anthony (1976) presented data on room temperature experiments with lumps of lignite two inches square or larger. These lumps were placed in various solvents. Hydrochloric acid, a 10% solution of caustic saturated with lime, or the aluminum hydroxide had no effect on the lignite lump. Sulfuric acid, methanol and potassium dichromate dissolved the lignite lump slightly. The sodium hydroxide and pyridine yielded the greatest degree of comminution. Increasing dissolutions were observed with increasing caustic concentration.

The breakdown of coal in the presence of hot, aqueous alkaline is well documented (Juettner et al. 1937, Smith



UNIVERSIDAD DE ING.
EN CIENCIAS DE LA TIERRA

et al. 1939, Ruof et al. 1951, Kamiya 1961). A common feature of all studies is the requirement of temperatures from 250° to 400° C. The aqueous alkaline was not used for our experiments due to the swelling problem (Anthony 1976). Aqueous alkaline causes Texas lignite to swell which tends to plug the lignite seam.

Several experiments were conducted by using hydrogenated creosote oil as the solvent. The experiments used a one gallon autoclave and lumps of Texas lignite from the Sandow mine. At 400° C and 100 atm 80% of the lignite was converted to gas, liquid, and comminuted solid particles.

Skidmore and Konya (1973) conducted experiments with Illinois #6 subbituminous coal in commercial motor oil. The motor oil was very unreactive.

Davies et al. (1977) studied the solubility of coal in various fractions of an anthracene oil distillate. They concluded that the high-boiling (>340° C) fractions were better solvents than the low-boiling (<340° C) fractions. They further concluded, by investigating the main components in each fraction, polynuclear aromatics with hydrogen-donor ability were good solvents. A comparison between hydrogenated and non-hydrogenated anthracene indicated that the former was a much better solvent.

Their conclusions reveal one interesting point about the role of the solvent in coal liquefaction. Solvent

action occurs by donating hydrogen to stabilize free radicals produced from coal due to thermal decomposition and by carrying the coal-derived liquid from the coal matrix to the bulk solvent.

Chemical Kinetics

The kinetics of coal liquefaction have been studied by several investigators. Curran et al. (1967) treated coal liquefaction as two first order reactions occurring in parallel. However Gun et al. (1979) believed that the reaction should be of a sequential nature. Brunson (1979) studied the kinetics of coal liquefaction in a flow reactor. He suggested a model by considering the coal as being composed of four different fractions. Each fraction reacts differently from the others. Hill et al. (1966) treated the coal liquefaction as one which included first and second order kinetics. Wen and Han (1975) fitted the rate data obtained by the others with an empirical rate expression of the form $r = kC_{A0}(X_e - X)$. Han and Wen (1979) considered coal liquefaction as a two-stage reaction. The initial stage requires little time to react, and a first order reaction is proposed for this stage. In the second stage, hydrogen has to be supplied from the gas phase and the reaction requires long residence times. An axial dispersion model was developed for a continuous liquefaction process (Lee et al. 1978).

The kinetic studies that have been reported were conducted at pressures greater than 70 atmospheres. No kinetic studies have been reported for low pressures, i.e. less than 70 atm.

Underground Coal Liquefaction

Skidmore and Konya (1973) presented the idea of underground coal liquefaction. Later, with the D.O.E. contract (EF-77-5-05-5579), Skidmore (1978) continued the study of the technical and economic feasibility of in situ coal liquefaction. The proposed solvents include supercritical toluene, carbon monoxide and steam, ammonia, and aqueous caustic. Coal seams to be considered include **Gulf** Coast lignites and Pacific Northwest coals. The proposed period of investigation was from September 1, 1977 to September 30, 1978. A final report from this investigation has not been published.

Roylance et al. (1977) did several experiments at conditions simulating a field test. They reached a conclusion that heat was necessary for extraction of coal to occur. The steady state extraction rate was attained in the first one to two hours. The coal sample used was approximately 20 cm in diameter.

Wise and Augenstein (1978) did a conceptual analysis of in situ liquefaction of coal. The preliminary calculations were based on hot aqueous alkaine extraction of coal.

The calculation showed that to produce 1.0×10^{11} KJ/day, the operating costs would be \$10,000/day and the capital costs would be \$36 million.

CHAPTER III
EXPERIMENTAL MATERIALS AND EQUIPMENT

Lignite

The lignite used for this research was furnished by Alcoa Co. at Rockdale, Texas. The freshly mined lignite chunks were stored in water to avoid air oxidation.

Before the experiment, the lignite was removed from the water and crushed by a Jaw crusher. The Jaw crusher was adjusted with an opening of about 12 mm. The crushed lignite was then screened. The lignite collected between U.S. Standard No. 2½ (with opening = 7.9 mm) and No. 5 (with opening = 4.0 mm) was used for all the experiments. The average size of the lignite was taken to be 5 mm.

The 5 mm lignite was treated in two ways. For the mini-reactor experiments, the lignite was air dried for several days. The moisture content of the dried lignite was less than 1%. The reason for drying the lignite was because the mini-reactor experiments were to be conducted at low pressures. At the reaction temperature, the vaporized water can cause significant reaction pressures. However, for the tubular reactor runs, the lignite was soaked in water. The water saturated lignite contained about 35% water (on wet basis).

The ash content of the lignite was determined in a furnace to be 14.7% (MFB). The sulfur content was also

determined in an analyzer to be 1.1% (MFB). Others (Anthony 1976) reported similar results.

Reagents

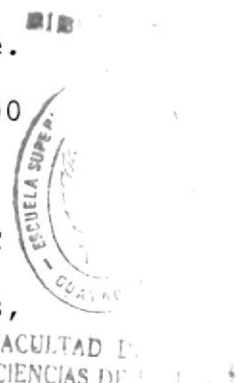
A. Tetralin:

Tetralin, known as a hydrogen donor solvent, was purchased from Fisher Scientific Co. The composition was reported with 99% tetralin, 1% other compounds.

Coal liquefaction involves the thermal disintegration of coal structures at about 400°C to form free radicals. The radicals are terminated by the hydrogen transferred from tetralin. As a result, the tetralin is converted to naphthalene.

Thermal dissociation of tetralin between 300 and 450°C was studied by Hooper et al. (1979). Less than 3% of the tetralin decomposed at 435°C for 1 hour. At the same temperature for 6 hours, 10% of the tetralin decomposed. 1-methyl indan appeared to be the main product of the decomposition. Further study was reported by Benjamin et al. (1979). He concluded that at 500°C for 1 hour, only 25% of the tetralin remained. Naphthalene was the major product.

Tetralin meets all of the requirements to be an active solvent. It is a donor solvent, a ring



type compound and has a rather high boiling point.

B. SRC Recycled Solvent:

Solvent Refined Coal (SRC) recycled solvent was obtained from the pilot plant at Wilsonville, Alabama. The quality of the SRC recycled solvent varies from run to run. An analysis (Ellington 1977) showed that 50% of the solvent had a boiling point between 210°C to 340°C. It contained about 3% tetralin, 12% naphthalene and 7% anthracene/phenanthrene. The approximate composition is shown in Table 1.

TABLE 1. COMPOSITION OF SRC RECYCLED SOLVENT

<u>Fraction</u>	<u>B.P. (°C)</u>	<u>Wt %</u>
Low boiling	< 206	13
Tetralin	207	3
Naphthalene	211	12
	211~339	50
Phenanthrene/ Anthracene	340	7
High boiling	> 340	15

SRC recycled solvent is a mixture of many components with most of the components being aromatics. Also, the majority of the compounds have a boiling point above 200°C and some of the components possess the ability to donate hydrogen.

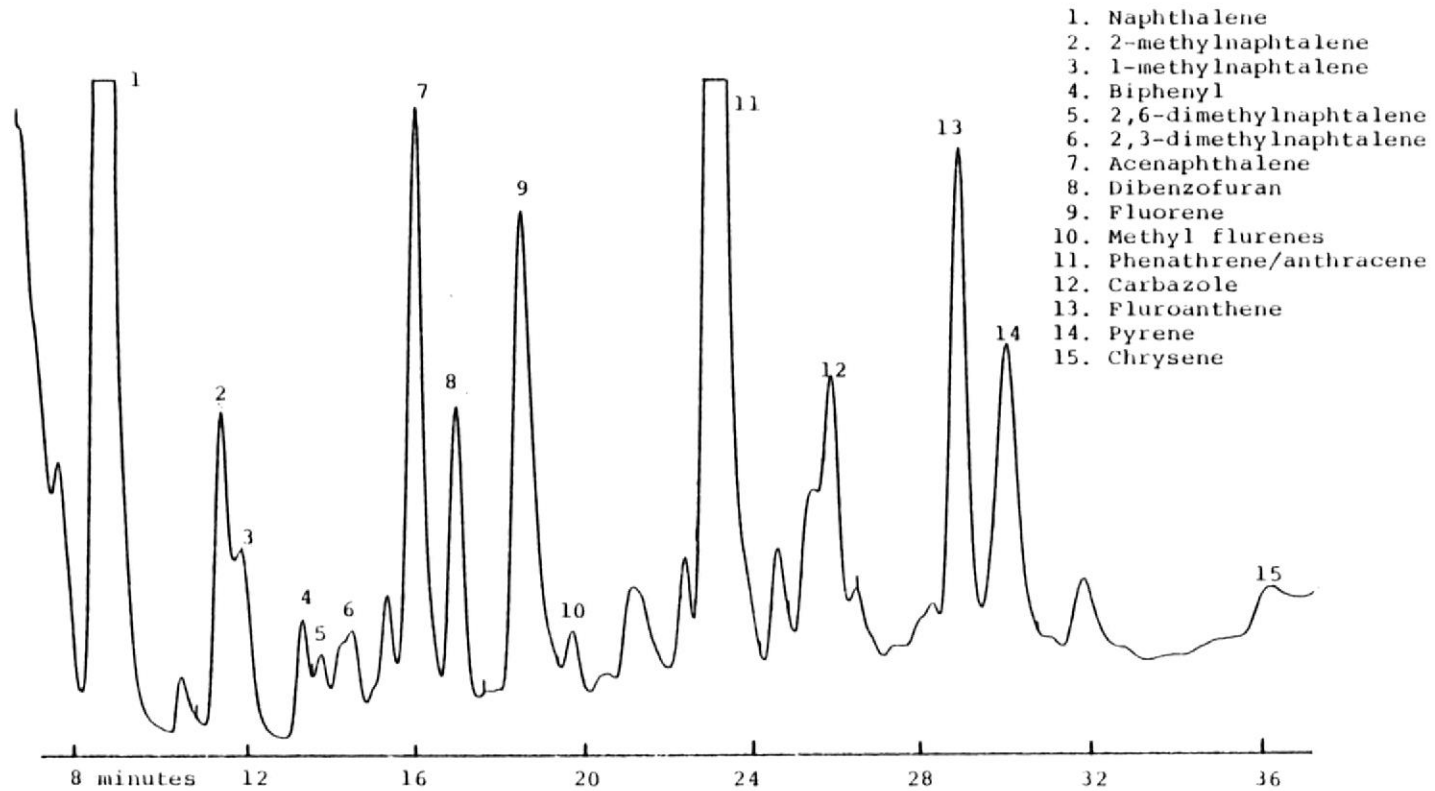
C. Creosote Oil:

Creosote oil was also used in this research because of its similarities in its chemical

properties to the coal substance. The creosote oil was analyzed by injecting it directly into a gas chromatograph. The column used in the analysis was purchased from Supelco, Inc.. The description of the column is as follows: 10% SP-2100 on 100/120 Supelcoport, 8ft x $\frac{1}{4}$ in S.S. The column temperature was programmed between 100°C to 300°C at a rate of 5°C/min. Helium was the carrier gas at 50 ml/min. The gas chromatograph, series 550 purchased from Gow Mac Instrument Co., has a thermal conductivity detector. The detector signal was connected to a Hewlett-Packard 3385A automation system to print the chromatogram shown in Figure 4.

The area percentage under each peak was also calculated by the automation system. Five runs were conducted and the results are shown in Table 2. The weight factors were reported by Max Nestler (1974). By multiplying the area by the weight factors, the weight percentage can be calculated by normalization.

The creosote oil was produced by T&R Chemical Inc. with advertised 60% coal tar creosote, 38.5% petroleum hydrocarbons and 1.5% water and free carbon. In the gas chromatograph analysis (Figure 4) the hydrocarbons were eluted at times less than 8 minutes. Therefore, the hydrocarbons



FACULTAD DE ING.
 EN CIENCIAS DE LA TIERRA



BIBLIOTECA

Figure 4. Gas Chromatogram of Creosote Oil.
 10% SP-2100 on 100/120 Supelcoport,
 8 ft x 1/4 in. S.S. Col. Temp.: 100-300°C
 @ 5°C/min., Flow Rate 50 ml/min, He,
 Sample Size 30 µl. Det.: T/C @ 260-310°C.

TABLE 2. COMPOSITION OF CREOSOTE OIL

No.	Components	AREA %					Ave.	Weight Factor	Weight %
		Run 1	Run 2	Run 3	Run 4	Run 5			
1.	Naphthalene	9.882	11.563	10.766	11.218	11.069	10.900	0.935	9.9
2.	2-Methylnaphthalene	1.539	1.531	1.336	1.362	1.189	1.391	0.952	1.3
3.	1-methylnaphthalene	0.802	0.785	0.649	0.856	0.993	0.817	0.952*	0.8
4.	Biphenyl	0.655	0.552	0.401	0.519	0.489	0.523	0.934	0.5
5.	2,6 dimethylnaphthalene	0.375	0.332	0.240	0.317	0.317	0.316	0.998*	0.3
6.	2,3 dimethylnaphthalene	0.575	0.447	0.416	0.500	0.748	0.537	0.998	0.5
7.	Acenaphthene	3.042	2.560	2.710	2.872	2.796	2.787	1.002	2.7
8.	Dibenzofuran	1.564	1.133	1.352	1.467	1.439	1.391	1.102	1.5
9.	Fluorene	3.536	2.635	3.067	3.257	3.570	3.213	1.061	3.3
10.	Methylfluorene	0.733	0.278	0.487	0.584	0.592	0.535	1.108*	0.6
11.	Phenanthrene/Anthracene	8.284	7.941	8.331	8.600	8.390	8.309	1.154	9.3
12.	Carbazole	2.279	2.440	2.760	1.985	1.894	2.372	1.217	2.8
13.	Fluoranthene	2.983	2.774	2.867	2.729	2.800	2.831	1.285	3.5
14.	Pyrene	2.341	2.643	2.651	2.154	2.793	2.516	1.299	3.2
15.	Chrysene	0.692	0.442	0.402	0.295	0.203	0.407	1.610	0.6
16.	others	7.744	7.764	8.591	8.746	9.058	8.380	1.00*	8.1
17.	Light Hydrocarbons (solvent)	52.922	54.190	52.792	52.584	51.652	52.530	1.00*	51.1
Total		100.000	100.000	100.000	100.000	100.000	100.000		100.0

* Author's estimation based on the adjacent component.

were light materials and were used as a solvent for the coal tar creosote.

Mini-reactor

The reactor for studying the kinetics of the lignite liquefaction was a 60 ml batch type mini-reactor (Figure 5). The reactor was made of 2.54 cm O.D. stainless steel tube. Swagelok caps were used to seal the ends. A pressure transducer was used to record the reaction pressure. The pressure transducer has a smaller internal volume than a conventional pressure gauge, therefore fewer problems with vapor condensation were encountered.

The response time for the reactor was short. The time required for heat-up was only 5 minutes and quench times were less than 10 seconds. Hence, experiments could be done in relatively less than by using the conventional autoclave or by using the tubular extraction flow-through system.

Tubular Reactor Continuous Extraction System

The concept of a two borehole underground liquefaction process is to inject hot solvent into one borehole. The solvent flows through the lignite seam, liquefying the lignite, and then a slurry is recovered from the other borehole.

In the laboratory, the process was simulated by a continuous extraction system (Figure 6). The major components

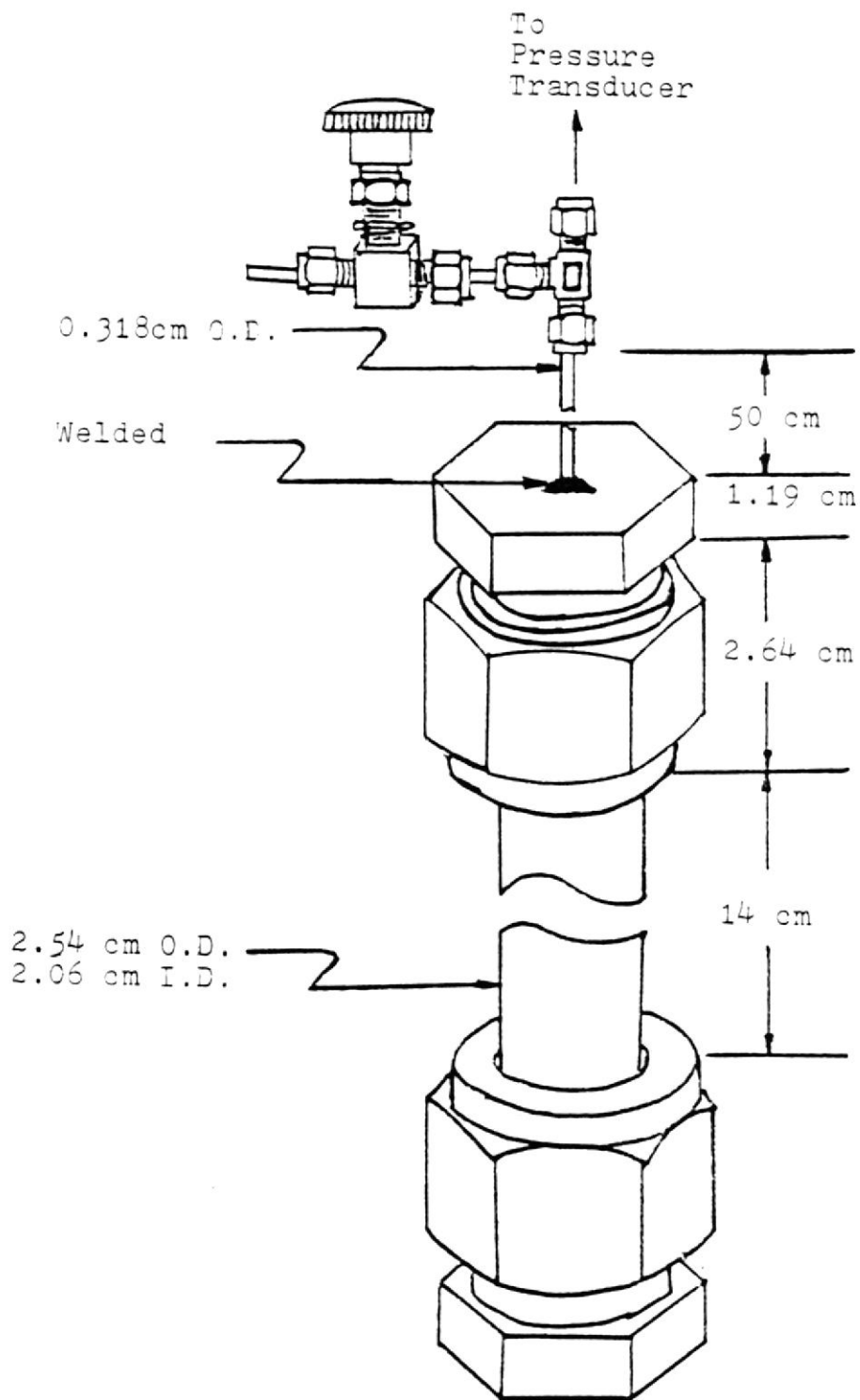


Figure 5. Mini-reactor

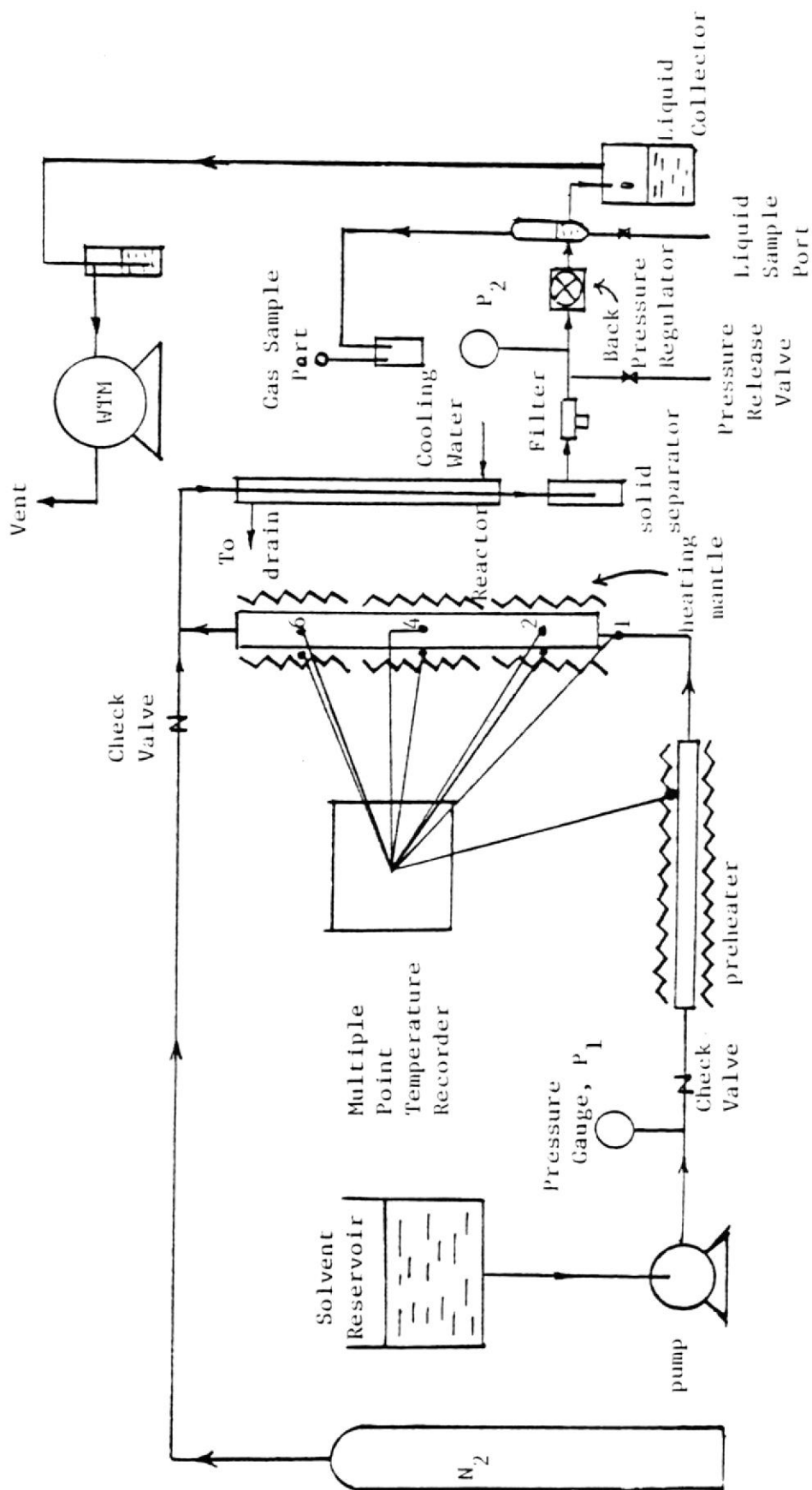


Figure 6. Laboratory Unit For Simulation of Underground Liquefaction.

of the system were a pump, a preheater, a tubular reactor, the sampling apparatus and the controlling and measuring instruments.

The pump, purchased from Lapp Insulator Co. Model LS-20, is a diaphragm pump with a theoretical capacity of 1040 ml/hr and a design pressure of 136 atm. The pump flow rate is adjustable from 0 to 1040 ml/hr.

The preheater, made up of a 2.54 x 60 cm stainless steel tube, was heated by a 2,600 watts furnace. The furnace temperature was controlled by an on-off controller-Thermolyne Furnatrol I, Model CP 18215, Syborn Corporation. Thermocouples were used to measure the temperatures of the solvent, the preheater surface and the furnace.

The tube between the preheater and the tubular reactor was heavily insulated with asbestos tape and the length, approximately 6 cm, was minimized to prevent heat loss.

The tubular reactor (Figure 7) constructed of type 304 stainless steel pipe. It was 5.08 cm I.D., 78.74 cm long, and was packed with lignite to be considered as the lignite seam. A thermocouple well was inserted into the reactor for the measurement of temperatures at three locations. The reactor length was divided evenly into three sections and the thermocouples were located at the centers of the sections. Corresponding to the thermocouples inside the reactor there were three thermocouples on the outside wall.

BIBLIO



FACULTAD DE CIENCIAS DE LA UNIVERSIDAD DE GUAYAQUIL

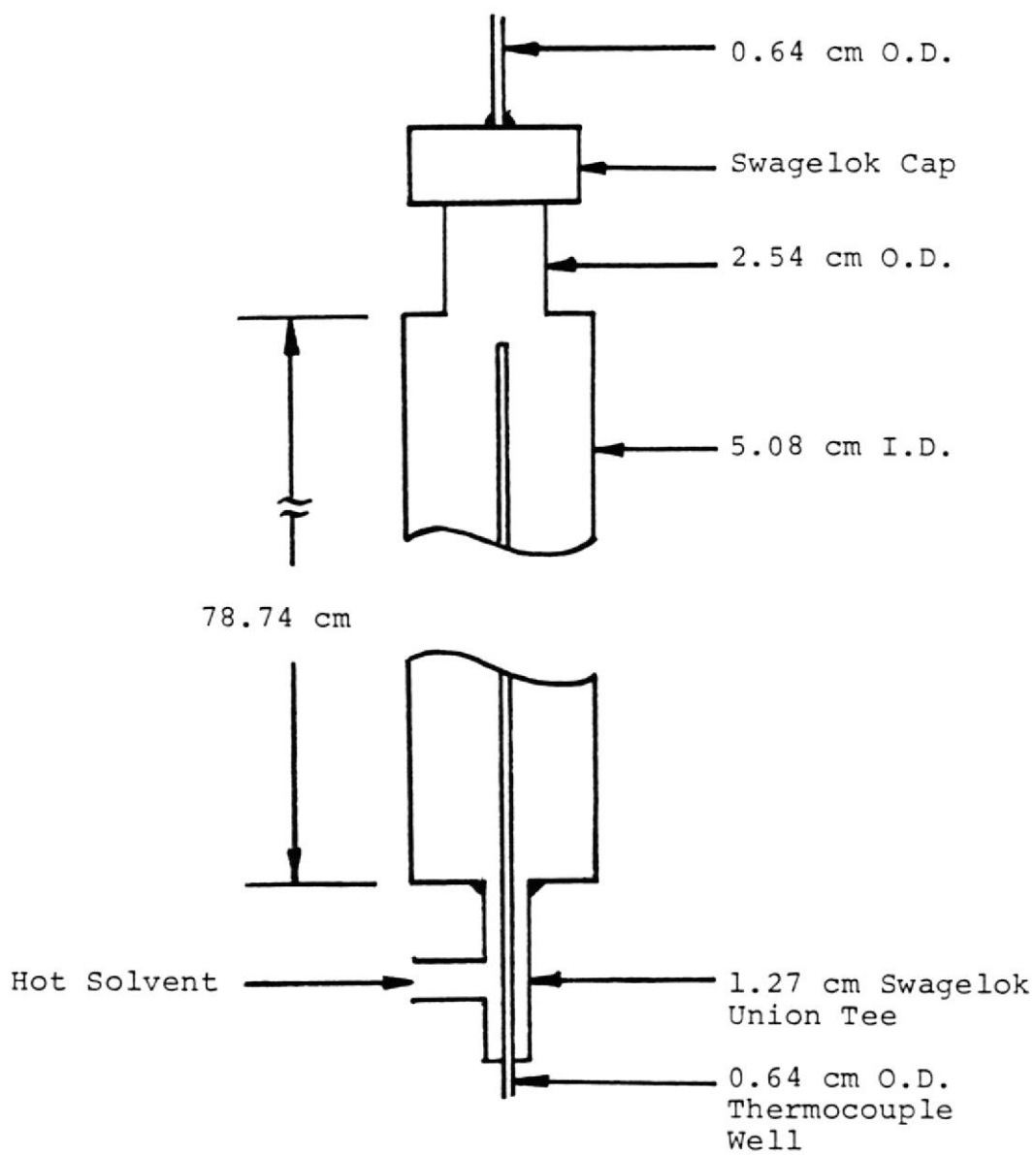


Figure 7. Tubular Reactor.

The outside ones measured the reactor surface temperature. Three heating mantles were wrapped around the reactor. The mantles were purchased from Glas-Col Co. and are made of quartz fabric with a design operating temperature of 650°C. The mantle temperatures which also represent the reactor surface temperatures were regulated with rheostats.

The hot liquid effluent from the reactor was cooled by using a double tube heat exchanger. The solid separator was for the removal of the suspensions in the effluent. The system pressure was controlled by the use of a back pressure regulator.

Two pressure gauges were used. The up-stream gauge is located between the pump and the preheater. The down-stream gauge is connected before the back pressure regulator. Under normal operating conditions, these two gauges indicate the same pressure. If the system plugs, the up-stream gauge will indicate the maximum pump pressure which is much higher than the pressure indicated by the down-stream gauge.

A multiple-point recorder was used to record the temperatures at various points. Figure 6 represents the final design. There were 9 runs conducted with the system and modifications were made between each run. The major modifications were the flow pattern and the use of heating mantles.

Figure 6 shows the hot solvent flowing into the reactor

from the bottom. This flow pattern was used only for run No. 9. For all the other runs, the hot solvent was introduced into the tubular reactor from the top. The reason for making such a change was based on the suspicion that the product gas might gradually fill the reactor if the hot solvent entered from the top. This flow pattern might result in the lignite in the reactor being surrounded by gas phase most of the time. The bottom entering pattern had the advantage that the lignite was soaked in the liquid phase most of the time because the gas is lighter and is continuously rising through the reactor and leaving at the top. The bottom entering style was considered to be closer to the situation which might be encountered in the real underground liquefaction. The existence of the assumed difference between these two flow patterns is to be examined in a subsequent section.

Run Nos. 1 through 4 used asbestos to insulate the tubular reactor. Some degree of heat loss was expected. The existence of the heat loss should be noticed from the temperature profile. The use of heating mantles for runs 5 through 9 should provide better insulation.

CHAPTER IV

EXPERIMENTAL PROCEDURES

Batch Reaction

A schematic diagram of the procedure is shown in Figure 8. Solvent and lignite were weighed and charged into the mini-reactor. After sealing and connecting the pressure transducer, the reactor was lowered into a hot fluidized sand bath which was maintained at a constant temperature. The sand bath quickly heated the reactor to the reaction temperature as indicated by the pressure curve (Figure 9).

The pressure is caused primarily by the solvent vapor pressure and the lignite-derived gases. Since the solvent vapor pressure is a constant at constant temperature, the reaction pressure is determined by the amount of the lignite - derived gases that are generated. The amount of the lignite-derived gases that are generated is proportional to the amount of lignite charged. Therefore, the reaction pressure can be regulated by the amount of lignite charged.

The heating time is estimated from the pressure curve to be 5 minutes. After a predetermined reaction time, the reactor was quenched in water. It took less than 10 seconds to cool the reactor to room temperature.

The final pressure prior to quenching is usually the maximum pressure and is taken to be the reaction pressure. A pressure drop during the experiment indicates a leaky

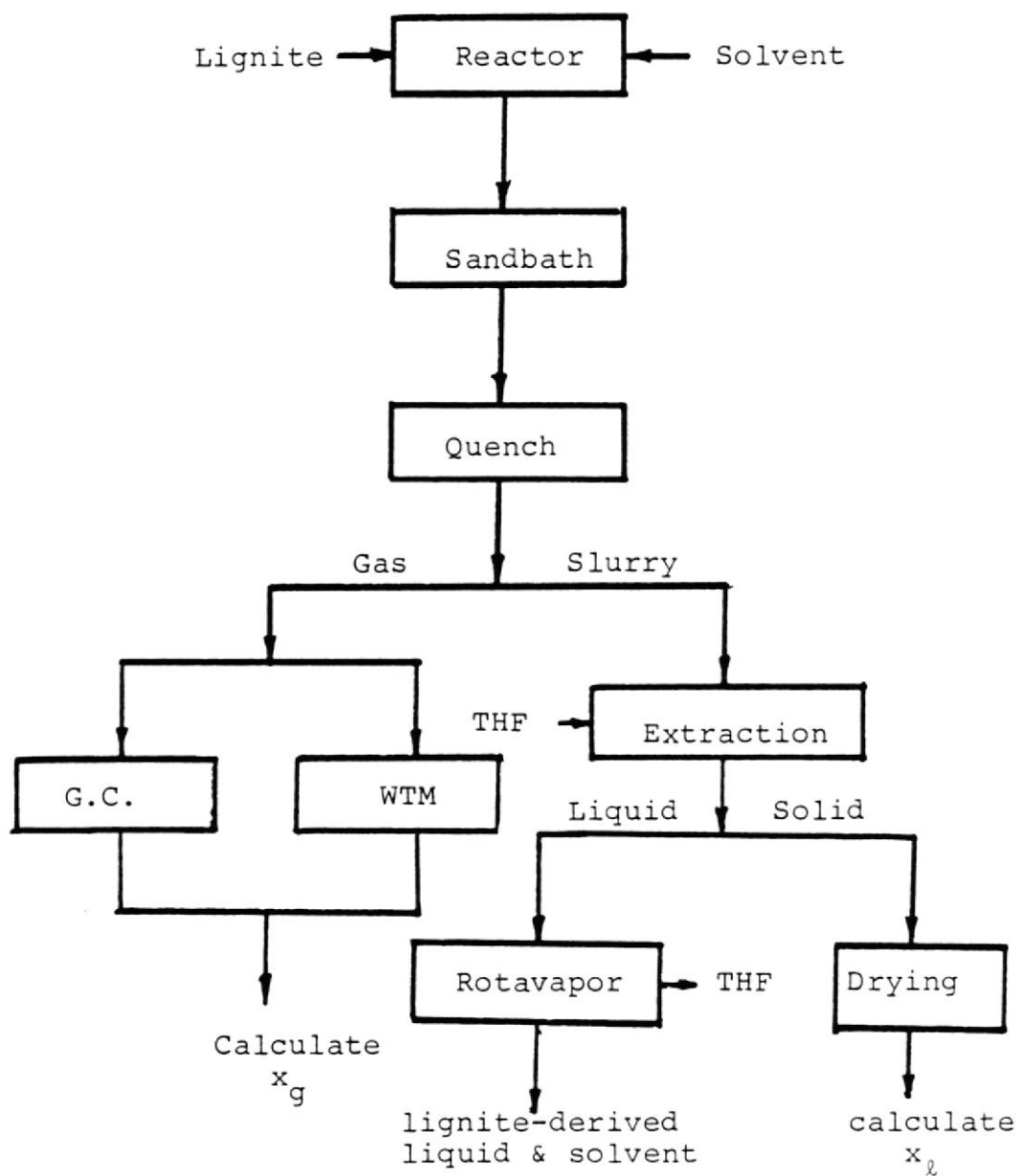


Figure 8. Mini-reactor Experimental Procedure

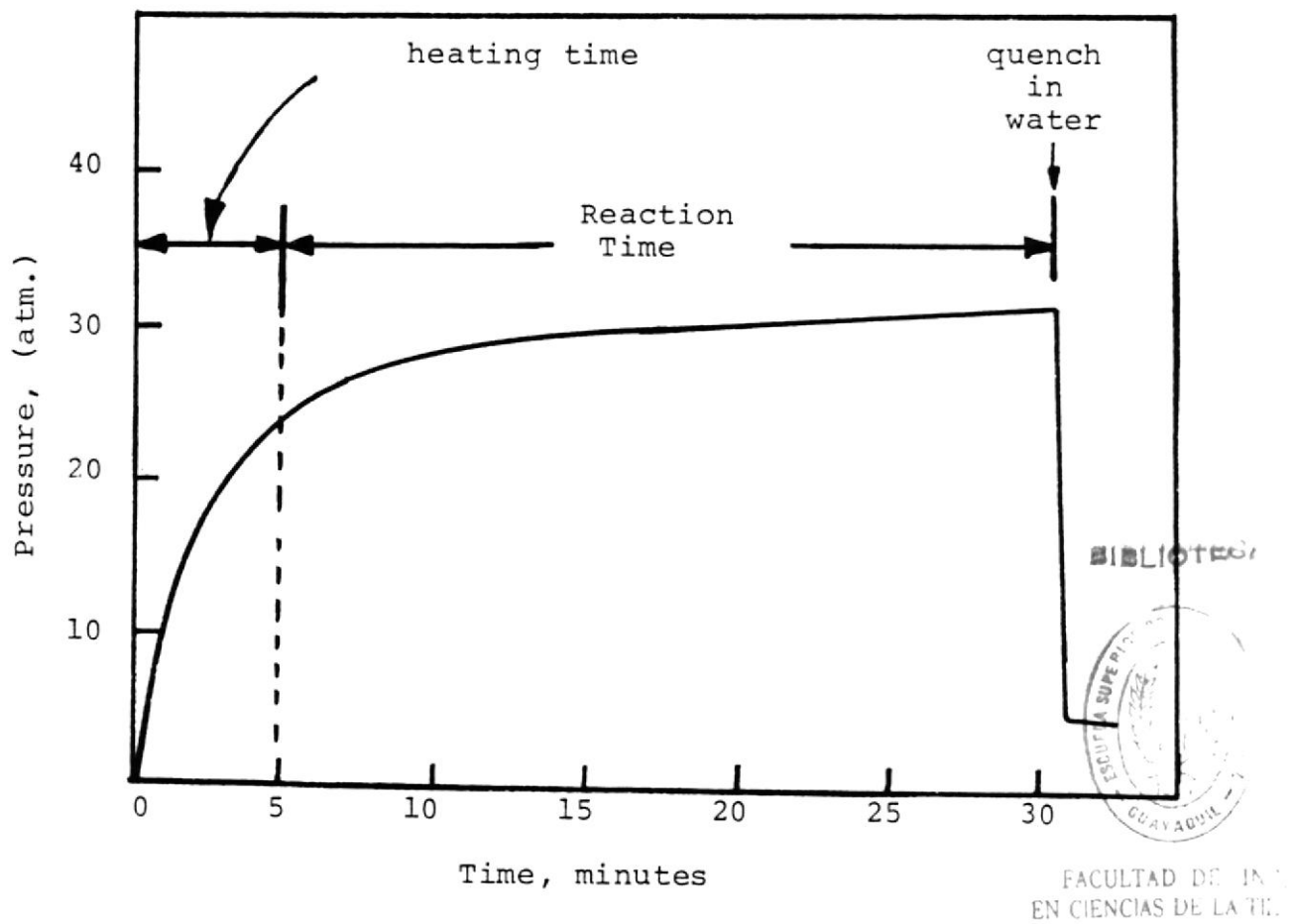


Figure 9. Mini-reactor Pressure Curve.

reactor.

The slurry in the reactor after the reaction contained the solid residue, the solvent and the lignite-derived liquid. The slurry was removed and put into a thimble and extracted by tetrahydrofuran (THF) for 6 hours. The solvent and the lignite-derived liquid were concentrated in the THF rich phase. Analysis of the lignite-derived liquid can be done by removing the THF with a rotavapor. The solid residue left in the thimble was then air dried and weighed. The lignite conversion was calculated.

Gas Product Measurement and Sampling

After the mini-reactor was cooled to room temperature, the gas product was released. The volume of the released gas was measured by a wet test meter (Figure 10).

Before measuring the volume and taking a sample, the system was flushed with nitrogen to ensure that no gases from the previous run remained. The 500 ml bottle provided proper mixing for the gas product. Because of the small volume of the gas product (ranged from 17 ml to 382 ml), the gas sample contained more than 50% (by mole) nitrogen used for purging. The sample was taken after all the gas product was released and was considered to be an average composition of the gas product.

Tubular Reactor Continuous Extraction

These experiments were conducted prior to the batch experiments.

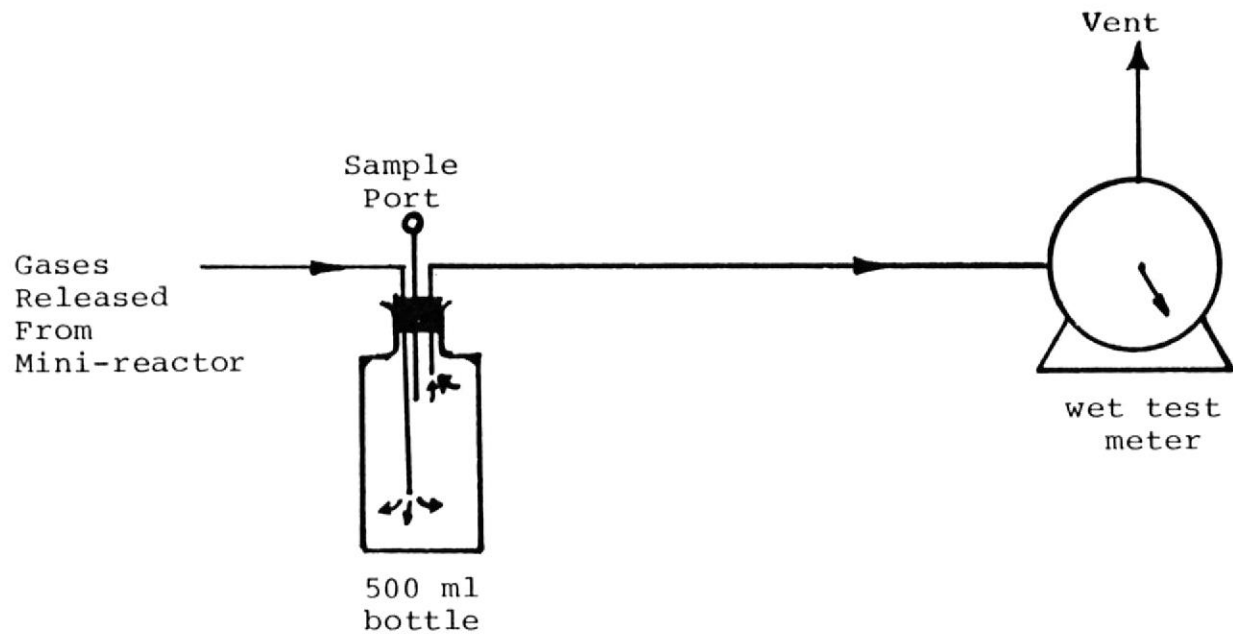


Figure 10. Gas Sampling and Volume Measurement.

FACULTAD DE CIENCIAS DE LA TIERRA
UNIVERSIDAD NACIONAL AUTÓNOMA DE MÉXICO
INSTITUTO DE QUÍMICA

The procedure to start-up the tubular reactor continuous extraction system is as follows:

1. Pack the tubular reactor with lignite. The amount of the lignite packed was weighed for subsequent determination of the conversion.
2. Prepare sufficient solvent in the reservoir.
3. Assemble the system.
4. Use nitrogen pressure to check for leaks and set the back pressure regulator. Then release the nitrogen.
5. Insert thermocouples as indicated in Figure 6.
6. Wrap the heating mantles (or insulation) around the reactor. Heating mantles were not used prior to Run No. 5.
7. Set the pump flow rate.
8. Set the temperature controller at 450°C. The setting is the preheater surface temperature.
9. Turn on the cooling water, the pump, the furnace, and the temperature recorder. The time is $t=0$.

During the experiment, the following things are to be done:

1. Take gas and liquid samples every hour. The gas sample is then immediately analyzed.
2. Record the cumulative volume of the product gas at various times.



FACULTAD DE CIENCIAS DE LA UNIVERSIDAD DE LOS AGOS, NIGERIA

3. Regulate the heating mantles manually so that the tubular reactor surface temperatures are equal to those inside the reactor. This step is not required prior to Run No. 5.
4. Observe the pressures constantly because of the possibility of a plug forming in the system.

The shut down procedure is as follows:

1. Turn off the furnace, the heating mantles and the temperature recorder.
2. Connect a water reservoir to replace the solvent reservoir. The water is then pumped to the system through the preheater to steam the lignite. The system is maintained at 400° C. This step lasts for approximately 15 minutes. It is then allowed to cool for several hours. This step was conducted only for runs 6 through 9. For the other runs the system was cooled and drained of any liquid.
3. Turn off the pump and the cooling water.
4. Release the system pressure and then flush with nitrogen to remove any toxic gases that may be remaining in the system.
5. Remove the heating mantles, the thermocouples and the asbestos tape.
6. Disassemble the system and clean the parts.
7. Remove the unreacted lignite in the reactor and weigh it.

The system was not operated without difficulties. The most serious one was caused by the carbonization of the solvent in the preheater. The carbonization tended to plug the preheater and allowed no solvent to flow. This problem is believed to be caused by local excessive temperatures near the preheater surface. The seriousness of the problem depends on the type of solvents. Packing ceramic beads in the preheater was found to be an undesirable move.

The local overheat problem was cured by controlling the preheater surface temperature. However, the temperature controller can sense only one temperature, either the solvent temperature or the preheater surface temperature in order to determine the furnace output. If the temperature of the preheater surface is to be controlled, then there can be no guarantee that the solvent is regulated at a constant exit temperature. If the solvent temperature is to be controlled (which is the desirable mode), then the surface overheat problem occurs. The compromise is to control the surface temperature at say 450°C.

The heat loss between the preheater and the reactor was another problem. This problem was solved by shortening the distance, adding a heating tape and increasing the thickness of insulation.

CHAPTER V
EXPERIMENTAL RESULTS AND DISCUSSIONS

Lignite Conversions - Mini-reactor

The lignite conversions along with the reaction conditions are listed in Table 3. The lignite charge had been air dried and the ash content was about 15% (DB).

The lignite conversion was calculated by using the following equation:

$$X_{\ell} = \frac{\text{lignite charged-residue}}{\text{lignite charged} \times 0.85} \quad (1)$$

The 0.85 factor is to correct for the mineral matter present in the lignite charge.

The lignite conversion, X_{ℓ} , includes the lignite converted to both gas and liquid products. The first term of the numerator in Equation (1) contains the ash. The assumption is made that the residue contains all of the mineral matter. Therefore, X_{ℓ} is on a dry and ash free basis.

The product gas composition determined by gas chromatography was used to calculate the average molecular weight by using

$$\bar{M} = \sum_{i=1}^N M_i y_i \quad (2)$$

where y_i = mole fraction of component i

M_i = molecular weight of component i

TABLE 3. LIGNITE CONVERSIONS EXPERIMENTAL DATA FOR KINETIC ANALYSIS

A. Tetralin

Run No.	Lignite ^a (g)	Solvent (g)	P (atm)	T(K)	t (hr)	X _g	X _g
T1	2.00	10.00	29.57	673	0.25	0.406	0.038
T2	2.00	10.00	30.59	673	0.50	0.536	(0.015) ^b
T3	2.00	10.00	31.61	673	0.75	0.624	0.062
T4	2.00	10.00	32.63	673	1.00	0.624	0.083
T5	4.00	20.00	45.90	673	1.00	0.677	0.078
T6	6.00	30.00	65.29	673	1.00	0.746	0.060
T7	8.00	40.00	130.59	673	1.00	0.814	0.075
T8	2.20	11.00	24.18	648	0.25	(0.270)	(0.082)
T9	2.00	10.00	25.49	648	1.00	0.448	0.053
T10	4.00	20.00	35.69	648	1.00	0.536	0.041
T11	6.00	30.00	49.98	648	1.00	0.550	0.061
T12	3.30	16.50	30.93	648	1.00	0.503	0.064
T13	3.30	16.50	33.65	648	0.75	0.478	0.061
T14	3.60	18.00	32.29	648	0.50	0.435	0.059
T15	3.70	18.50	32.97	648	0.25	0.360	0.048
T16	1.80	9.00	35.01	698	0.25	0.595	0.052
T17	1.50	7.50	34.67	698	0.50	0.754	(0.094)
T18	1.40	7.00	35.69	698	0.75	0.799	---

TABLE 3 continued:

<u>Run No.</u>	<u>Lignite^a (g)</u>	<u>Solvent (g)</u>	<u>P (atm)</u>	<u>T(K)</u>	<u>t(hr)</u>	<u>X_g</u>	<u>X_g</u>
T19	2.00	10.00	25.49	673	1.00	--	0.047
T20	4.00	20.00	38.41	673	1.00	--	(0.027)
T21	6.00	30.00	39.78	673	0.67	--	(0.024)
T22	6.00	30.00	49.98	673	1.00	--	0.051
T23	8.00	40.00	101.68	673	1.00	--	0.081
T24	4.00	20.00	49.98	673	0.75	--	0.056

B. Wilsonville - SRC Recycled Solvent

S1	2.00	10.00	21.41	673	1.00	(0.501)	0.088
S2	4.00	20.00	33.65	673	1.00	0.557	0.085
S3	6.00	30.00	52.02	673	1.00	0.573	0.082
S4	8.00	40.00	70.39	673	1.00	0.599	0.077
S5	4.00	20.00	35.01	673	0.75	0.533	0.088
S6	4.00	20.00	32.63	673	0.50	(0.468)	0.080
S7	4.00	20.00	31.61	673	0.25	0.442	0.053
S8	6.00	30.00	34.33	648	0.25	0.349	0.043
S9	5.00	25.00	33.65	648	0.50	0.426	0.064
S10	4.50	22.50	32.29	648	1.00	0.466	0.073
S11	4.80	24.00	31.61	648	0.75	0.439	(0.081)

Table 3 continued:

<u>Run No.</u>	<u>Lignite^a(g)</u>	<u>Solvent (g)</u>	<u>P (atm)</u>	<u>T(K)</u>	<u>t(hr)</u>	<u>X_l</u>	<u>X_g</u>
S12	3.00	15.00	32.63	698	1.00	(0.589)	0.137
S13	3.20	16.00	32.63	698	0.50	(0.784)	0.103
S14	3.00	15.00	34.33	698	0.25	0.522	0.102
C. Creosote Oil							
C1	2.00	10.00	30.93	673	1.00	(0.300)	0.088
C2	4.00	20.00	44.88	673	1.00	0.368	0.085
C3	6.00	30.00	69.71	673	1.00	0.426	0.082
C4	2.00	10.00	31.61	673	0.75	(0.412)	(0.106)
C5	2.00	10.00	29.57	673	0.50	0.336	0.077
C6	2.00	10.00	28.21	673	0.25	0.353	0.053
C7	3.90	19.50	34.67	648	0.25	0.269	0.051
C8	3.60	18.00	35.69	648	0.25	0.232	0.056
C9	3.00	15.00	30.25	648	1.00	0.314	(0.055)
C10	3.30	16.50	33.65	648	0.50	0.253	0.071
C11	3.20	16.00	33.65	648	0.75	0.272	0.066
C12	1.00	5.00	27.53	698	1.00	0.436	[0.236]
C13	2.00	10.00	34.33	698	0.25	0.406	[0.106]

Table 3 continued:

<u>Run No.</u>	<u>Lignite^a (g)</u>	<u>Solvent (g)</u>	<u>P (atm)</u>	<u>T (K)</u>	<u>t (hr)</u>	<u>X_l</u>	<u>X_g</u>
C14	1.80	9.00	35.69	698	0.50	0.406	[0.137] ^c
C15	1.60	8.00	34.33	698	1.00	0.420	[0.199]
C16	1.70	8.50	32.29	698	0.75	0.423	[0.159]

- a Dry lignite charged, ash content is about 15% of the weight
- b the data in the barcket () are considered with large errors and will not be used to determine the model parameter. This treatment is suggested by Himmelblau (1970)
- c the data in the bracket [] are not used to determine the parameters



With the measured volume of the gas and the average molecular weight, the weight of the gas product is calculated by

$$W_g = \frac{\bar{M} PV}{R_1 T} \quad (3)$$

where $P = 1 \text{ atm}$

$R_1 = 0.082 \text{ l-atm/(g mole K)}$

$T = 698 \text{ K}$

$\bar{M} = \text{average molecular weight (g/g mole)}$

$V = \text{volume of product gas (l)}$

The conversion of lignite to gas, X_g is calculated by the following equation:

$$X_g = \frac{\text{Wt. of the gas product (or } W_g)}{\text{Wt. of the dry lignite charged} \times 0.85} \quad (4)$$

X_g , like X_l , is on dry and ash free basis.

Several figures are derived from Table 3. The pressure effects are shown in Figures 11 and 12. It appears that X_l increases and X_g decreases with increasing pressure. Both X_l and X_g increase with increasing temperature as shown in Figures 13 and 14. These figures also show that X_l (tetralin) $>$ X_l (SRC) $>$ X_l (Creosote) at the same condition. However, the reverse is true for X_g . These conclusions are to be discussed in more detail in a subsequent section. The conversions for different solvents are shown

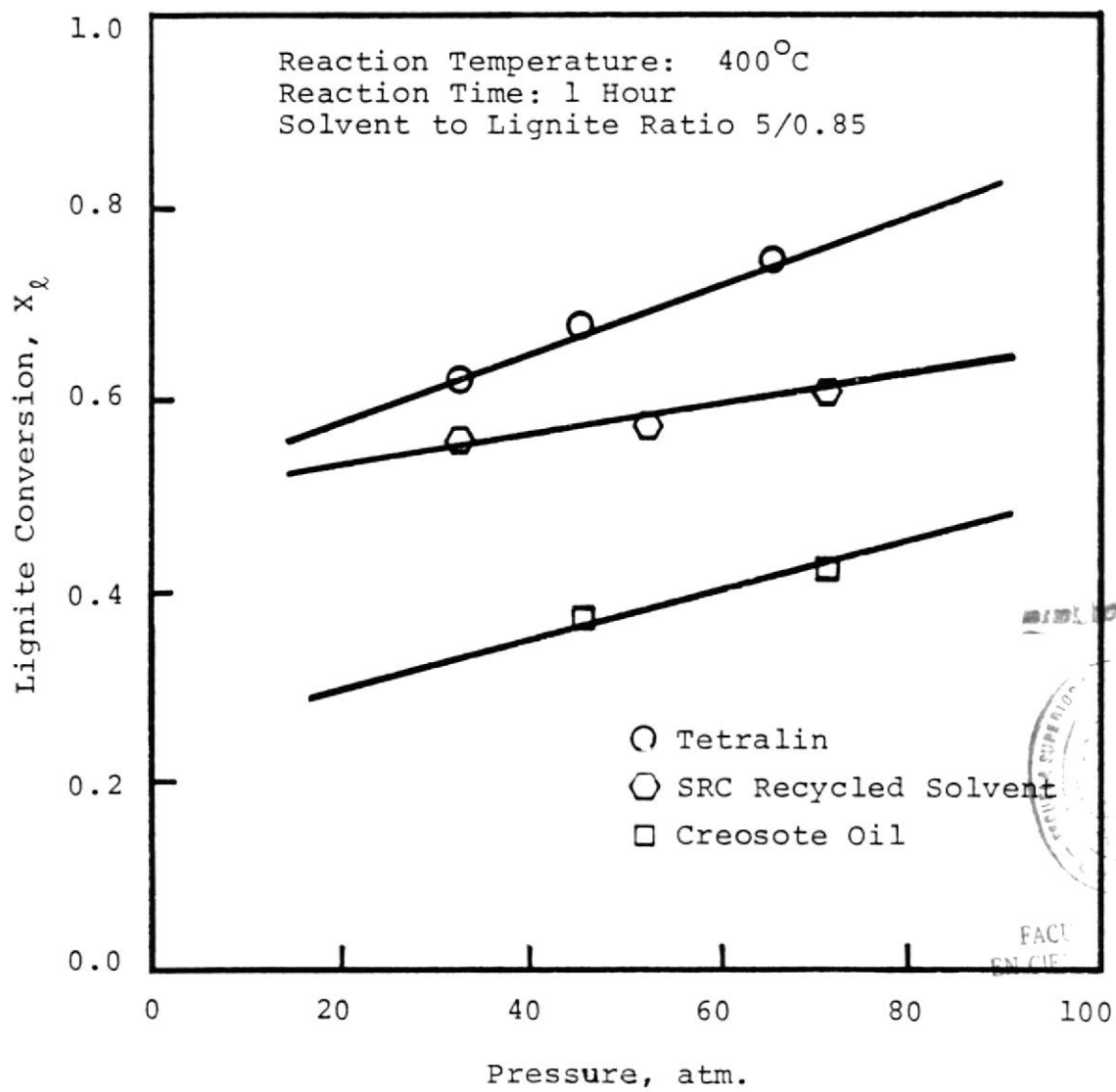


Figure 11. The Effect of Pressure on Lignite Conversion.

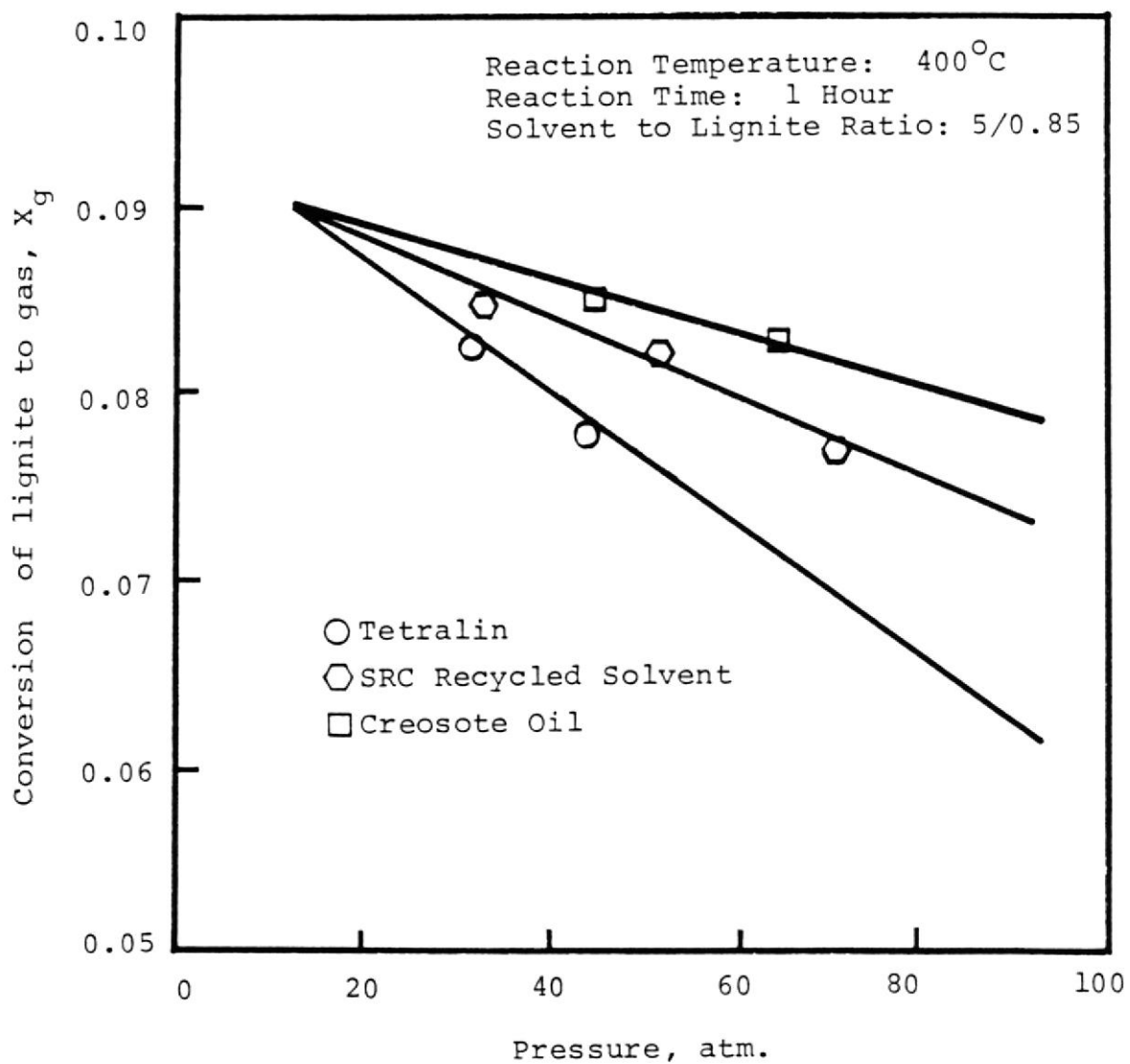


Figure 12. The Effect of Pressure on the Conversion of Lignite to Gas.

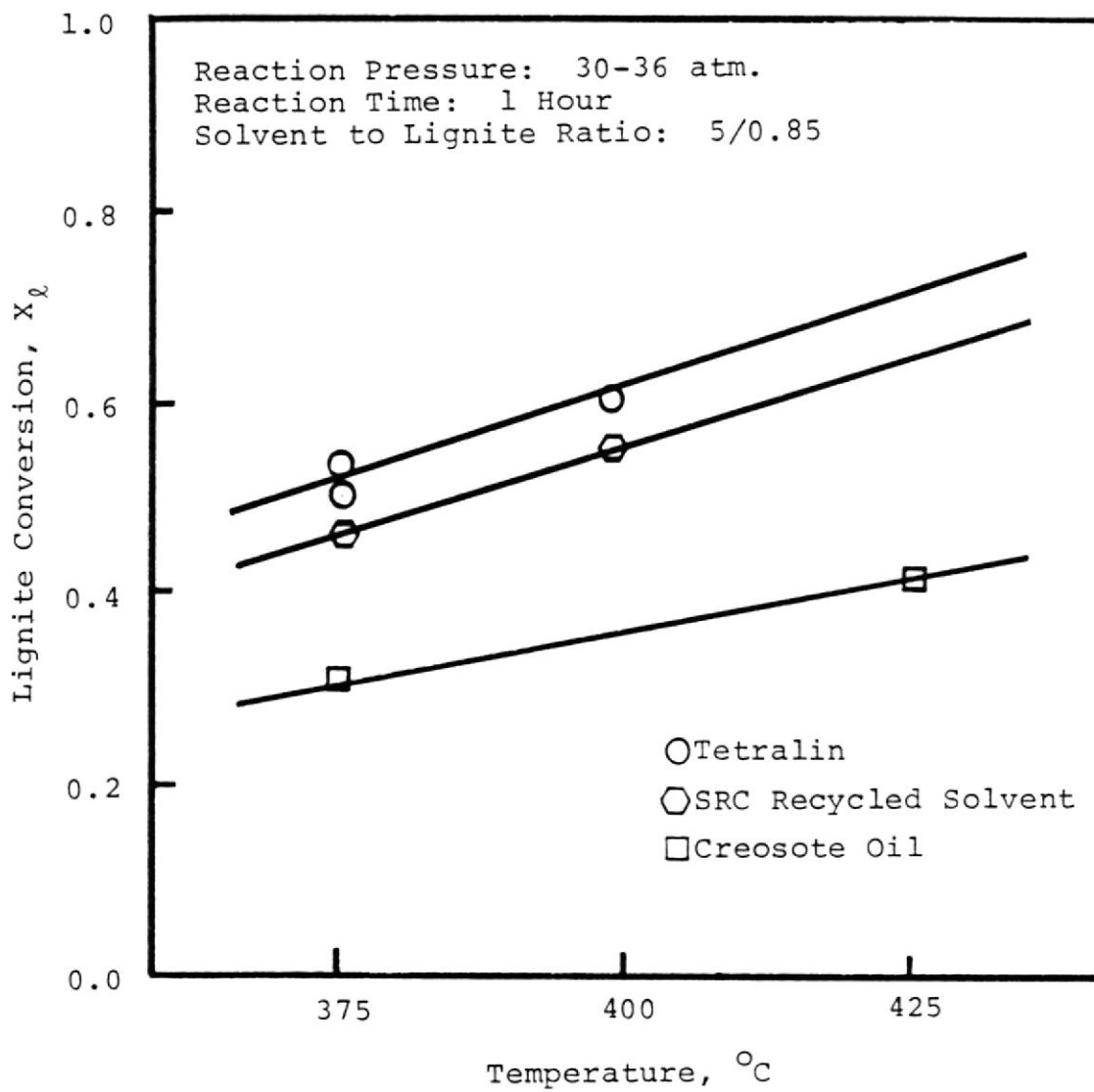


Figure 13. The Effect of Temperature on Lignite Conversion.

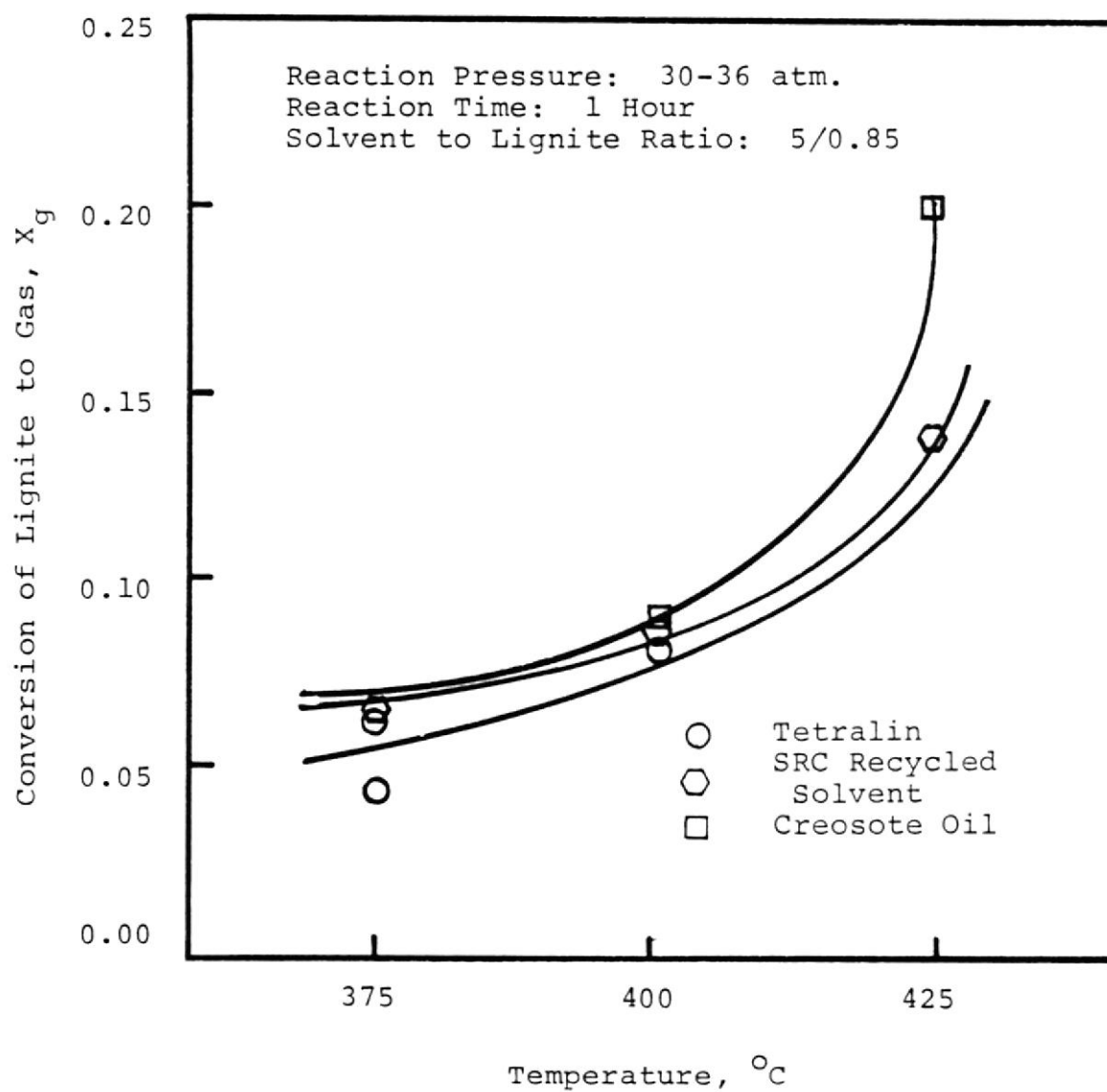


Figure 14. The Effect of Temperature on the Conversion of Lignite to Gas.

in Figures 15 through 20. Figure 20 illustrates the fact that at 425°C, X_g continues rising even after the 1 hour reaction time. This rise indicates that the decomposition of creosote oil occurs at this temperature. A similar, but not as drastic a situation, is also observed for SRC recycled solvent as shown in Figure 19.

The tetralin according to Figure 18 does not appear to be decomposing thermally. Others (Hooper et al. 1979) have reported decomposition of less than 1% at these temperatures and reaction times.

Miscellaneous Runs

The results for several additional runs conducted with the mini-reactor are shown in Table 4.

Run No. A1 used anthracene oil as the solvent. By comparing the result with that of other solvents in Table 5, anthracene oil appears to be a slightly better solvent than creosote oil but not as good as tetralin or SRC recycled solvent. Anthracene was not used for more experiments, because it was very viscous and difficult to handle.

Three blank runs (B1, B2 and B3) were conducted. These experiments used no solvent. The lignite was simply placed in the mini-reactor and then heated in the sand bath. The lignite conversions obtained from these runs are as high as those obtained with creosote oil. The results imply that the lignite conversions obtained by using creosote oil as the solvent are simply the results of devolatilization.

BIBLIOTECA

FACULTAD DE ING.
UNIVERSIDAD DE LA TIERRA

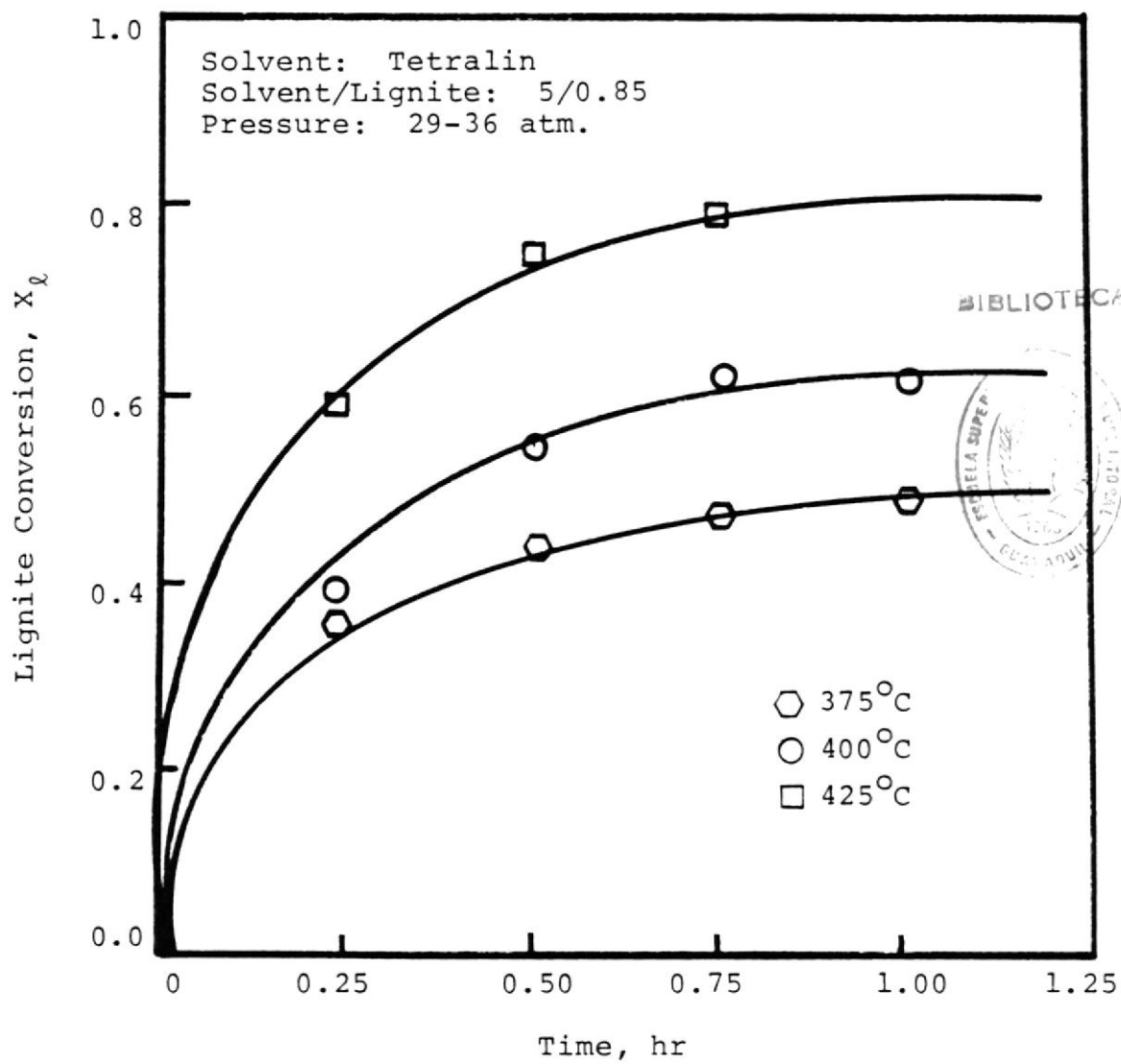


Figure 15. The Effect of Time on Lignite Conversion
-- Tetralin.

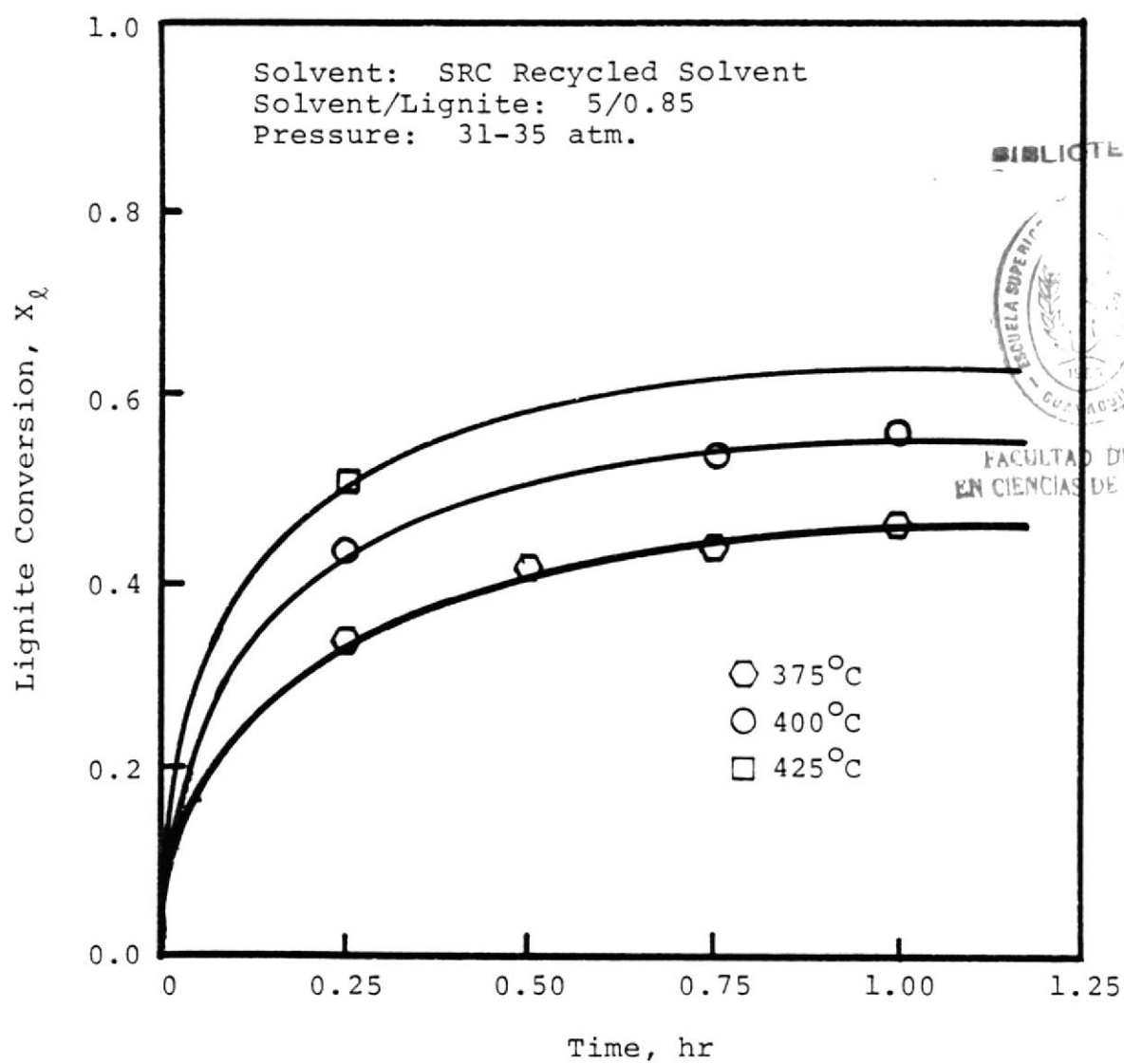


Figure 16. The Effect of Time on Lignite Conversion
-- SRC Recycled Solvent.

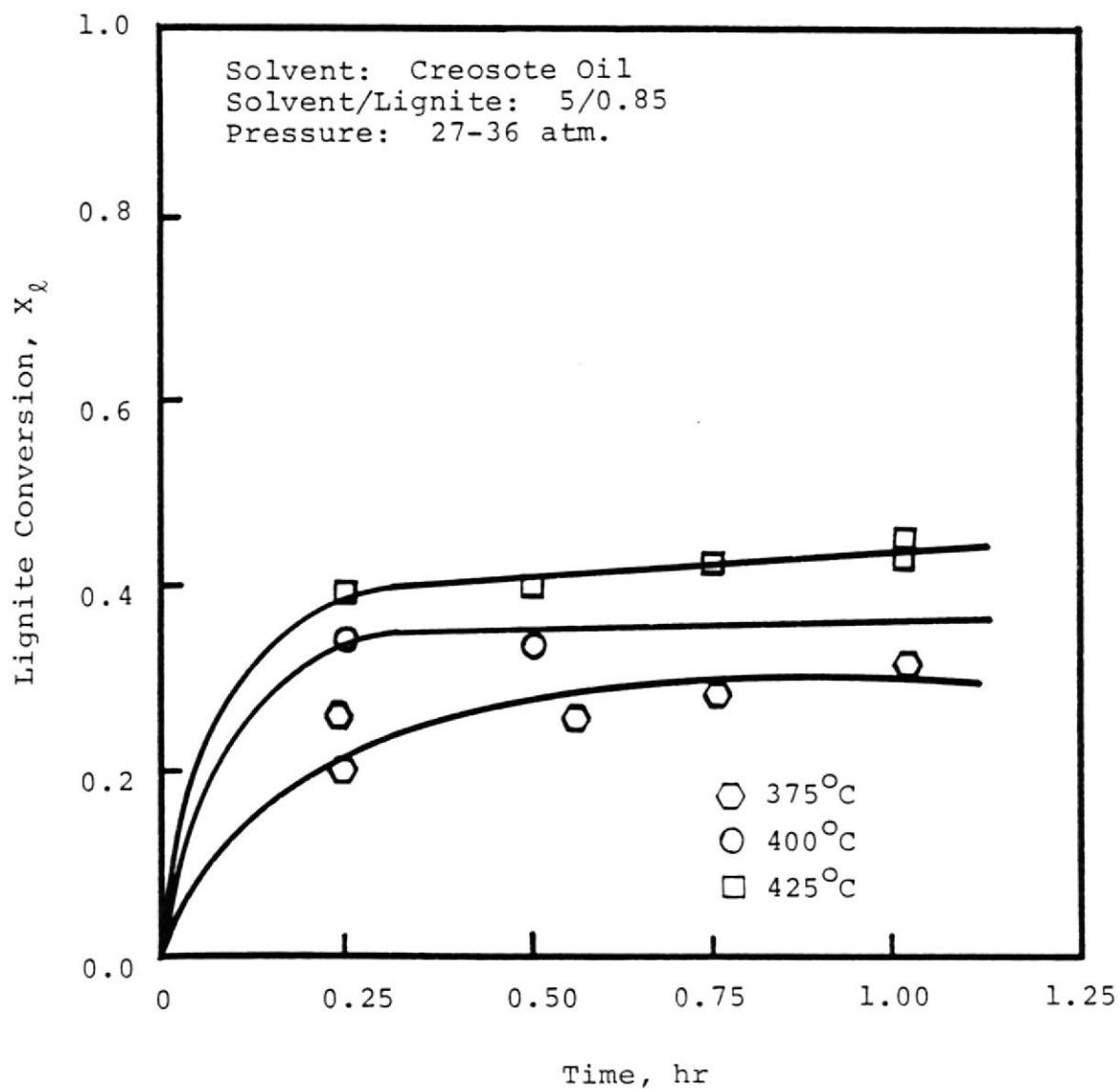


Figure 17: The Effect of Time on Lignite Conversion
-- Creosote Oil.

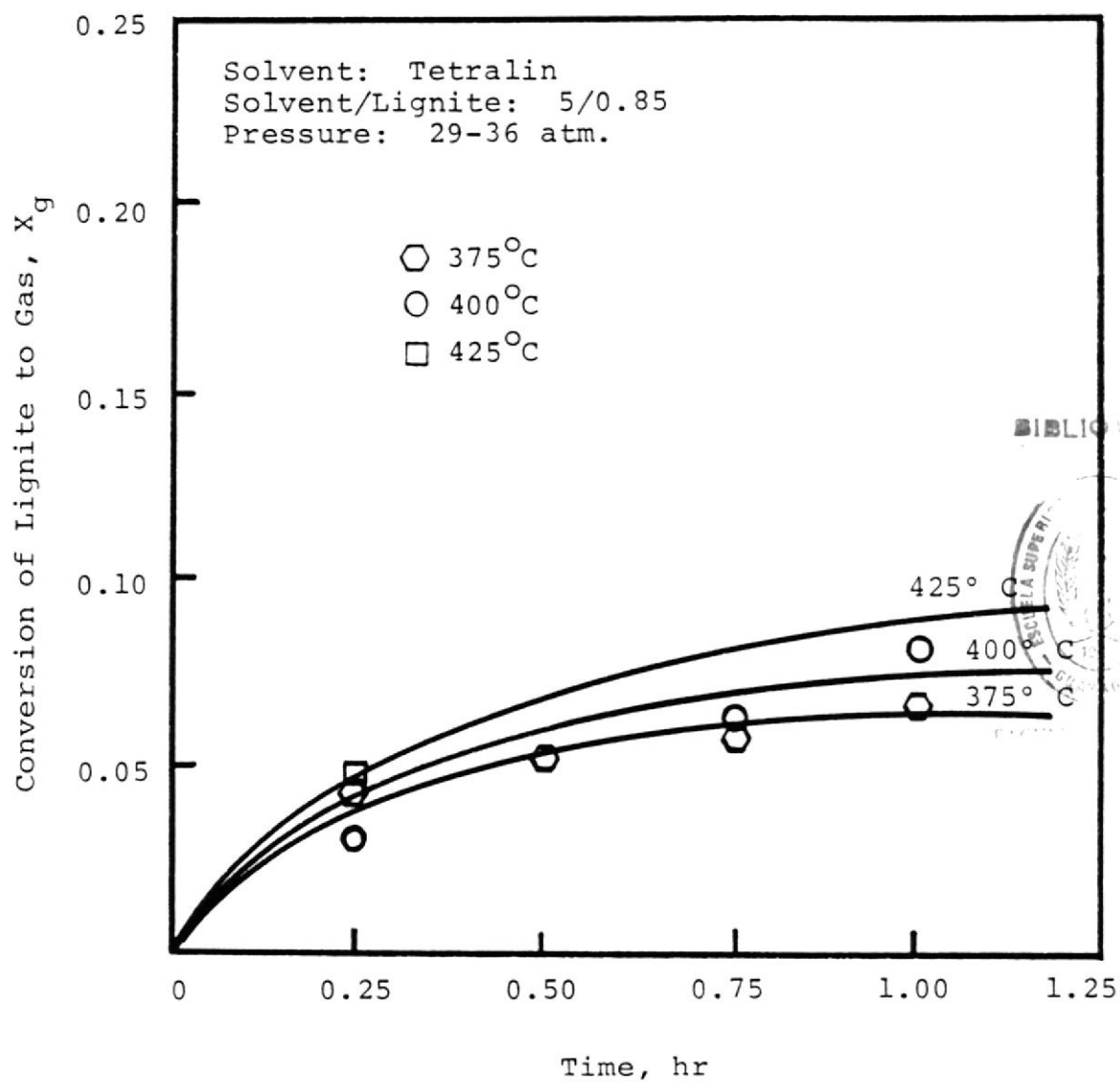


Figure 18. The Effect of Time on the Conversion of Lignite to Gas -- Tetralin.

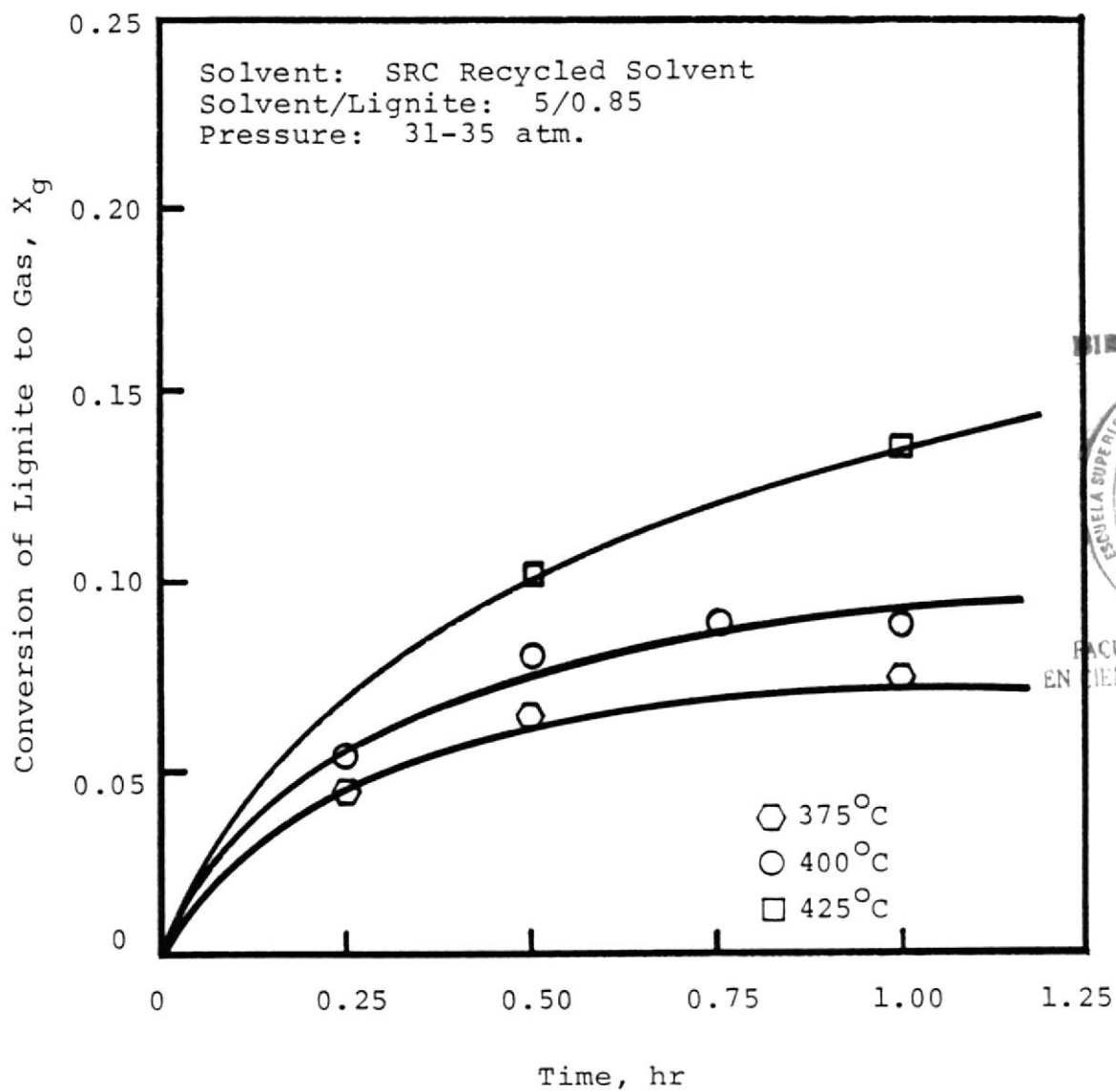


Figure 19. The Effect of Time on the Conversion of Lignite to Gas -- SRC Recycled Solvent.

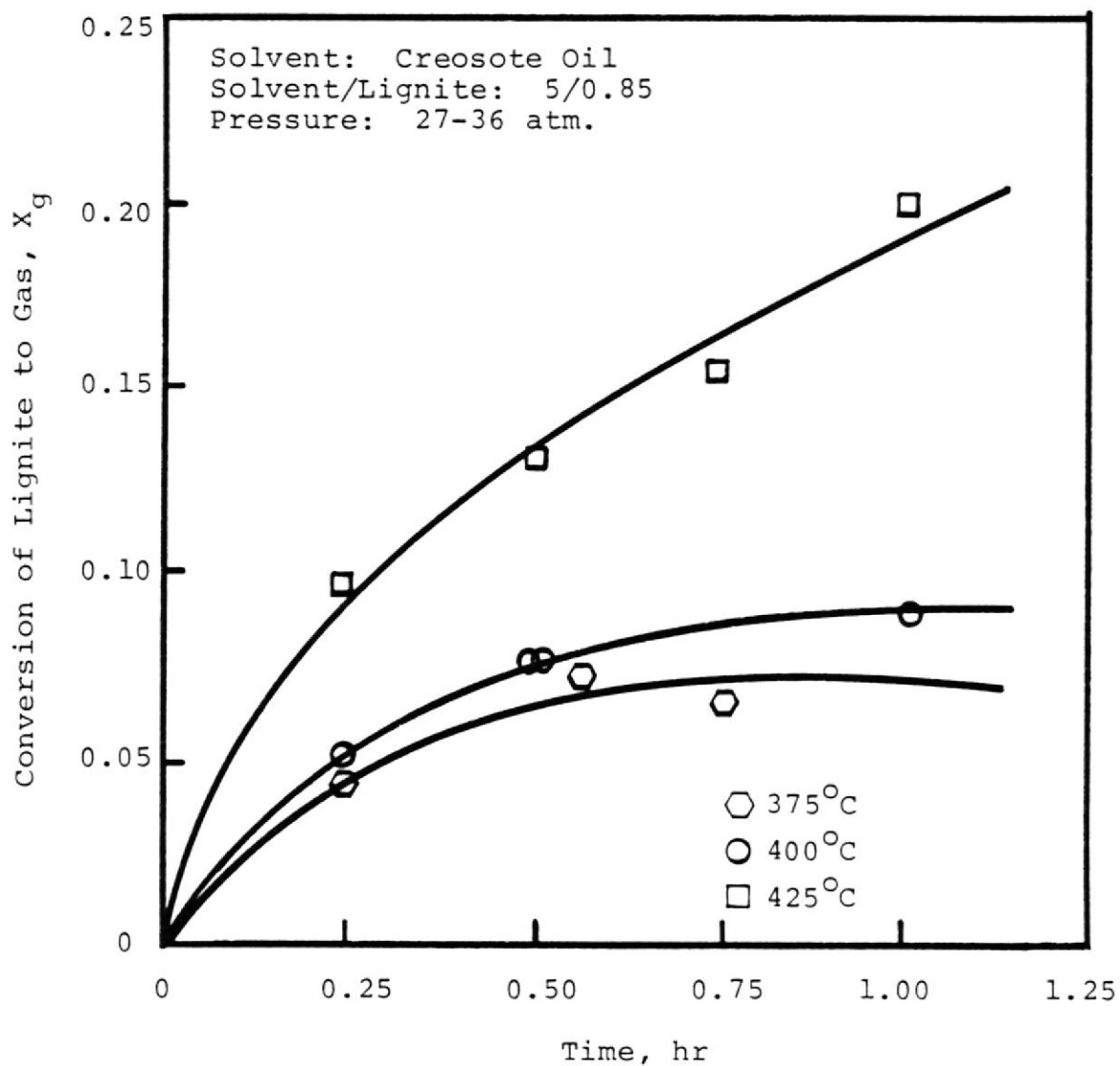


Figure 20. The Effect of Time on the Conversion of Lignite to Gas -- Creosote Oil.

TABLE 4. MISCELLANEOUS MINI-REACTOR EXPERIMENTS

Run No.	Lignite ^c (g)	Solvent	Solvents (g)	P (atm)	T (K)	t (hr)	X_{ℓ}	X_g
A1	4.00	d	39.13	27.5	648	1.0	0.368	0.071
B1	20.00	none	0.00	90.8	673	1.0	0.360	0.065 ^a
B2	5.00	none	0.00	32.6	673	1.0	0.318	0.090
B3	12.75	none	0.00	86.0	700	1.0	0.435	0.094
W1	5.00	water	0.75	33.7	673	1.0	0.320	0.078
W2	5.00	water	1.50	50.7	673	1.0	0.344	0.097
BB1	5.00	e	0.00	1.0	298	---	0.031	0.000
CW1	2.00	f	10.60 ^b	40.5	673	1.0	0.424	0.130

a. slight leak observed

b. creosote oil 10 g and water 0.6 g

c. dry lignite particles 5 mm diameter were charged to the reactor.

d. anthracene oil

e. soxhlet extraction

f. creosote-water

TABLE 5. SOLVENT COMPARISON

<u>Solvent</u>	<u>Run No.</u>	<u>P (atm)</u>	<u>T (K)</u>	<u>t (hr)</u>	<u>X_l</u>	<u>X_g</u>
Anthracene	A1	27.5	648	1.0	0.368	0.071
Creosote	C9	30.3	648	1.0	0.314	--
Tetralin	T12	30.9	648	1.0	0.503	0.064
SRC	S10	32.3	648	1.0	0.466	0.073

BIBLIOTECA

FACULTAD DE ING.
EN CIENCIAS DE LA TIERRA

Two experiments (W1 and W2) were conducted by adding water to the dry lignite. Although W2 shows a slightly higher lignite conversion than W1, the increased conversion is probably due to the increased pressure instead of the water content.

Run No. BBl is the simple soxhlet extraction of the original lignite. The lignite conversion is so low that it can virtually be considered to be zero.

Run No. CW1 used creosote oil and water. The same conversion can be obtained with creosote only. The water content didn't show much effect on conversion.

Product Gas Composition - Mini-reactor

The composition of the gas product is shown in Table 6. The data exclude the nitrogen content in the sample. We assumed that nitrogen was not produced during lignite liquefaction. The majority of the gases were CO_2 , CH_4 , CO , H_2 , and C_2H_6 .

Tubular Reactor - Continuous Extraction Unit

The continuous extraction unit was designed, constructed, and operated prior to the experiments conducted in the mini-batch reactors. The purpose of these experiments was to determine the extent of extraction under conditions similar to those which might be encountered in underground liquefaction extraction. The experiments involved low heating rates, near adiabatic operation and low pressures.

TABLE 6. COMPOSITION OF MINI-REACTOR GAS PRODUCT

A. Solvent - Tetralin															
Run	H ₂	CO ₂	C ₂ H ₄	C ₂ H ₆	CH ₄	CO	C ₃ H ₈	C ₄ H ₆	i-C ₄ ^a	n-C ₄ ^b	u-C ₄ ^b	V(ml)	\bar{n}^d	W(g)	^e
T1	0.20	77.28	0.00	0.00	8.17	12.18	0.73	0.26	0.00	1.18	0.00	46	40	0.07	
T2	5.30	68.79	0.00	0.00	11.20	11.97	1.04	0.35	0.00	1.17	0.00	17	37	0.03	
T3	10.34	59.43	0.00	2.48	11.60	13.86	1.10	0.31	0.00	0.78	0.10	76	34	0.11	
T4	15.50	57.15	0.00	2.70	11.75	10.41	0.90	0.21	0.00	1.38	0.00	108	32	0.14	
T5	13.88	58.73	0.00	3.15	12.98	9.05	1.12	0.14	0.04	0.81	0.10	198	33	0.26	
T6	11.99	59.60	0.00	3.25	14.11	9.00	1.09	0.08	0.04	0.75	0.09	227	33	0.31	
T7	9.81	62.27	0.00	3.72	15.55	6.55	1.09	0.05	0.04	0.84	0.08	368	34	0.51	
T8	0.00	78.70	0.00	0.00	5.80	12.47	1.51	0.89	0.07	0.24	0.32	85	40	0.14	
T9	3.50	0.00	0.00	0.00	42.19	45.78	3.05	0.54	0.00	4.94	0.00	57	22	0.05	
T10	2.74	78.43	0.00	0.23	7.90	9.70	0.42	0.10	0.00	0.48	0.00	85	39	0.14	
T11	3.63	77.11	0.00	1.06	8.06	9.06	0.46	0.07	0.00	0.55	0.00	198	38	0.31	
T12	1.51	79.94	0.00	0.00	7.53	9.64	0.48	0.11	0.00	0.79	0.00	113	40	0.18	
T13	0.80	80.30	0.00	0.00	7.16	10.18	0.41	0.13	0.00	0.94	0.00	102	40	0.17	
T14	0.17	82.00	0.00	0.00	6.06	10.26	0.31	0.10	0.00	0.30	0.00	110	41	0.18	
T15	0.00	82.90	0.00	0.00	5.03	11.27	0.18	0.05	0.00	0.57	0.00	91	41	0.15	
T16	7.08	62.61	0.00	3.08	12.06	11.59	1.52	0.53	0.00	1.42	0.11	57	35	0.08	
T17	18.89	44.65	0.19	4.75	15.51	10.05	2.25	0.62	0.11	1.85	0.33	99	29	0.12	
T18	22.86	42.87	0.00	5.08	15.06	9.04	2.29	0.55	0.13	1.77	0.35	424	28	0.49	
T19	29.03	38.47	0.00	4.72	15.72	8.54	1.93	0.47	0.00	0.92	0.20	76	25	0.08	

Table 6 continued:

B. Solvent - SRC recycled solvent

Run	H ₂	CO ₂	C ₂ H ₄	C ₂ H ₆	CH ₄	CO	C ₃ H ₈	C ₃ H ₆	i-C ₄ ^a	H ₂ S	n-C ₄ ^b	V(ml)	\bar{M} ^d	W(g) ^e
S1	4.11	46.96	0.00	9.56	23.08	7.14	5.31	1.20	0.53	0.85	1.26	108	33	0.15
S2	4.44	49.55	0.00	8.95	22.18	6.49	4.89	0.82	0.48	1.15	1.05	207	34	0.29
S3	5.06	52.42	0.00	7.76	22.64	6.15	3.54	0.44	0.33	1.01	0.65	309	33	0.42
S4	4.68	53.79	0.00	7.64	24.68	6.25	2.00	0.20	0.16	0.31	0.29	382	33	0.52
S5	3.65	55.72	0.00	7.43	19.41	6.57	3.79	0.69	0.37	1.55	0.82	212	35	0.30
S6	2.18	62.62	0.00	5.68	16.23	7.32	2.95	0.66	0.27	1.51	0.58	184	36	0.27
S7	0.37	71.23	0.00	3.55	12.09	8.30	1.85	0.56	0.14	1.59	0.32	113	38	0.18
S8	0.00	83.16	0.00	0.00	6.69	8.45	0.57	0.21	0.00	0.92	0.00	133	41	0.22
S9	0.06	80.54	0.00	1.72	8.15	7.30	0.88	0.24	0.06	0.95	0.10	164	40	0.27
S10	0.26	73.75	0.00	3.23	11.52	7.06	1.79	0.40	0.13	1.59	0.27	176	39	0.28
S11	0.12	77.57	0.00	2.38	9.94	6.91	1.37	0.33	0.09	1.09	0.20	207	39	0.33
S12	7.59	28.53	0.18	13.93	31.01	4.78	8.16	1.01	0.86	1.81	2.14	292	29	0.35
S13	5.97	38.00	0.39	11.73	27.60	6.25	5.69	1.22	0.57	1.22	1.36	218	31	0.28
S14	3.87	51.85	0.54	8.23	20.60	7.89	4.03	0.92	0.38	1.27	0.86	190	34	0.26

Table 6 continued:

Run	H ₂	CO ₂	C ₂ H ₄	C ₂ H ₆	CH ₄	CO	C ₃ H ₈	C ₃ H ₆	i-C ₄ ^a	n-C ₄ ^b	V(ml) ^c	\bar{M} ^d	W(g) ^e
C1	0.21	61.86	1.04	5.33	13.83	10.99	3.55	1.41	0.32	0.76	0.70	96	0.15
C2	1.64	59.48	0.62	5.74	16.13	9.84	3.55	0.91	0.33	1.10	0.66	198	0.29
C3	1.60	63.29	0.00	5.59	17.60	7.29	2.78	0.45	0.26	0.69	0.45	283	0.42
C4	0.37	59.15	1.43	4.73	14.40	15.96	2.11	0.85	0.16	0.48	0.36	113	0.17
C5	0.28	58.99	0.79	3.53	12.85	19.26	2.08	0.93	0.13	0.85	0.31	85	0.13
C6	0.00	68.73	1.35	0.00	9.41	15.67	1.64	1.68	0.00	1.26	0.26	57	0.09
C7	0.00	81.26	0.00	0.00	6.13	12.61	0.00	0.00	0.00	0.00	0.00	102	0.17
C8	0.00	78.25	1.18	0.00	6.17	13.40	0.45	0.40	0.00	0.15	0.00	105	0.17
C9	0.00	71.42	1.62	1.89	8.32	14.93	0.93	0.55	0.05	0.17	0.12	85	0.14
C10	0.00	73.19	1.09	0.00	8.33	15.48	0.81	0.55	0.00	0.55	0.00	125	0.20
C11	0.00	74.73	0.00	0.00	8.72	13.26	1.33	0.81	0.00	1.15	0.00	113	0.18
C12	3.01	43.54	2.06	10.38	18.14	10.39	6.79	2.67	0.66	0.64	1.72	142	0.20
C13	2.84	44.41	2.29	9.60	17.55	12.29	5.80	2.43	0.56	0.77	1.46	127	0.18
C14	1.06	55.77	1.66	8.56	15.58	9.53	4.61	1.67	0.37	0.21	0.98	142	0.21
C15	2.50	47.59	1.38	10.25	16.86	6.83	7.89	2.59	0.85	1.07	2.19	184	0.27
C16	2.75	37.27	1.95	12.54	21.44	9.82	7.85	2.68	0.88	0.68	2.14	170	0.23

a. iso-butane

b. n-butane

c. volume of gas production measured by wet test meter at 1 atm. and 298k

d. average molecular weight

e. weight of gas production

Nine runs were conducted in this system and many problems were encountered. A detailed discussion of each experiment is presented in Appendix B. The grams of lignite put into the reactor for each experiment is shown in Table 7. The reaction conditions, solvent utilized, run time and the extent of extraction are presented in Table 8. The total conversion is based on the lignite charged less the residue in the reactor after it had been extracted with THF.

The total conversions can be reduced by the amount extracted in the soxhlet extraction. For Runs 6-9 as shown in Table 9, this correction is less than 3%. In the procedure the reactor contents were purged with steam and cooled with water flowing through the system. Run 4 with the tetralin had a considerable quantity extracted in the soxhlet extractor. The lignite conversion would therefore be reduced to approximately 50%. However, had the reactor been flushed by steaming and allowed to cool with water flowing through it, only a small amount of extractable material would probably have been obtained in the soxhlet extractor.

The temperature profiles for the 9 experiments are shown from Figures 21 through 29. Run No. 1, 2, 3 used water as the solvent. The effect of the phase change (water to steam) on the temperature profiles are easily seen in Figures 21, 22 and 23. Run No. 6 using creosote has a similar profile (Figure 26), indicating the vaporization of

TABLE 7. LIGNITE CHARGE TO THE TUBULAR REACTOR

<u>Run No.</u>	<u>Wet (g)</u>	<u>% Water</u> [*]	<u>MFB (g)</u>	<u>% Ash</u> ^{**}	<u>MAF (g)</u>
1	--	---	---	---	---
2	1142	37.8	710	(15)	604
3	(residue from run no. 2)				
4	(residue from run no. 3)				
5	1052	31.5	721	(15)	613
6	1024	32.0	696	(15)	592
7	1049	39.6	634	(15)	539
8	1047	40.0	628	(15)	534
9	1034	34.4	678	(15)	576

*on the wet basis

**on the dry basis

***value with parenthesis represents the estimated value

TABLE 8. CONVERSIONS FOR THE TUBULAR REACTOR EXPERIMENTS

<u>Run No.</u>	<u>Solvent</u> ^d	<u>Flow Rate (ml/hr)</u>	<u>P (atm)</u>	<u>T (°C)</u>	<u>T (hr)</u>	<u>X_ℓ (MAF)</u>	<u>X_g (MAF)</u>
1	Water	1000	21.4	365-435	3.75	---	---
2	Water	1000	14.6	308-338	6.50	---	0.037
3	Water	1000	17.3	372-435	8.00	---	---
4	Tetralin	1000	14.6	378-445	6.00	0.587 ^b	---
5	Kolineum	1000	14.6	430	5.00	0.281 ^c	0.329 ^c
6	Creosote	1000	21.4	400	6.50	---	0.121
7	Creosote	500	21.4	110-310	2.50	---	0.059
8	Creosote ^a	757	25.0	400	6.00	0.041	---
9	Creosote	941	21.4	425	6.00	0.314	0.139

a. 99% creosote plus 1% Tetralin

b. The result of Run No 2, 3, 4. The same lignite has been run through 3 runs.

c. Result of two trials on the same lignite

d. The water was vaporized in the preheater. On entering the reactor part or all of it may have recondensed. At the final reaction temperatures water and tetralin would be in the gas phase within the reactor.

TABLE 9. LIGNITE RESIDUE OF THE TUBULAR REACTOR

<u>Run No.</u>	<u>Wet (g)</u>	<u>MFB (g)</u>	<u>% Extraction^a</u>	<u>% Ash^b</u>	<u>% Sulfur^c</u>	<u>MAF^d (g)</u>
1	---	---	---	---	---	---
2	---	---	---	---	---	---
3	---	---	---	---	---	---
4	---	406	12.4	14.1	0.54	298
5	---	536	(2.8) ^e	(15)	---	441
6	545	532	2.8	13.1	0.64	447
7	---	---	---	9.6	0.93	---
8	704	620	(2.8)	14.6	---	512
9	---	499	(2.8)	18.1	0.59	395

- a. % extractable by soxhlet extraction with THF for 4 hours on the dry basis. The original lignite can not be extracted.
- b. On the dry basis, the original lignite contains 14.7% ash.
- c. On the dry basis, the original lignite contains 1.11% sulfur.
- d. Includes the sulfur content.
- e. Value with parenthesis represents the estimated value.

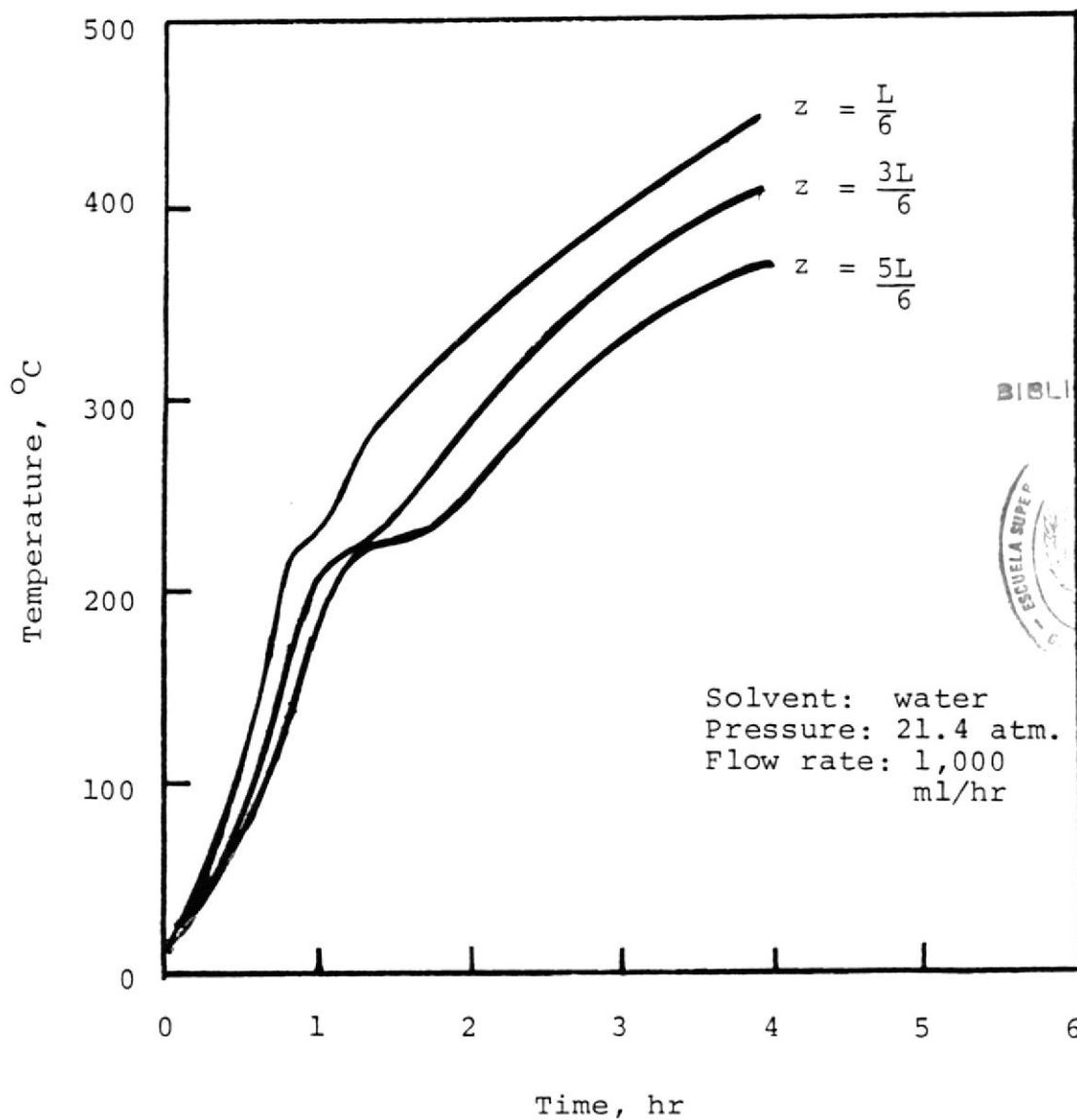


Figure 21: Experimental Temperature Profile for Tubular Reactor Run No. 1 (No external heat on the reactor).

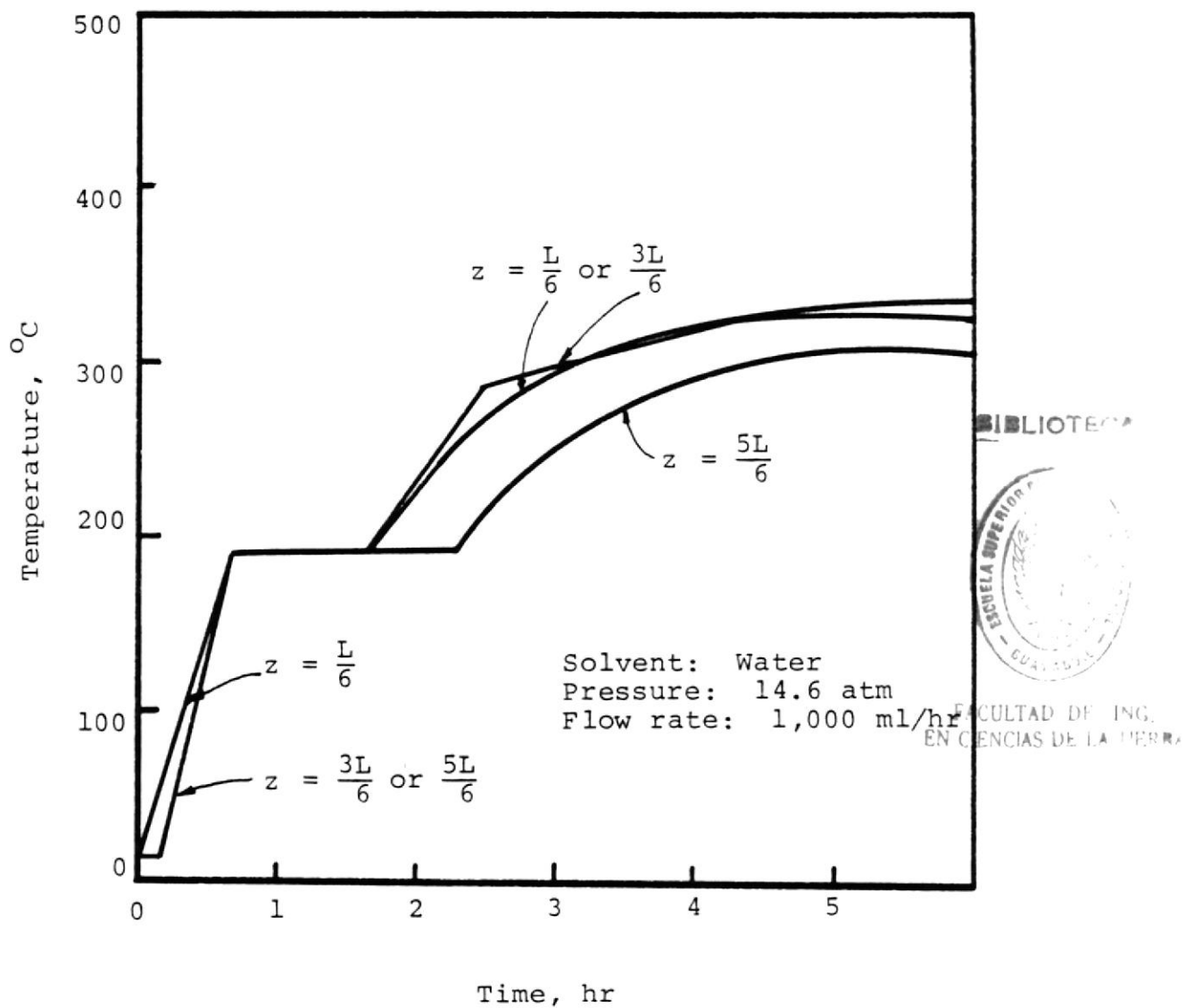


Figure 22: Experimental Temperature Profile for Tubular Reactor Run No. 2 (no external heat on the reactor).

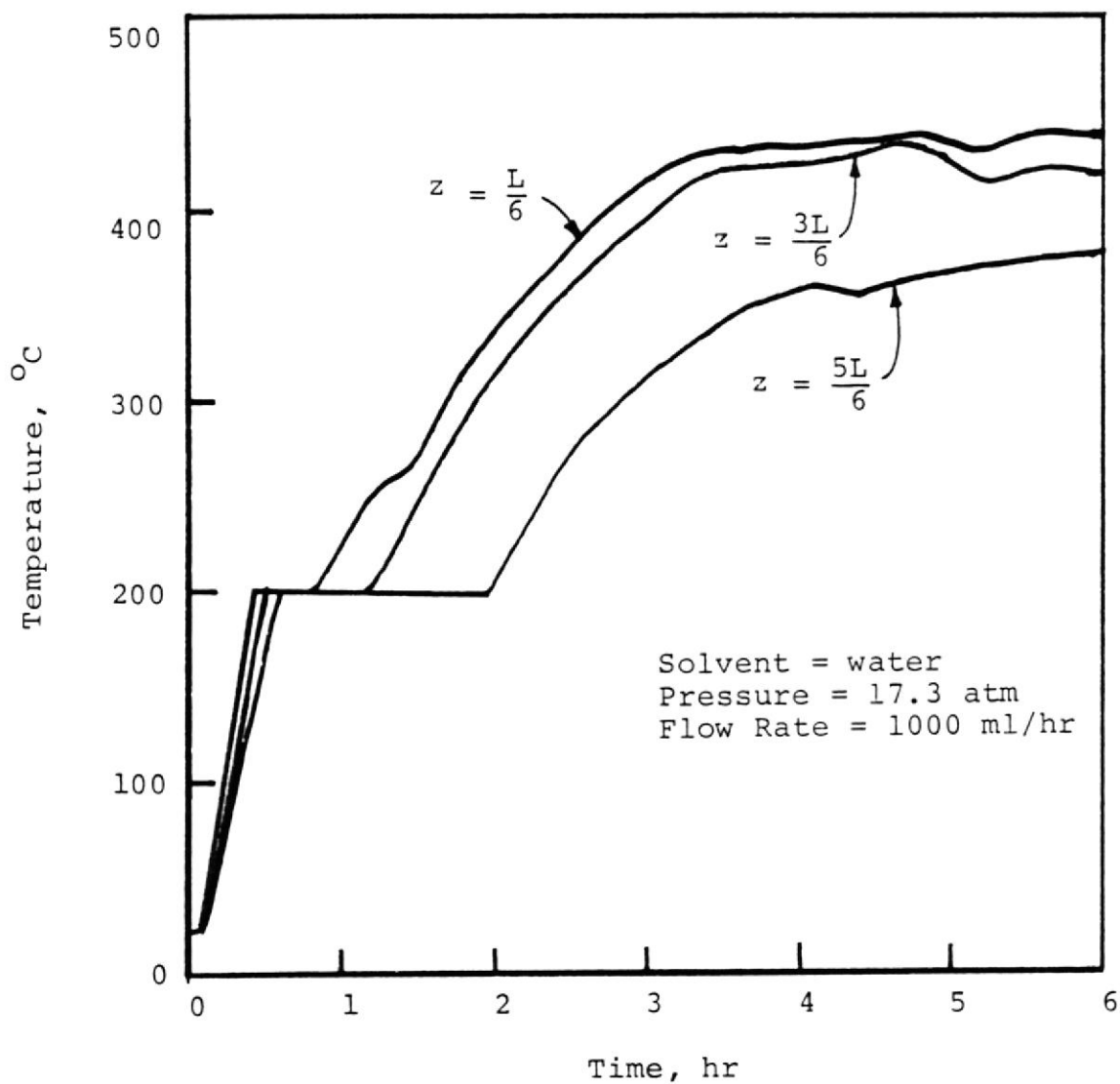


Figure 23. Experimental Temperature Profile for Tubular Reactor Run No. 3 (No external heat on the reactor).

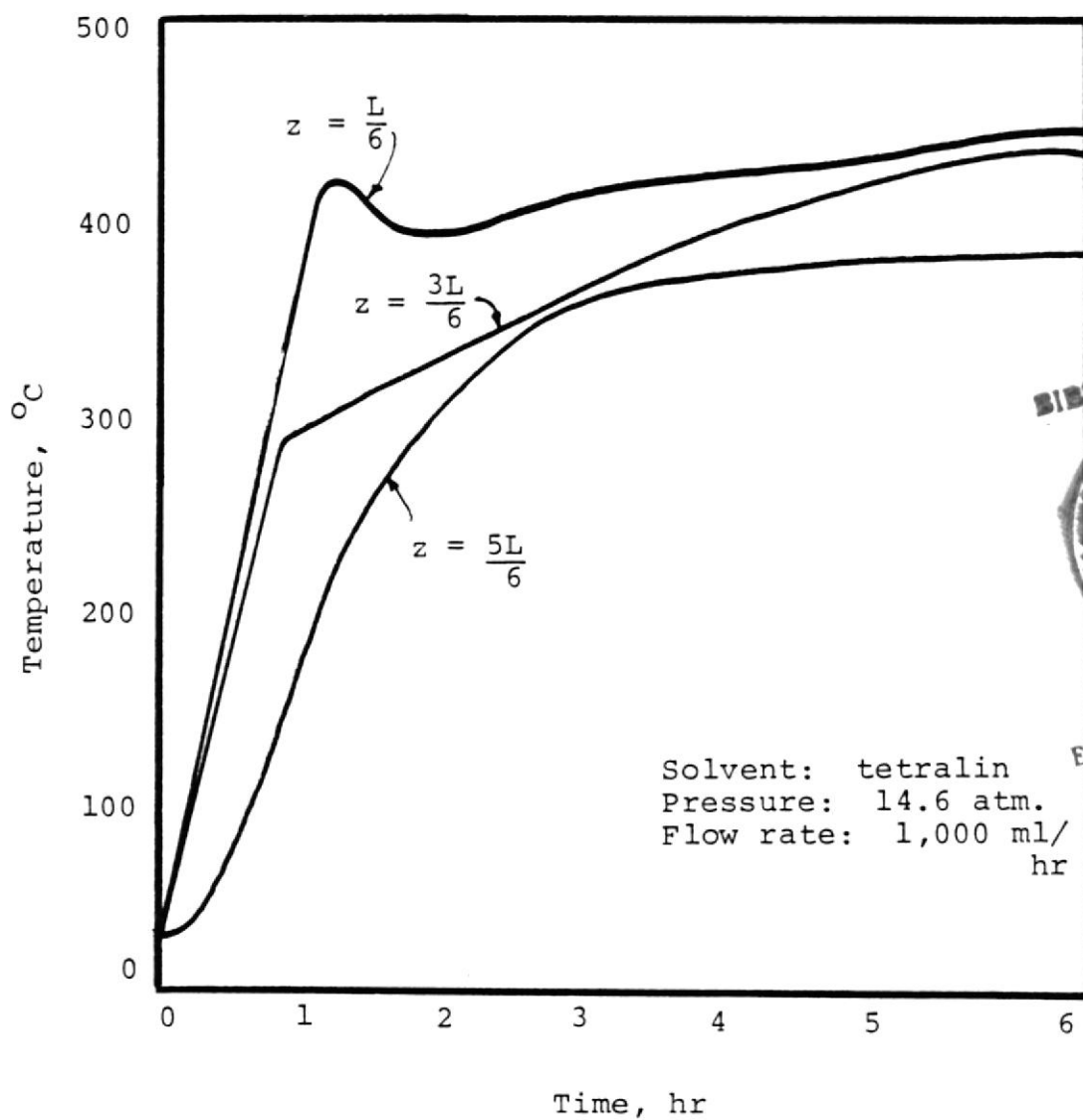


Figure 24: Experimental Temperature Profile for Tubular Reactor Run No. 4 (No external heat on the reactor).

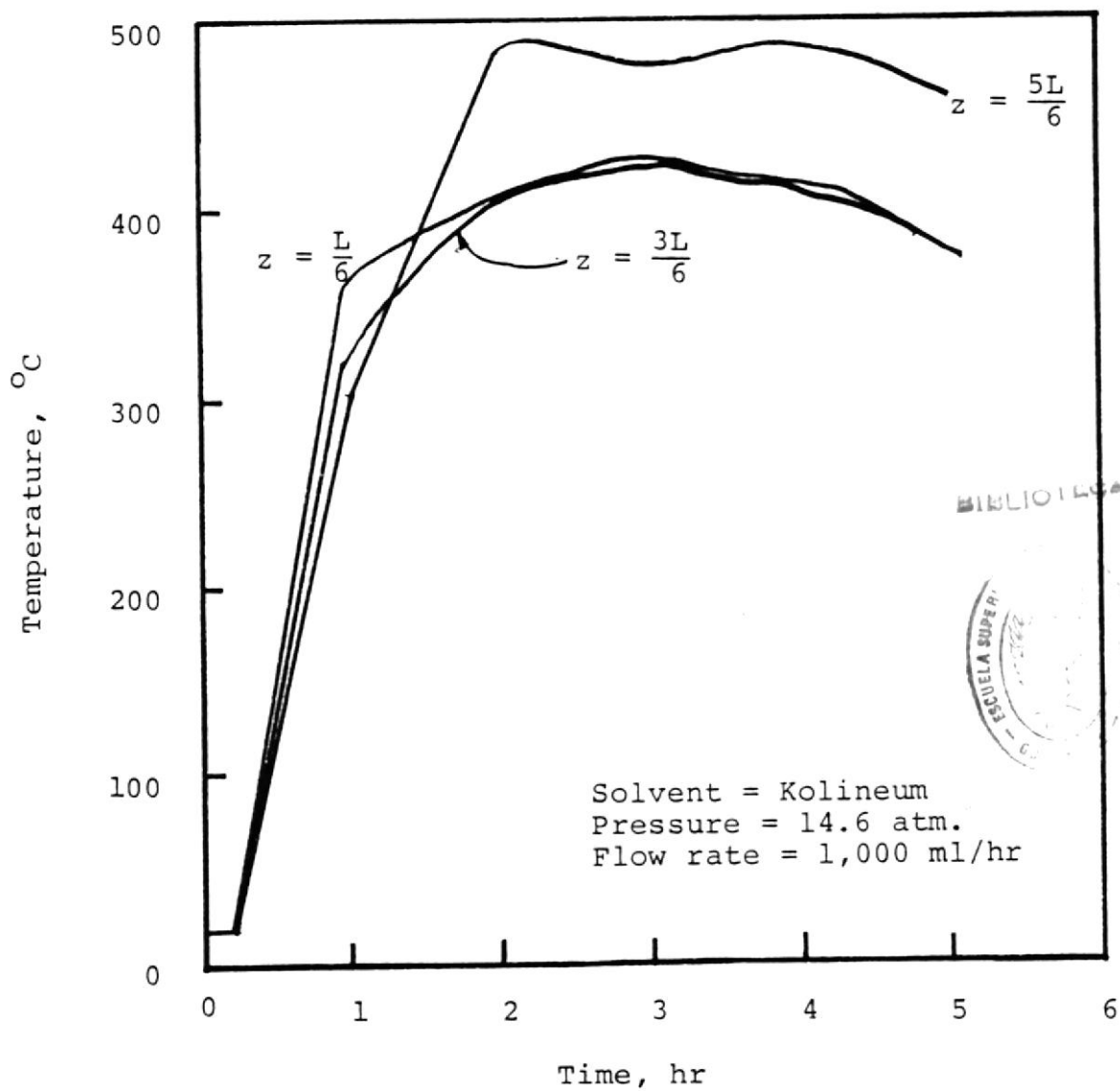


Figure 25. Experimental Temperature Profile for Tubular Reactor Run No. 5, Trial No. 2 (Thermocouple at $z = \frac{5L}{6}$ may be a bad one).

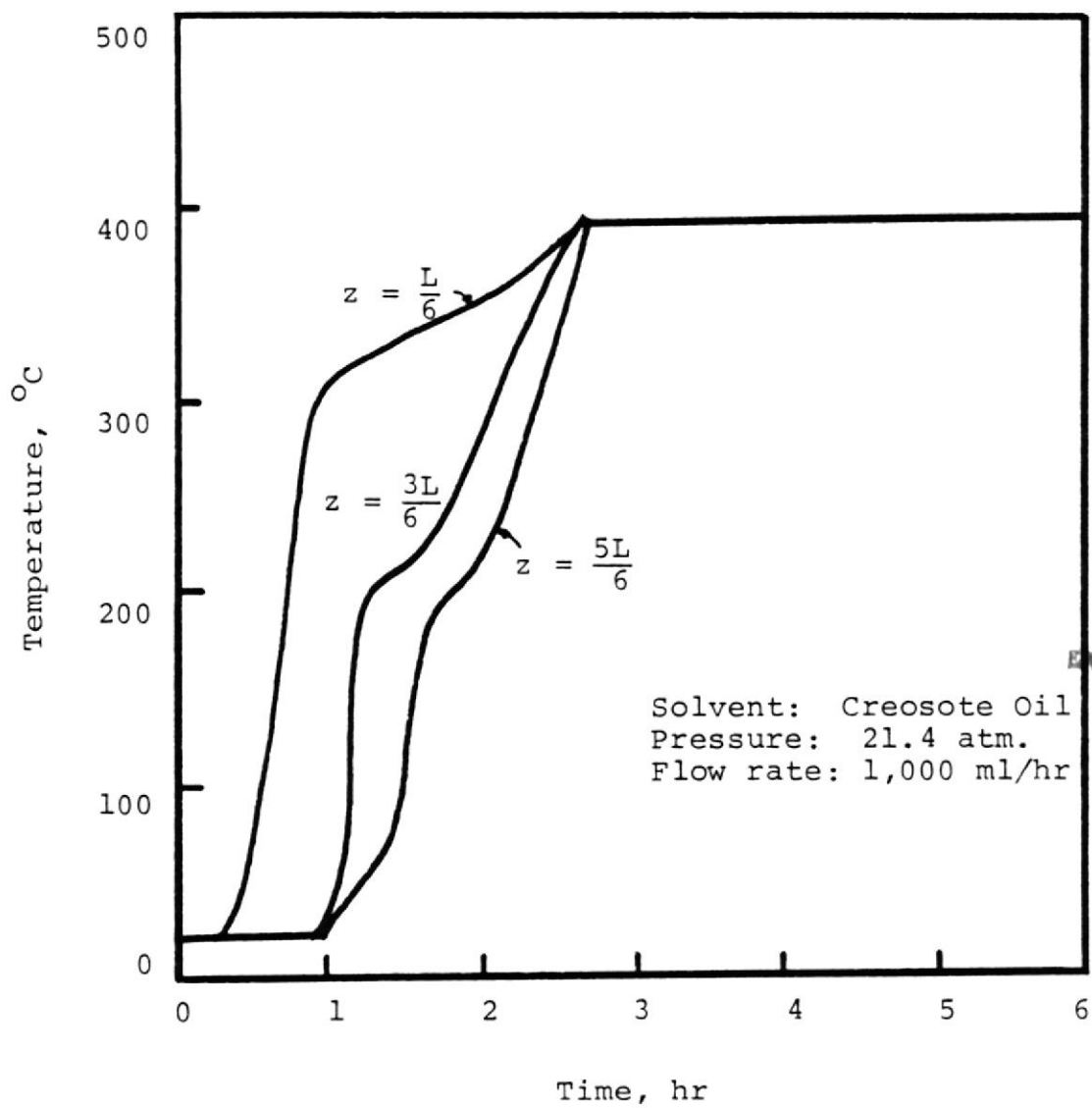


Figure 26. Experimental Temperature Profile for Tubular Reactor Run No. 6.

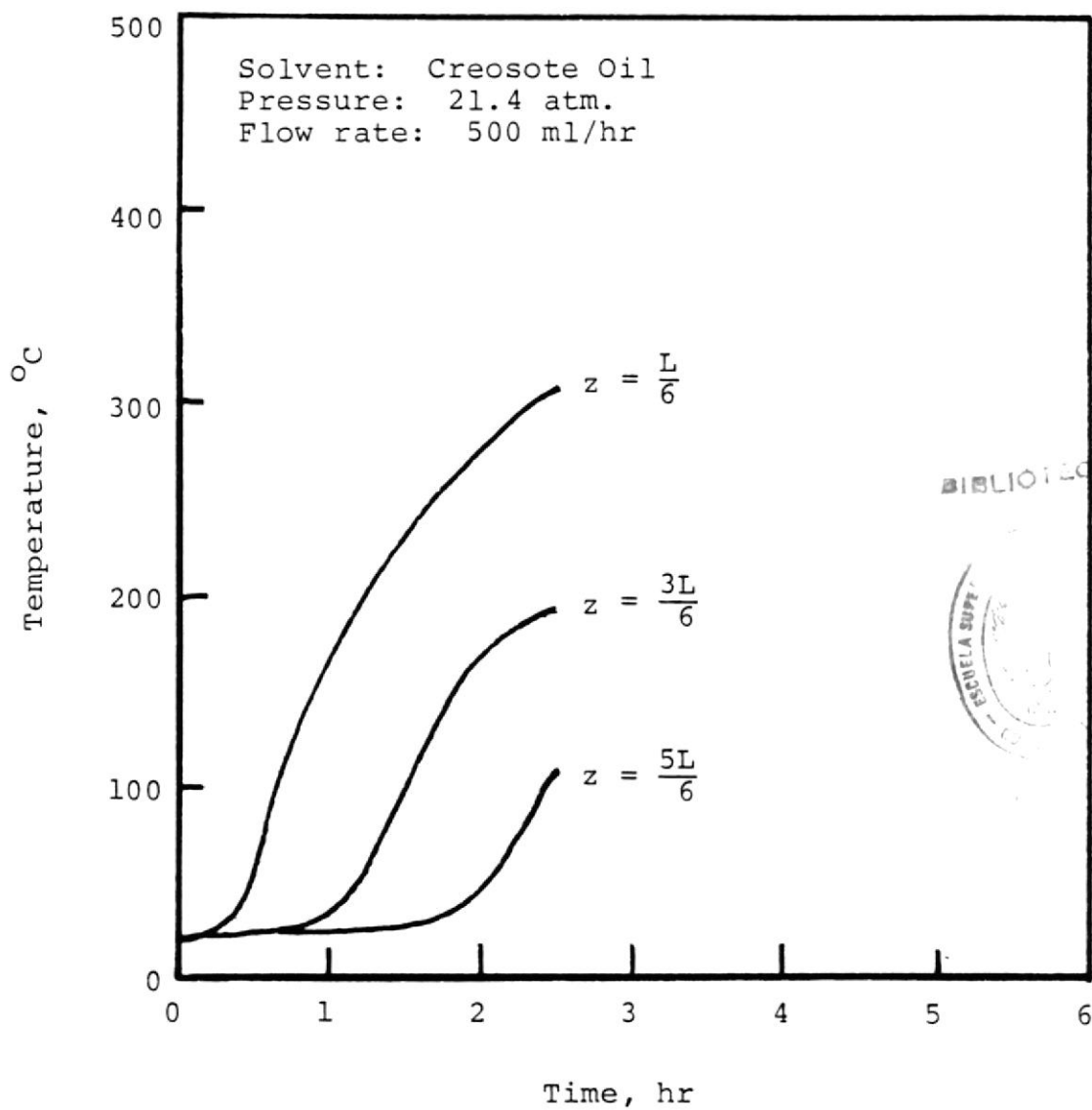


Figure 27. Experimental Temperature Profile for Tubular Reactor Run No. 7.

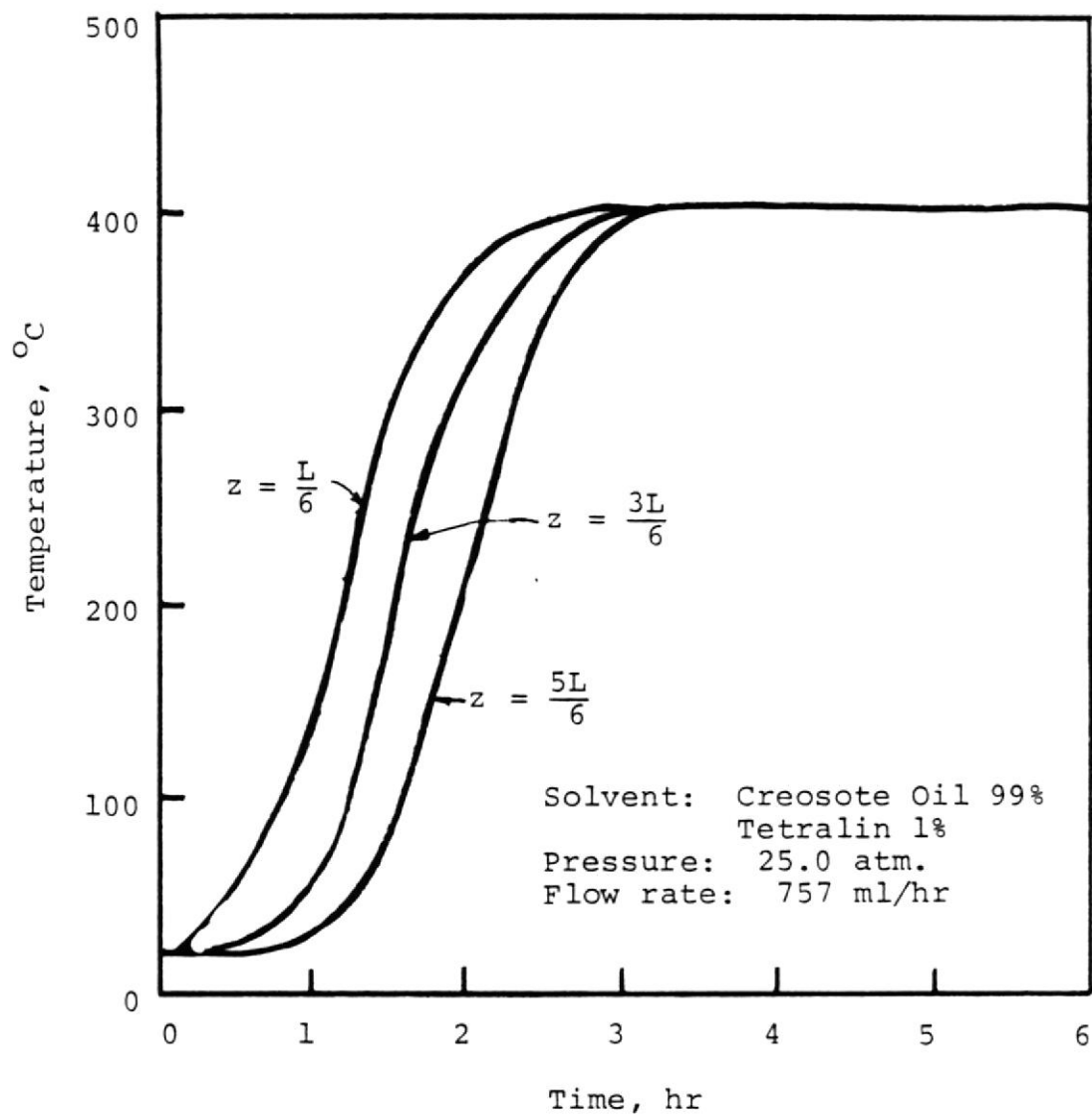


Figure 28. Experimental Temperature Profile for Tubular Reactor Run No. 8, Trial No. 5.

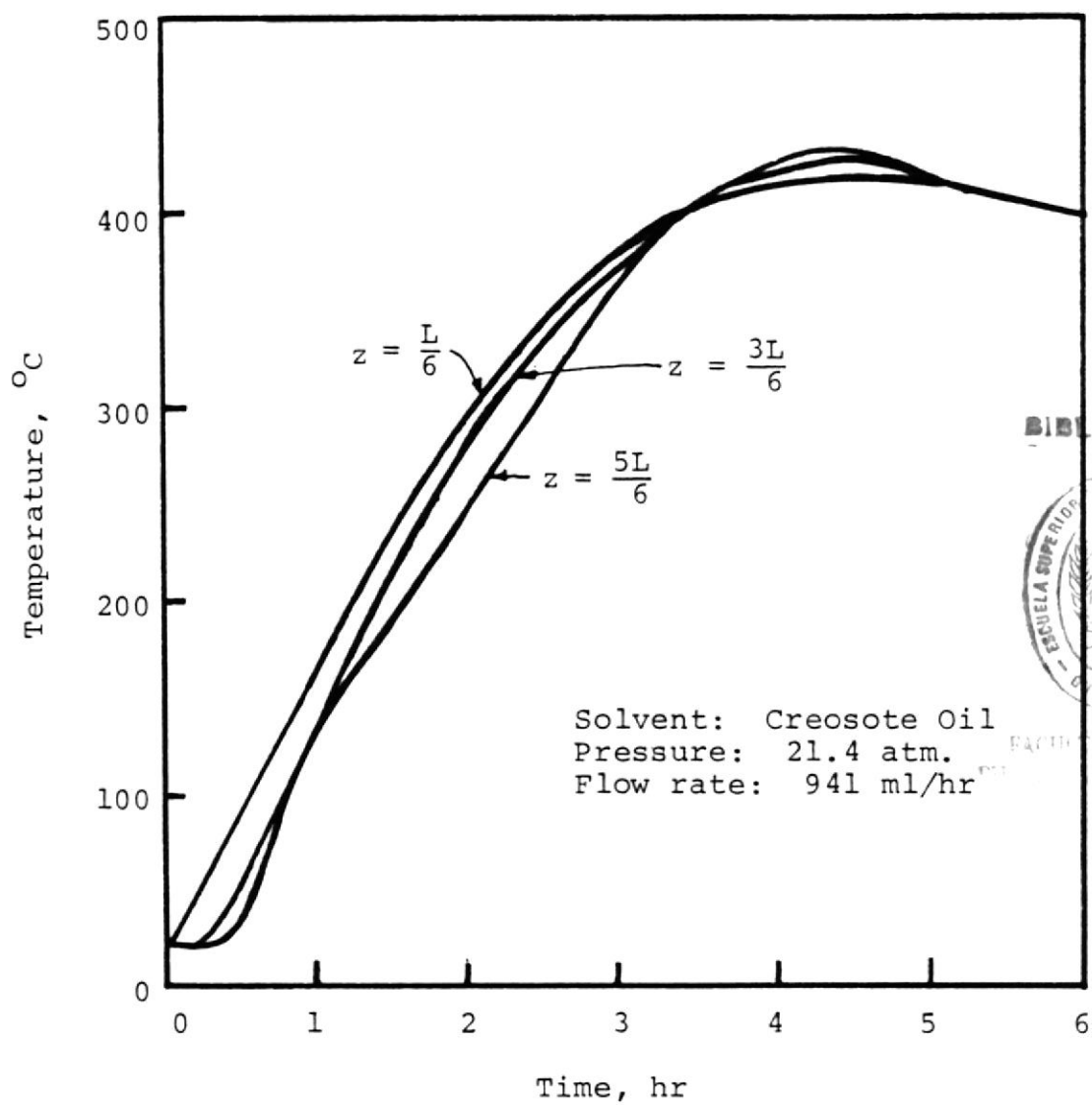


Figure 29. Experimental Temperature Profile for Tubular Reactor Run No. 9.

the water within the lignite.

Run No. 6 and Run No. 9 were conducted under the similar conditions. The only difference in these two runs was the solvent flow pattern. The hot solvent entered the reactor from the top for Run No. 6 while for Run No. 9 the solvent was introduced from the bottom of the reactor. The effect of the flow pattern on the temperature profiles is shown by comparing Figures 26 & 29. Run No. 6 shows a greater temperature gradient at the unsteady state than Run No. 9. A slightly higher conversion was also observed for Run No. 9, but this could be due to the higher final temperature of 425°C versus 400°C . The minibatch experiments showed a substantial effect of temperature on conversion.

Runs Nos. 6 and 9 are the only two runs using the fresh lignite that were completed without interruption. Therefore, these two experiments are treated in more details.

First, the pressures for these runs are shown in Figure 30. Run No. 6 used a back pressure regulator to control the pressure. It is seen from Figure 30 that the relief valve did a better job in giving a steady back pressure. However, the relief valve has a viton gasket which cannot stand a temperature higher than 477K . The pressure curve of Run No. 9 shows the failure of the relief valve. The pressure of the later part of Run No. 9 was controlled by the back pressure regulator.

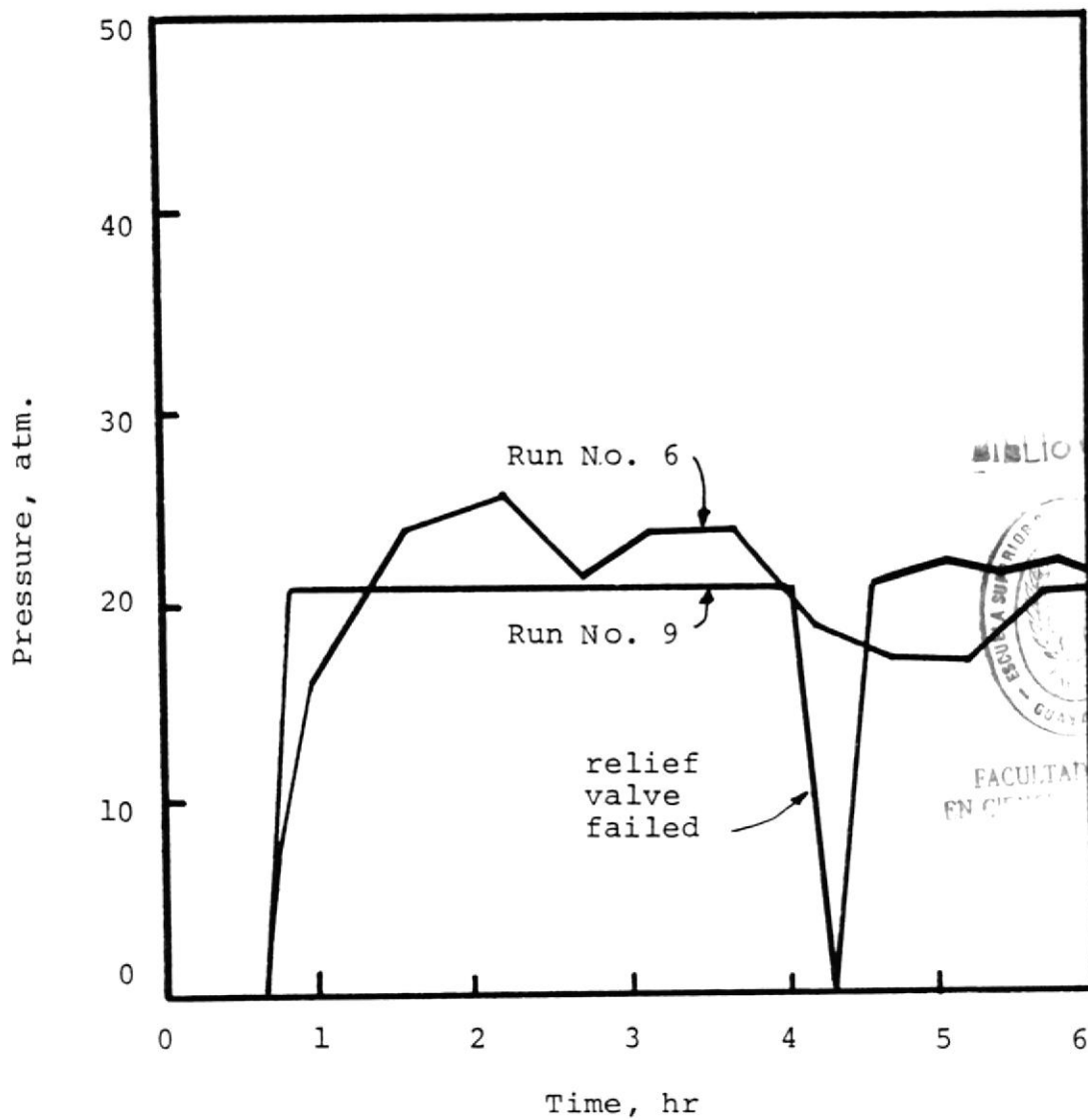


Figure 30. Pressures of the Tubular Reactor Experiments.

The cumulative gas production of Runs No. 6 and 9 are shown in Figure 31. Run No. 9 has higher gas production. This can be explained by the higher reaction temperature of 425°C relative to 400°C. The curves also suggest that a maximum rate of gas production occurs between 2 and 3 hours, which correlates with the rise in temperature. At t=6 hours, even though at a low rate, gas is still being produced.

The compositions of the produced gases are shown in Figures 32 through 35. The major components are carbon dioxide, methane, ethane, hydrogen, carbon monoxide and propane. Other detected components are hydrogen sulfide, ethylene, propylene, n-butane and iso-butane.

The carbon dioxide concentration decreases as the reaction time increases. Methane, ethane and hydrogen show the opposite trend. The increase in the hydrogen concentration is interesting, because it is generally believed that the liquefaction requires hydrogen. The concentration of hydrogen sulfide is important because it represents the sulfur removal rate. The hydrogen sulfide concentration increases during the first 3 hours, then it starts decreasing. By examining the temperature profile, the reactor reaches steady state temperature at about 3 hours. It seems that after the reactor reaches the steady state, the hydrogen sulfide is generated at a lower rate.

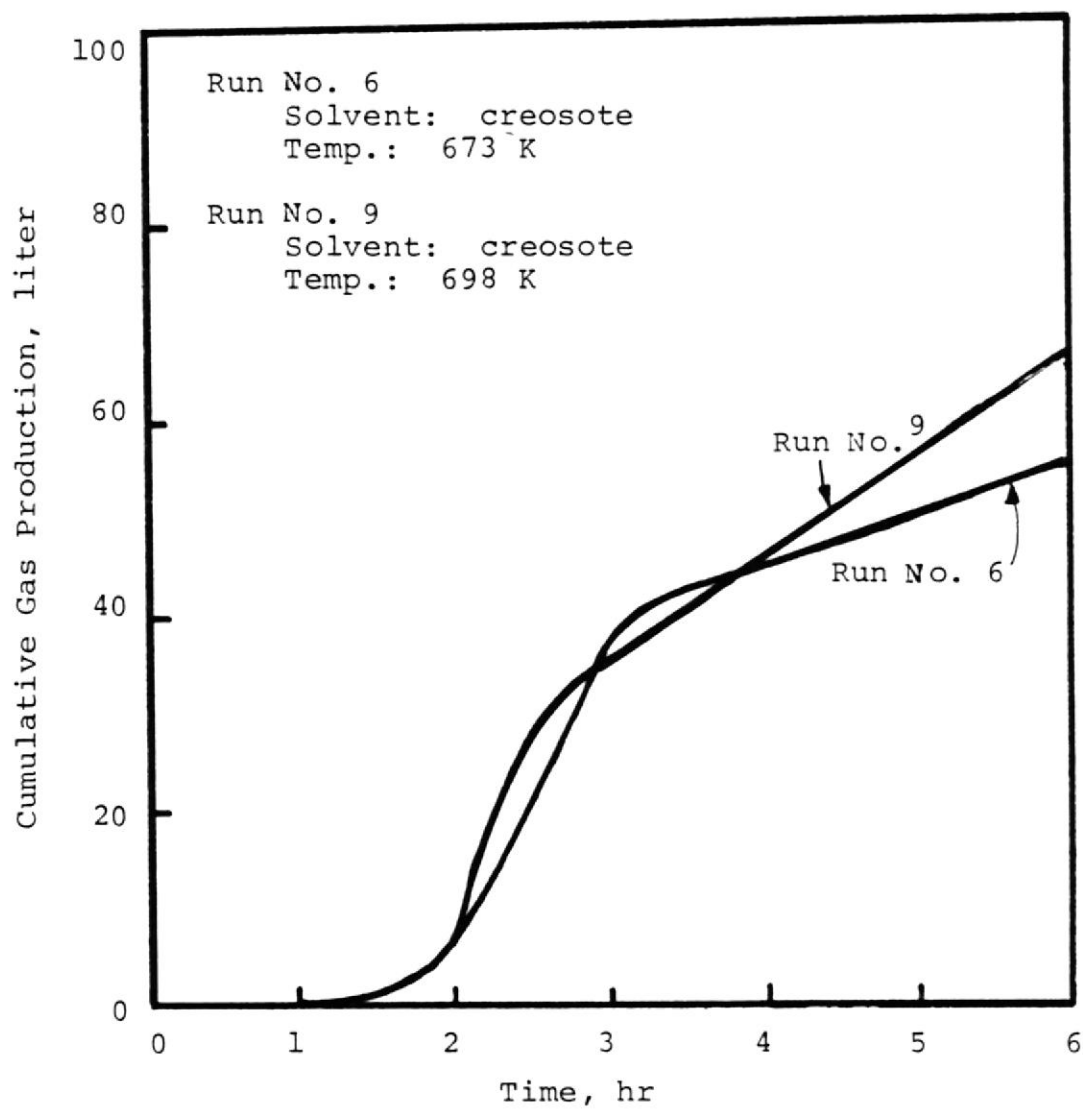


Figure 31. Experimental Gas Productions.

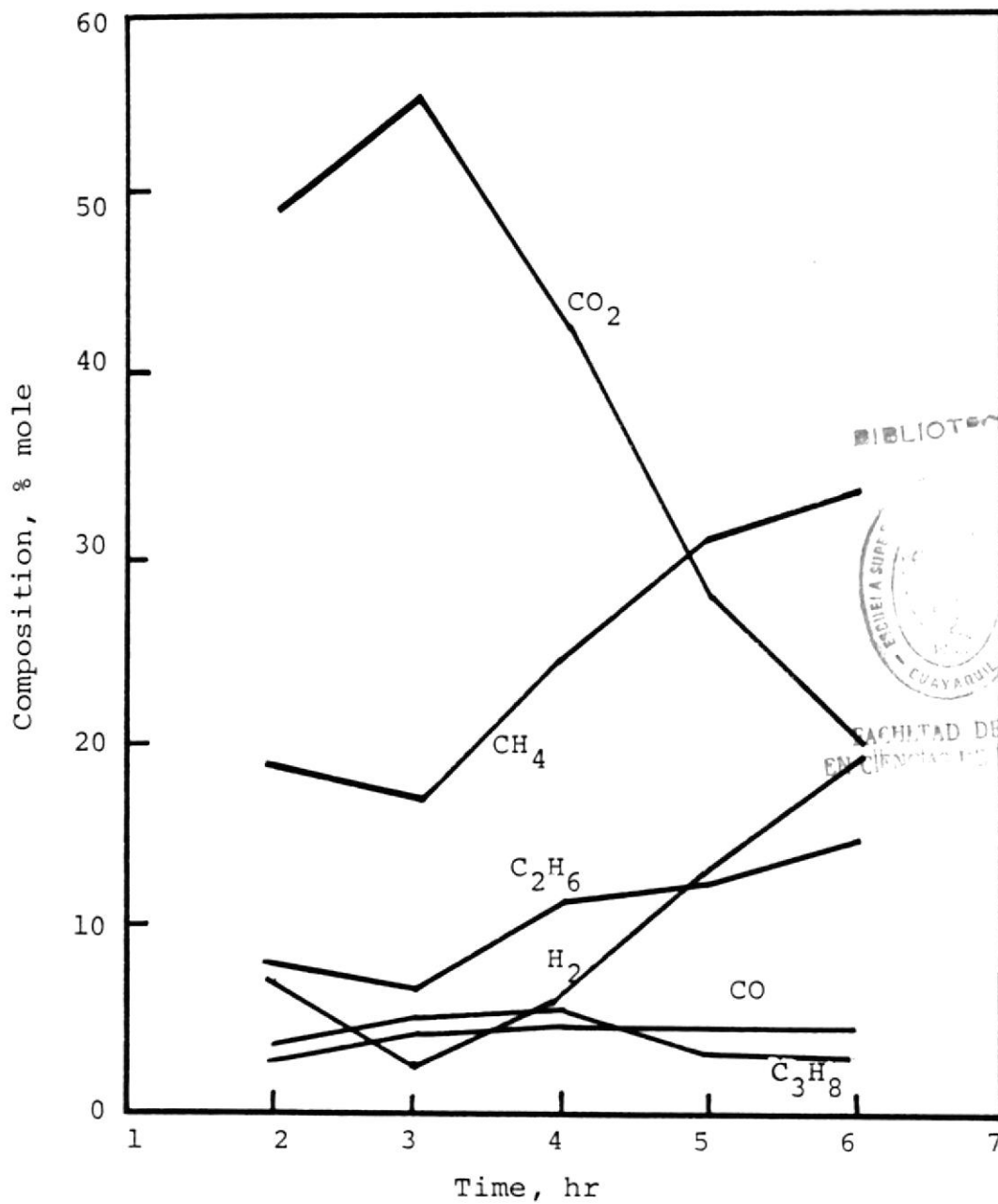
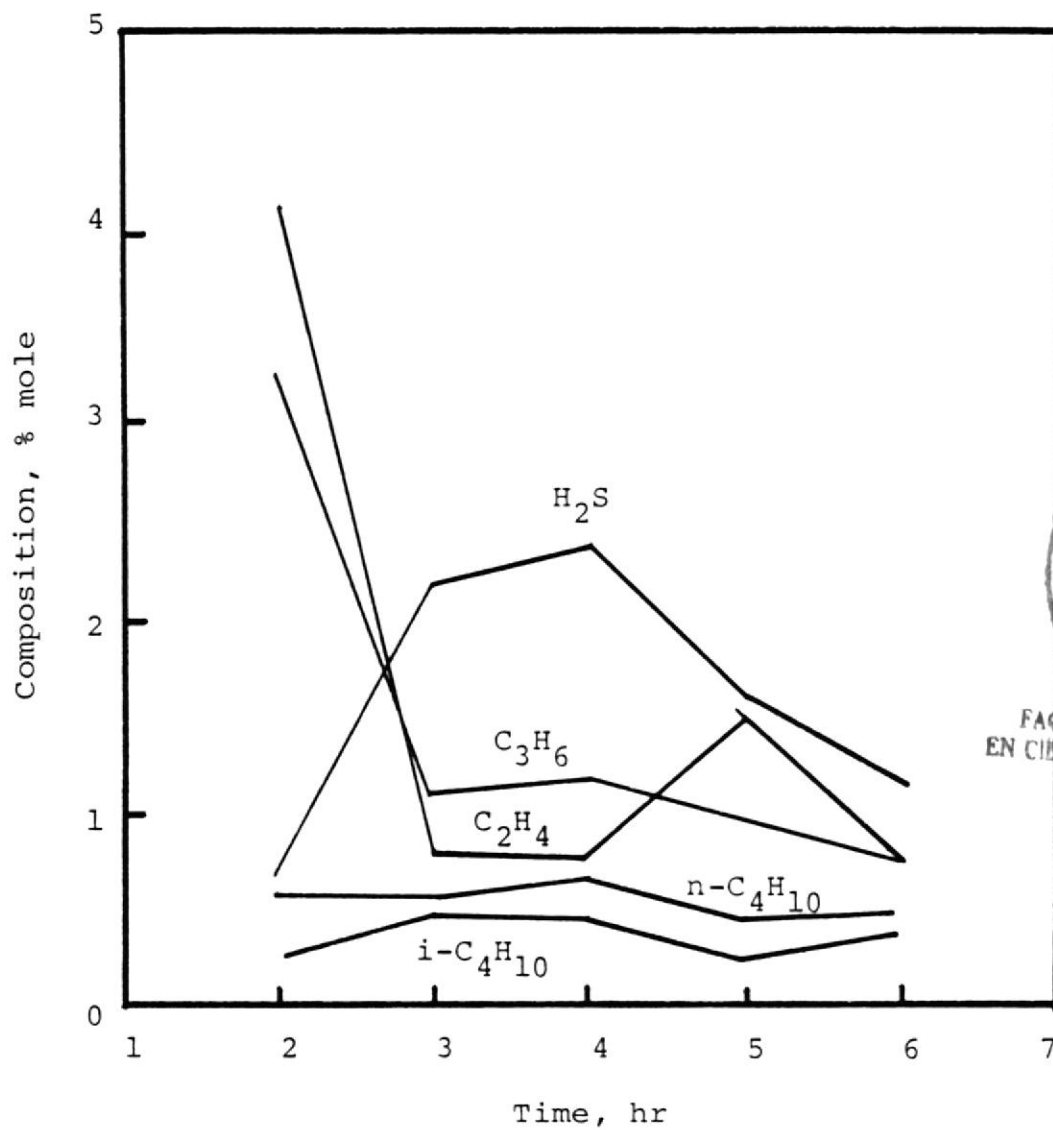


Figure 32. Gas Composition of Tubular Reactor Run No. 6 - Major Components. Solvent: Creosote.



BIBLIOTECA

ESCUELA SUPERIOR DE INGENIERIA

GUAYABUIL

FACULTAD DE ING.
EN CIENCIAS DE LA TIERRA

Figure 33. Gas Composition of Tubular Reactor Run No. 6 - Minor components. Solvent: Creosote.

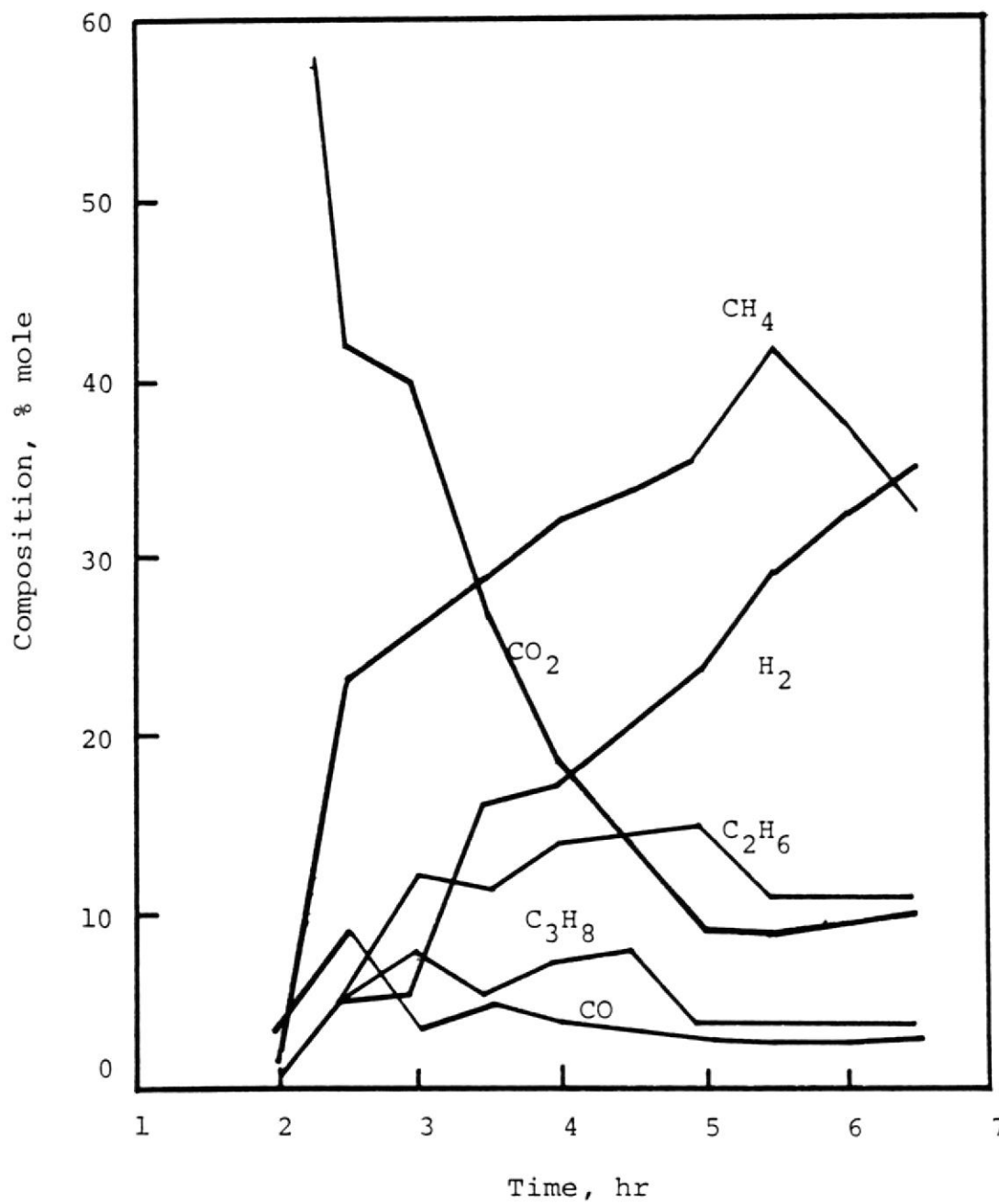


Figure 34. Gas Composition of Tubular Reactor Run No. 9 - Major Components. Solvent: Creosote.

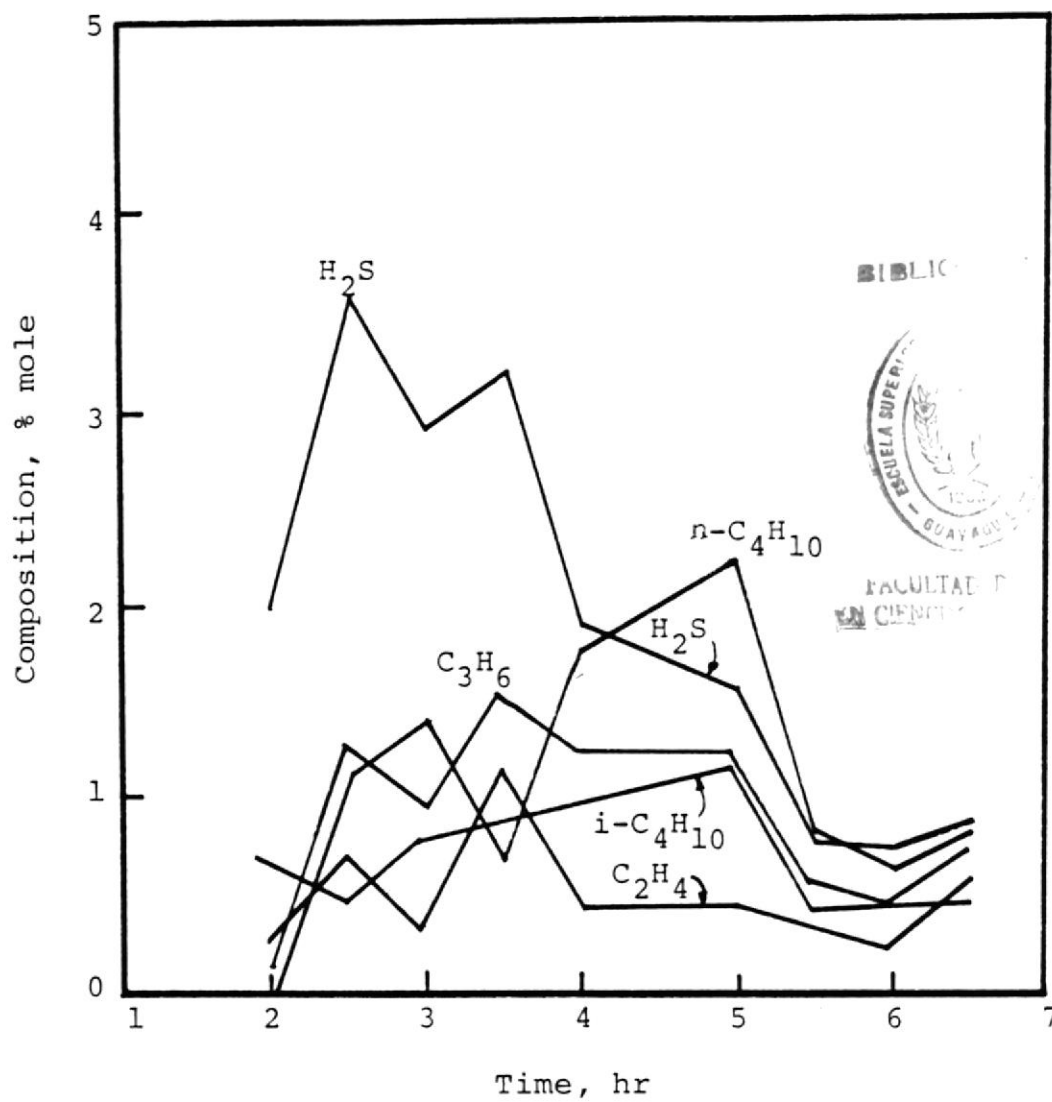


Figure 35. Gas Composition of Tubular Reactor Run No. 9 - Minor Components. Solvent: Creosote.

Concentration of Lignite-derived Liquid

A gel permeation chromatograph (GPC) was used to determine the concentration of the lignite-derived liquid. The GPC, Waters Associate Co. Model ALC/GPC 202, was equipped with a refractometer (Model R401) and a UV detector. Two 100 Å μ -Styragel columns, 7.8 mm I.D. X 300 mm, were used. The carrier solvent was tetrahydrofuran (THF).

The technique for determining the concentration by a GPC is illustrated by the chromatogram shown in Figure 36. For creosote oil, only A_2 appears. When the sample contains creosote oil and lignite-derived liquid, the area becomes $A_1 + A_2$. Apparently, the shaded area, A_1 , is caused by the lignite-derived liquid. Hence, A_1 is correlated with the lignite-derived liquid concentration.

To obtain the relationship between the concentration and the Area A_1 , four samples of different known concentrations were prepared. The samples were then injected into the GPC. As expected, the highest concentration results in the largest A_1 (for creosote $A_1=0$). Since the chromatographic area depends on the GPC system pressure and the type of column used, the absolute relationship between concentration and A_1 is abandoned. Instead, the correlation is placed on a relative basis. In this way, the pressure and column effect can be neglected. The relative (or normalized) concentration is obtained by dividing by the highest concentration. A similar treatment is applied to A_1 .

1873



LIBRARY OF CONGRESS
WASHINGTON, D. C.

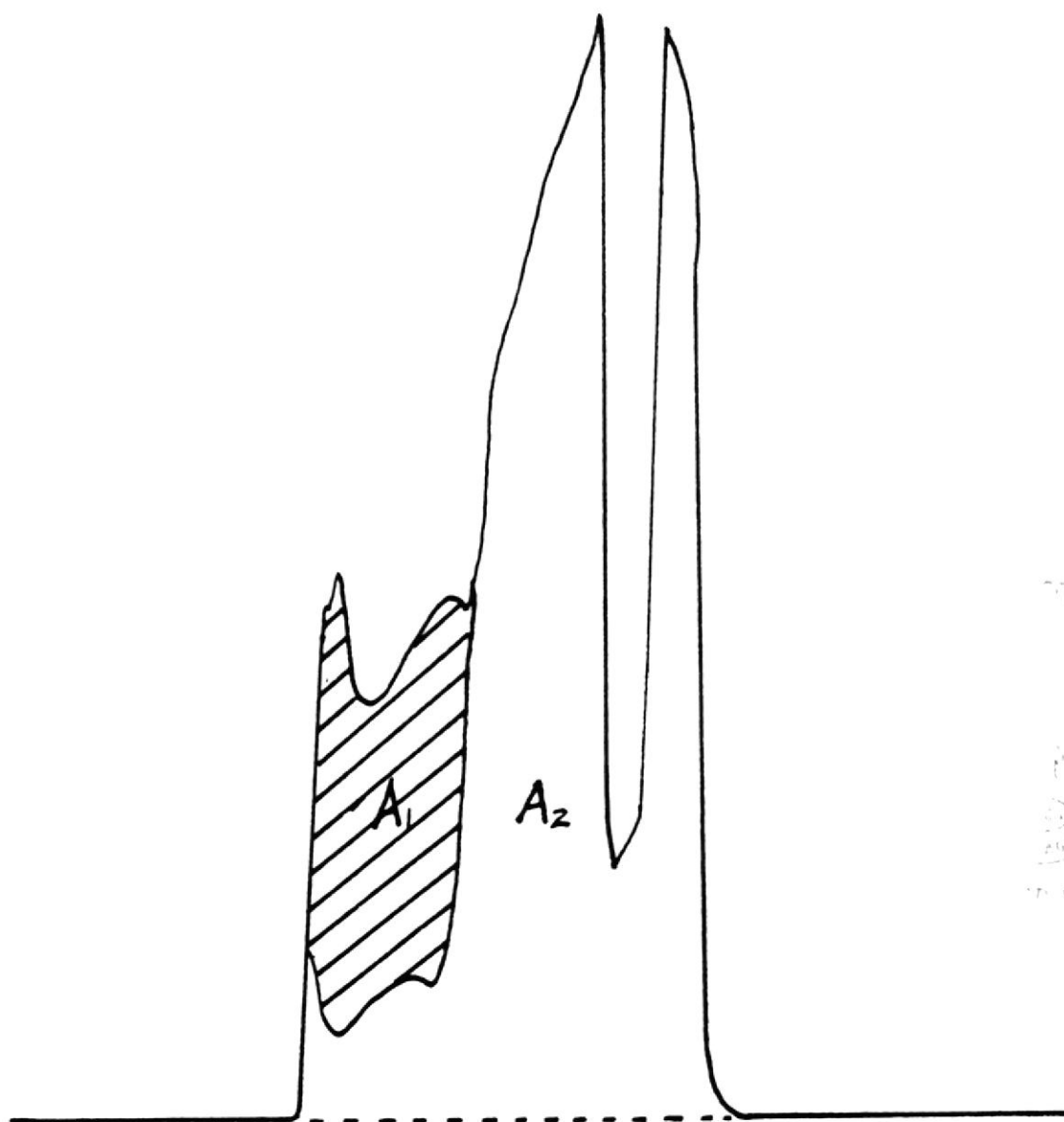


Figure 36. Concentration of Lignite-derived Liquid Analyzed by GPC.

The result is plotted in Figure 37. The conclusion is that there is a linear relation between the concentration and the lignite-derived liquid.

The liquid samples of Run No. 6 were analyzed. The results are listed in Table 10.

This technique allows a rapid monitoring of the rate of conversion of the lignite to liquids.

BIBLIOTECA

FACULTAD DE I
EN CIENCIAS DE LA

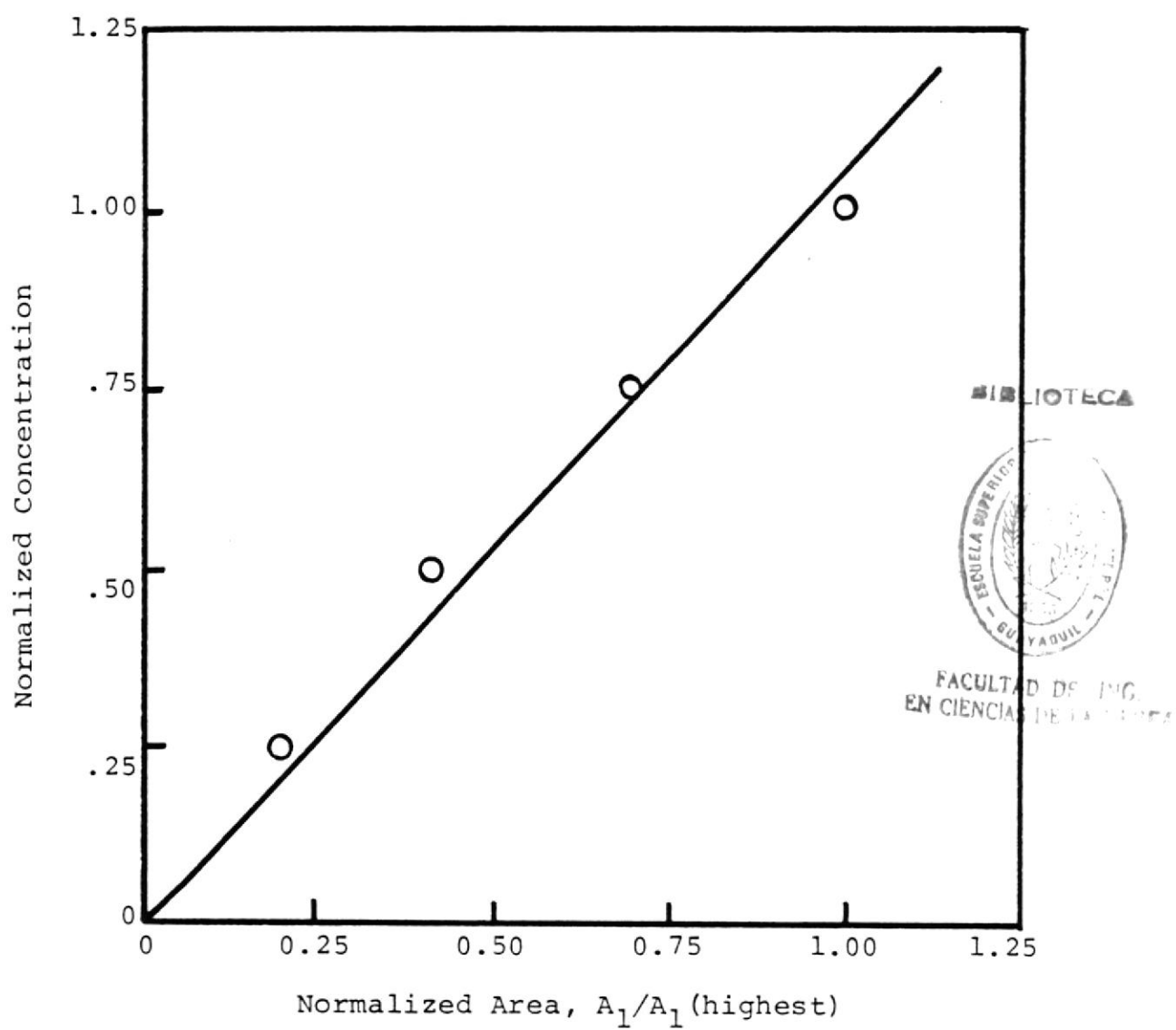


Figure 37. Correlation of Lignite-Derived Liquid Concentration.

TABLE 10. EXPERIMENTAL CONCENTRATION OF THE TUBULAR REACTOR EFFLUENT RUN NO. 6

<u>t (hr)</u>	<u>A₁</u>	<u>Normalized Concentration</u>
2	0.6	0.14
4	4.2	1.00
5	1.6	0.38
6	0.0	0.00

BIBLIO

FACULTAD DE ING.
EN CIENCIAS DE LA TIE.

CHAPTER VI
KINETIC MODELING

Equilibrium Conversion

The pressure effects on conversion are shown in Figure 11 and 12. The figures were plotted using data of 400°C and 1 hour in Table 3. With both the reaction temperature and time being kept constant, the pressure becomes the only variable.

Figure 11 also reveals that the effectiveness of the solvent has the order: tetralin > SRC > creosote oil. However, for the gas production, the reverse is true as can be seen from Figure 12.

Many equations can be used to describe the curves in the figures. However, the equation with some theoretical background, even though it may suffer in goodness of fit to the data, is the best choice. The reason is that a theoretically derived equation offers the best chance of success to extrapolate the equation to a region of conditions not experimentally explored. Extrapolation of a purely empirical equation is never safe.

For the lignite liquefaction, 1 hour is long enough to reach the equilibrium conversion. Therefore, the figures are actually showing the pressure effect on the equilibrium conversions.

On the basis of thermodynamic first and second laws,

the pressure effect on the equilibrium conversion can be expressed as (Denbigh 1971):

$$\left(\frac{\partial \ln X_e}{\partial P} \right)_T = \frac{-\Delta v}{R_1 T} \quad (5)$$

Where R_1 = gas constant

Δv = a characteristic difference in volumes of the products and of the reactants.

Equation (5) is a general expression for equilibrium, and X_e can be other equilibrium quantities such as the vapor pressure of a liquid, the solubility of a solid, or the equilibrium constant of a reaction. In this case, X is either the lignite conversion, X_ℓ , or the conversion of lignite to gas, X_g .

The data from Table 3 with pressures between 30 atm to 36 atm and 1 hour reaction time were plotted in Figure 13 and Figure 14. These figures show that both X_ℓ and X_g are increased with increasing temperature.

For 1 hour reaction time, these curves are considered to be the equilibrium conversions. The temperature effect can be written as (Denbigh 1971):

$$\left(\frac{\partial \ln X_e}{\partial T} \right)_P = \frac{\Delta h}{R_2 T^2} \quad (6)$$

Where R_2 = gas constant

Δh = a characteristic difference in the energy of the products and the reactants

The equilibrium conversion, X_e , is a function of pressure and temperature. The relationship can be obtained by integrating Equation (5) and Equation (6).

The integration of Equation (5) is from P_0 to P at a constant temperature, T_0 . The integration of Equation (6) is from T_0 to T at a constant pressure, P . The results of the integrations for constant Δv and Δh are:

$$\ln \left(\frac{X_{e1}}{X_{eo}} \right) = \frac{-\Delta v}{R_1 T_0} (P - P_0) \quad (7)$$

$$\ln \left(\frac{X_e}{X_{e1}} \right) = \frac{-\Delta h}{R_2} \left(\frac{1}{T} - \frac{1}{T_0} \right) \quad (8)$$

X_{eo} , X_{e1} , and X_e are equilibrium conversion at (P_0, T_0) , (P, T_0) and (P, T) respectively. Because the equilibrium conversion is a state function, X_{e1} should have the same value in both equations. Furthermore, X_{e1} can be eliminated by adding the above equations to obtain

$$\ln \left(\frac{X_e}{X_{eo}} \right) = \frac{-\Delta v}{R_1 T_0} (P - P_0) - \frac{\Delta h}{R_2} \left(\frac{1}{T} - \frac{1}{T_0} \right) \quad (9)$$

or to express in another form:

$$X_e = X_{eo} \exp \left[\frac{-\Delta v}{R_1 T_0} (P - P_0) - \frac{\Delta h}{R_2} \left(\frac{1}{T} - \frac{1}{T_0} \right) \right] \quad (10)$$

Equation (10) is the equilibrium equation which is used to calculate the equilibrium conversion, X_e , at a given set of conditions, (P, T) , providing that X_{ep} is known at (P_0, T_0) .

Rate Equation

Let the rate equation be written as:



FACULTAD DE INGENIERIA
EN QUIMICA

$$\frac{dX}{dt} = k (X_e - X) \quad (11)$$

Where X is the MAF conversion based on THF solubles. X_e , the equilibrium conversion, is expressed by Equation (10). X_e is a function of pressure, temperature and the type of lignite. The rate constant is k . A similar rate expression was proposed by Wen and Han (1975). Equation (11) can be integrated to become:

$$X = X_e \left[1 - \exp(-kt) \right] \quad (12)$$

The rate constant, k , follows the Arrhenius type relation, i.e.:

$$k = k_o \exp \left(-E/R_2T \right) \quad (13)$$

By substituting Equation (10) and Equation (13) into Equation (12) yields a rate equation with five parameters-- X_{e0} , Δv , Δh , k_o , and E . These parameters are to be determined by the data in Table 3 and by a Statistical Analysis System (SAS) non-linear regression program. The statistical result shows that there is a strong correlation, (>0.99), between k_o and E . The estimated E carries a large error and the confidence interval spans from negative to positive (Appendix E). These results lead to the conclusion that E equals zero. Hence k becomes a constant and is not a function of temperature. Physically, this suggests that k is a mass transfer coefficient and the lignite liquefaction under the conditions studied is controlled by mass transfer.

By substituting Equation (10) into Equation (12) the rate equation can be expressed as:

$$X = X_{eo} \exp \left[\frac{-\Delta v}{R_1 T_0} (P - P_0) - \frac{\Delta h}{R_2} \left(\frac{1}{T} - \frac{1}{T_0} \right) \right] X \quad (14)$$

$$[1 - \exp(-kt)]$$

where: $R_1 = 0.082 \text{ \AA atm/g-mole K}$
 $R_2 = 8.314 \times 10^{-3} \text{ KJ/g-mole}$
 $P_0 = 32 \text{ atm}$
 $T_0 = 673 \text{ K}$

Results and Discussion of Kinetic Models

The parameters were determined by using the data in Table 3 and a non-linear regression SAS program. They are listed in Table 11 for each solvent.

TABLE 11. ESTIMATED PARAMETERS*				
<u>Solvent</u>	<u>X_{eo}</u>	<u>Δv (ℓ/mol)</u>	<u>Δh (KJ/mol)</u>	<u>k (hr⁻¹)</u>
A. For the conversion of lignite				
Tetralin	0.65	-0.145	37.8	4.47
SRC	0.55	-0.124	28.9	6.18
Creosote	0.34	-0.265	32.2	11.77
B. For the conversion of lignite to gas				
Tetralin	0.070	-0.028	23.8	4.28
SRC	0.096	0.238	47.5	3.52
Creosote	0.086	0.035	19.9	4.51
* Data of X _g for creosote oil at 698K were not used.				

In Table 11, X_{eo} is the equilibrium conversion at the reference state - 32 atm and 673 K. The value of X_{eo} is an indication of the effectiveness of the solvent. For the conversion of lignite, tetralin appears to be the best

solvent, followed by SRC and creosote oil. For the amount of gas generated during the liquefaction, the order becomes SRC > creosote oil > tetralin.

The value of Δv represents the effect of pressure on the conversion. A negative Δv means that a higher pressure yields a greater conversion. A positive value means the opposite. The magnitude of the pressure effect can be also measured by Δv as it is proportional to the absolute value of Δv . The values in Table 11 suggest that the lignite conversion increases with the increasing pressure. For the conversion of lignite to gas, the same statement is true only when tetralin is the solvent. When SRC or creosote oil is the solvent, increasing the pressure will result in a small value of X_g .

The temperature effect on X_e is expressed by the value of Δh . Positive values of Δh in Table 11 indicate that the conversion increases with increasing temperature regardless of solvent and that the magnitude of the effect is proportional to the magnitude of Δh . The rate constant, k , appears to increase as X_{e0} decreases.

Equation (14) and Table 11 are used to predict the conversion at given pressure, temperature, and time. The predicted conversions, the errors and the conditions are listed in Table 12.

The errors in model predictions can also be shown

TABLE 12. PREDICTED CONVERSIONS AND ERRORS

Run	P (atm)	T (K)	t (hr)	\hat{X}_l	$\xi_l(\%)$	\hat{X}_g	ξ_g
A. Tetralin							
T1	29.57	673	0.25	0.435	-6.7	0.046	-17.6
T2	30.59	673	0.50	0.579	-7.5	---	---
T3	31.61	673	0.75	0.627	-0.6	---	---
T4	32.63	673	1.00	0.644	-3.1	0.067	-8.1
T5	45.90	673	1.00	0.667	1.4	0.069	19.7
T6	65.29	673	1.00	0.702	6.2	0.070	-14.9
T7	130.59	673	1.00	0.834	-2.4	0.073	2.8
T8	24.18	648	0.25	---	---	---	---
T9	25.49	648	1.00	0.487	-8.1	0.059	-9.6
T10	35.69	648	1.00	0.501	7.1	0.059	-30.5
T11	49.98	648	1.00	0.520	5.8	0.059	2.7
T12	30.93	648	1.00	0.494	1.7	0.059	8.9
T13	33.65	648	0.75	0.486	-1.7	0.057	6.5
T14	32.29	648	0.50	0.448	-3.0	0.053	12.1
T15	32.97	648	0.25	0.338	6.4	0.039	22.4
T16	35.01	698	0.25	0.563	5.8	0.053	-3.2
T17	34.67	698	0.50	0.746	1.1	---	---
T18	35.69	698	0.75	0.808	-1.1	---	---

$$\bar{\xi}_l = 4.1$$

$$\bar{\xi}_g = 12.2$$

TABLE 12. (continued)

<u>Run</u>	<u>P (atm)</u>	<u>T (k)</u>	<u>t (hr)</u>	<u>\hat{X}_l</u>	<u>ξ (%)</u>	<u>\hat{X}_g</u>	<u>ξ_g (%)</u>
B. SRC recycled solvent							
S1	21.41	673	1.00	---	---	0.097	-9.4
S2	33.56	673	1.00	0.550	1.2	0.092	-7.7
S3	52.02	673	1.00	0.573	-0.1	0.085	-3.7
S4	70.39	673	1.00	0.598	0.2	0.079	-2.1
S5	35.01	673	0.75	0.548	-2.7	0.088	0.4
S6	32.63	673	0.50	---	---	0.079	1.4
S7	31.61	673	0.25	0.432	2.4	0.056	-5.4
S8	34.33	648	0.25	0.356	-2.0	0.040	7.8
S9	33.65	648	0.50	0.431	-1.2	0.057	13.0
S10	32.29	648	1.00	0.451	3.6	0.067	9.3
S11	31.61	648	0.75	0.445	-1.5	---	---
S12	32.63	698	1.00	---	---	0.125	9.3
S13	32.63	698	0.50	---	---	0.107	-3.7
S14	34.33	698	0.25	0.523	-0.1	---	---
					$\bar{\xi}_l = 1.5$		
						$\bar{\xi}_g = 6.1$	

TABLE 12. (continued)

Run	P (atm)	T (K)	t (hr)	\hat{X}_ℓ	$\bar{\epsilon}_\ell$ (%)	\hat{X}_g	$\bar{\epsilon}_g$ (%)
C. Creosote Oil							
C1	30.93	673	1.00	---	---	0.085	3.8
C2	44.88	673	1.00	0.368	0.1	0.084	1.1
C3	69.71	673	1.00	0.414	2.9	0.083	-0.9
C4	31.61	673	0.75	---	---	---	---
C5	29.57	673	0.50	0.340	-1.3	0.077	0.2
C6	28.21	673	0.25	0.321	9.9	0.058	-8.8
C7	34.67	648	0.25	0.266	1.3	0.050	1.1
C8	35.69	648	0.25	0.269	-13.1	0.050	11.1
C9	30.25	648	1.00	0.274	14.4	---	---
C10	33.65	648	0.50	0.279	-9.2	0.069	2.7
C11	33.65	648	0.75	0.279	-2.5	0.072	-8.4
C12	27.53	698	1.00	0.415	5.0	---	---
C13	34.33	698	0.25	0.407	-0.1	---	---
C14	35.69	698	0.50	0.431	-5.8	---	---
C15	34.33	698	1.00	0.429	-2.1	---	---
C16	32.29	698	0.75	0.425	-0.5	---	---

$$\bar{\epsilon}_\ell = 4.9$$

$$\bar{\epsilon}_g = 4.2$$

* \hat{X} = predicted conversion

** ϵ = percent error = $[(X - \hat{X}) / \hat{X}] \times 100$

*** $\bar{\epsilon}$ = average error = $\frac{1}{N} \sum_{i=1}^N |\epsilon_i|$

by a scatter plot as illustrated by Figure 38 and Figure 39. An exact model will have all points on the 45° line. The deviation from the line is an indication of the error.

The reaction times for the tubular reactor experiments are long enough to reach equilibrium conversion. The experimental results and the results calculated from Equation (10) are shown in Table 13. Only three runs are listed in Table 13; the other experiments are not listed because of the difficulties encountered during the experiments. The difficulties make the interpretation of the experimental result extremely difficult.

Table 13 shows that the experimental lignite conversions, X_{ℓ} , are always lower than the predicted conversions, \hat{X}_{ℓ} . However, the reverse is true for X_g . The large value obtained for experimental conversion, X_g , could be caused by the decomposition of the creosote oil. The creosote could be decomposing as a result of high temperature in the preheater.

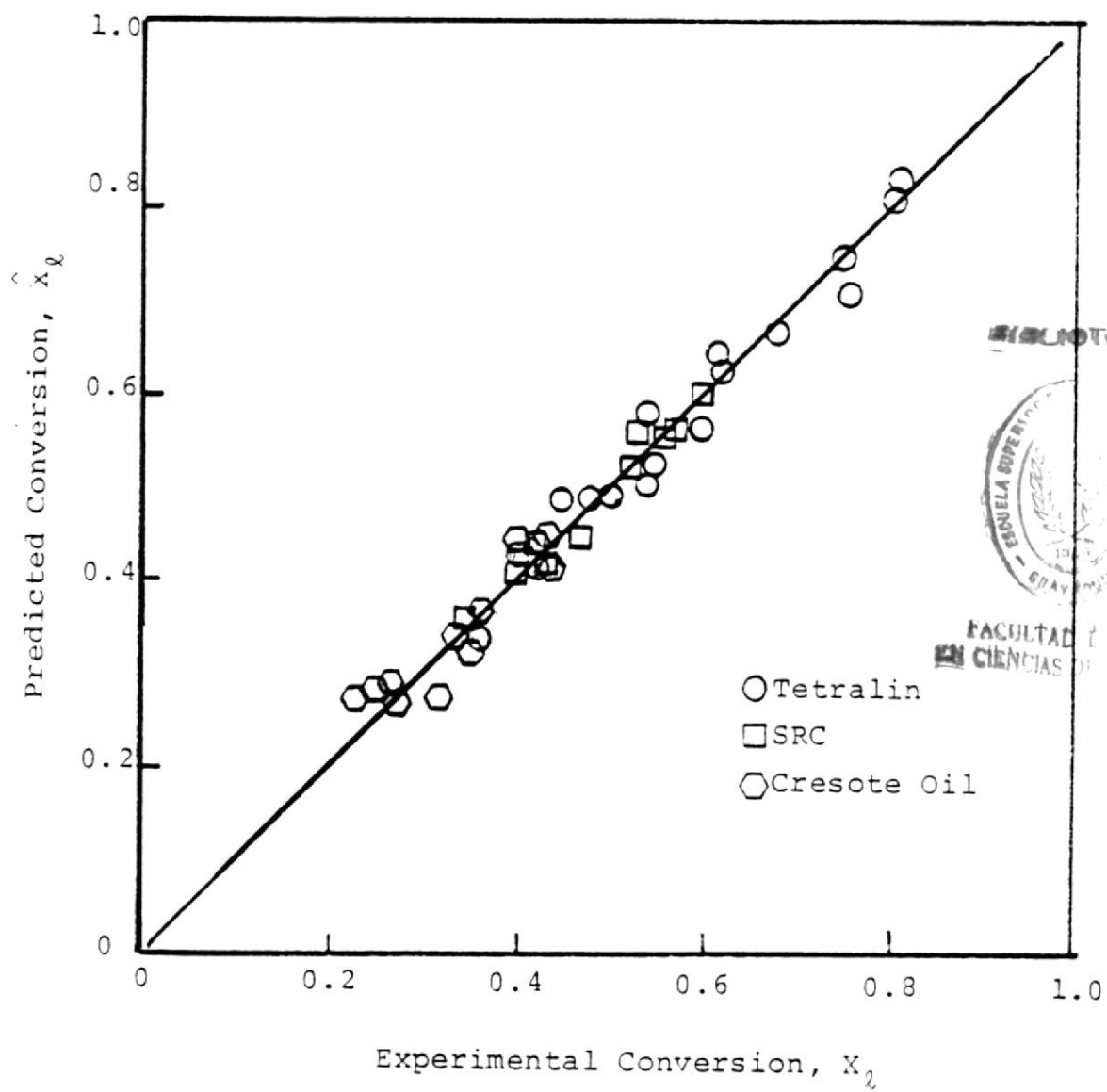


Figure 38. Scatter Plot of Lignite Conversion.

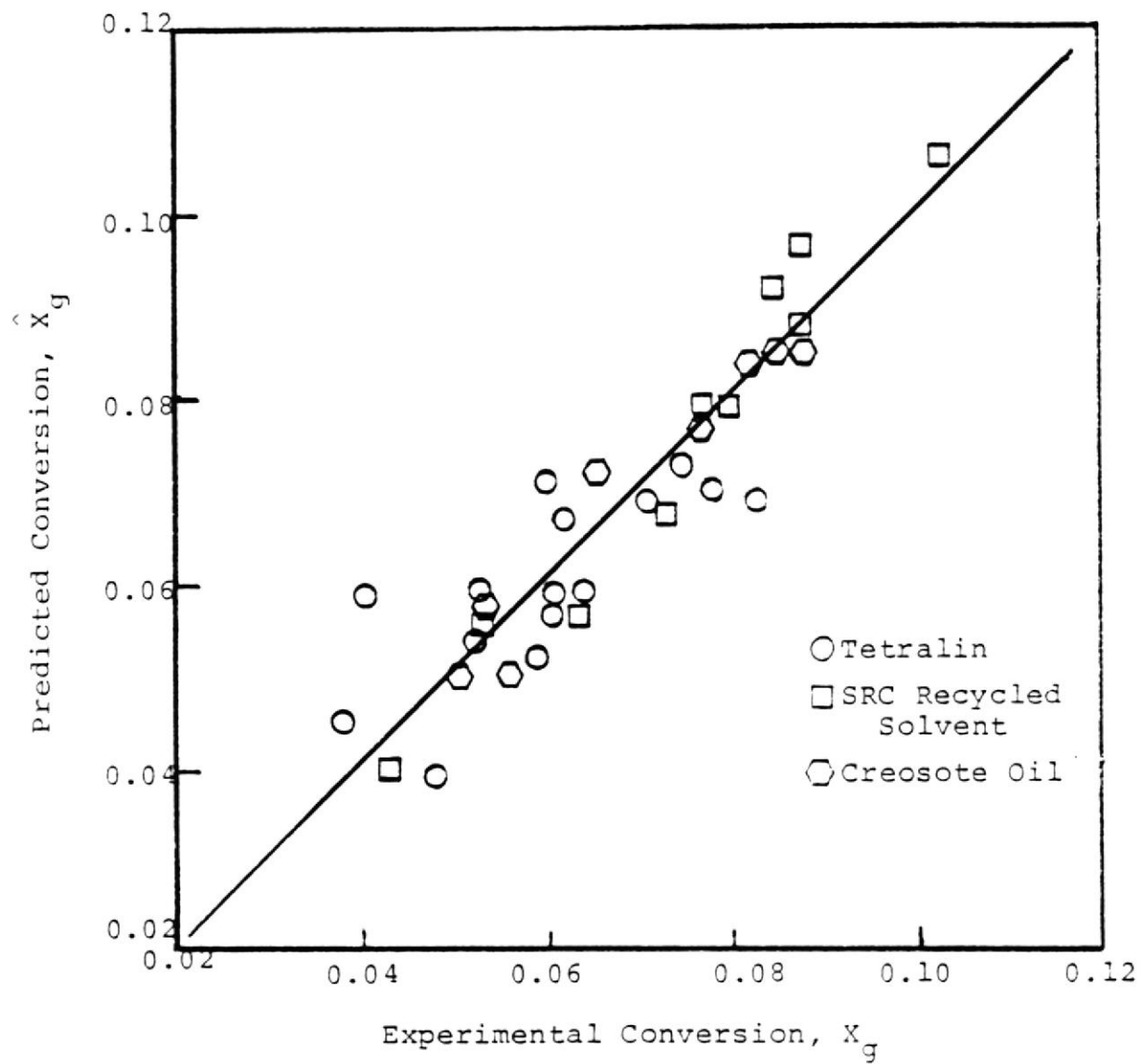


Figure 39. Scatter Plot of Lignite Converted to Gas.

TABLE 13. PREDICTED AND EXPERIMENTAL
CONVERSIONS FOR THE TUBULAR REACTOR

<u>Run No.</u>	<u>Solvent</u>	<u>P (atm)</u>	<u>T (K)</u>	<u>X_l</u>	<u>\hat{X}_l</u>	<u>X_g</u>	<u>\hat{X}_g</u>
4	Tetralin	14.6	685 ^a	0.587 ^b	0.699	--	0.075
6	Creosote	21.4	673	0.245	0.323	0.121	0.087
9	Creosote	21.4	698	0.314	0.397	0.139	0.098

a. estimated average, the temperature was measured
between 651 and 718K.

b. the lignite has been treated with steam.

FACULTAD DE INGENIERIA EN QUIMICA



IMPRESA

CHAPTER VII

MATHEMATICAL SIMULATION OF THE
TUBULAR REACTOR CONTINUOUS EXTRACTION UNITTubular Reactor Temperature Profile

The tubular reactor was operated in a near adiabatic mode. Heat loss was prevented by wrapping three heating mantles around the reactor. The heating mantles were controlled independently at temperatures according to those inside of the reactor. The reactor was gradually heated by the hot solvent. A mathematical model was written to predict the temperature profile and the result was used to compare with the experimental data. The comparison was made for tubular reactor Run No. 6 in order to demonstrate the procedure.

One assumption made in deriving the model is that the heat of reaction is negligible. This assumption makes it possible to decouple the energy equation from the continuity equation. Therefore, temperature distribution for the tubular reactor can be calculated independently. No temperature difference in the radial direction was assumed. This assumption is acceptable considering the reactor diameter (5 cm) relative to its length (79 cm). Heat involved in condensation or evaporation was also neglected. Physical properties were assumed to be constant, i.e. independent of temperature. In other words, all physical properties were assumed to be some average values between 25°C

and 400°C. Then the heat balance on the fluid can be written as (Bird et al. 1960, Holland and Anthony 1979).

$$\rho C_v \left(\epsilon \frac{\partial T}{\partial t} + v_z \frac{\partial T}{\partial z} \right) = K_e \frac{\partial^2 T}{\partial z^2} - Q_1 - Q_2 \quad (15)$$

Where

ρ = fluid density
 C_v = fluid heat capacity
 ϵ = porosity of the packed tubular reactor
 T = temperature
 t = time
 v_z = superficial velocity of the fluid flow in the z direction
 z = direction of flow
 K_e = effective conductivity of the packed bed
 Q_1 = heat loss to the lignite particles
 Q_2 = heat loss through the reactor boundary

Equation (15) is based on a unit volume of the reactor. The effective conductivity, K_e , was estimated by the following equation:

$$K_e = K\epsilon + K_\ell (1-\epsilon) \quad (16)$$

where

K = solvent conductivity
 K_ℓ = lignite conductivity

Q_1 is the heat transferred to the lignite and can be expressed as:

$$Q_1 = (1 - \epsilon) \rho_\ell C_{v\ell} \frac{\partial T_\ell}{\partial t} \quad (17)$$

The subscript ℓ in Equation (17) stands for solid lignite. If there is no temperature difference between the

lignite and the surrounding fluid, then $T_{\ell} = T$ and Equation (17) becomes:

$$Q_1 = (1 - \epsilon) \rho_{\ell} C_{V\ell} \frac{\partial T}{\partial t} \quad (18)$$

The heat loss through the reactor boundary per unit volume per unit time is:

$$Q_2 = h \Delta A (T - T_b) / \Delta V \quad (19)$$

where

h = heat transfer coefficient
 ΔA = reactor surface area;
 ΔV = reactor volume;
 T_b = Temperature outside reactor surface
 R = radius of the reactor

By substituting the values of ΔA and ΔV into Equation (19), the following result is obtained:

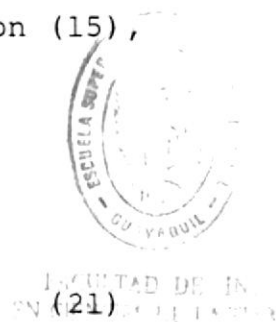
$$Q_2 = \frac{2h}{R} (T - T_b) \quad (20)$$

In equation (20), R is the radius of the reactor. substituting Equations (16), (18), (20) into Equation (15), the energy equation becomes:

$$\rho C_V \left(\epsilon \frac{\partial T}{\partial t} + v_z \frac{\partial T}{\partial z} \right) = \left[K\epsilon + K_{\ell} (1-\epsilon) \right] \frac{\partial^2 T}{\partial z^2} - (1-\epsilon) \rho_{\ell} C_{V\ell} \frac{\partial T}{\partial t} - \frac{2h}{R} (T - T_b)$$

Rearranging Equation (21), gives:

$$\left[\epsilon \rho C_V + (1-\epsilon) \rho_{\ell} C_{V\ell} \right] \frac{\partial T}{\partial t} + \left[\rho C_V v_z \right] \frac{\partial T}{\partial z} = K_e \frac{\partial^2 T}{\partial z^2} - \frac{2h}{R} (T - T_b) \quad (22)$$



Here, a new variable is defined as

$$(\rho C_v)_e = \epsilon \rho C_v + (1 - \epsilon) \rho_s C_{vs} \quad (23)$$

Then, Equation (18) becomes:

$$(\rho C_v)_e \frac{\partial T}{\partial t} + (\rho C_v v_z) \frac{\partial T}{\partial z} = K_e \frac{\partial^2 T}{\partial z^2} - \frac{2h}{R} (T - T_b) \quad (24)$$

Equation (24) is put into dimensionless form by use of the following:

$$\bar{T} = \frac{T - T_\infty}{T_m - T_\infty} = \text{dimensionless temperature} \quad (25)$$

$$\bar{z} = \frac{z}{L} = \text{dimensionless length} \quad (26)$$

$$\bar{t} = \frac{v_z z}{L} t = \text{dimensionless time} \quad (27)$$

$$\bar{R} = \frac{R}{L} = \text{dimensionless radius} \quad (28)$$

where

- T_∞ = room temperature 25° C
- T_m = entrance solvent temperature (which is maximum in this system)
- L = total reactor length
- R = reactor radius

By substituting Equations (25) through (28) into Equation (24) and then dividing, the resulting equation by $\frac{(T_m - T_\infty) v_z}{L (\rho C_v)_e}$ gives

$$\frac{\partial \bar{T}}{\partial \bar{t}} + \frac{\rho C_v}{(\rho C_v)_e} \frac{\partial \bar{T}}{\partial \bar{z}} = \frac{K_e}{L (\rho C_v)_e v_z} \frac{\partial^2 \bar{T}}{\partial \bar{z}^2} - \frac{2h}{R (\rho C_v)_e v_z} (\bar{T} - \bar{T}_b) \quad (29)$$

New variables are defined as:

$$R_a = \frac{\rho C_v}{(\rho C_v)_e} = \text{a ratio} \quad (30)$$

$$Pe_h = \frac{L(\rho C_v)_e v_z}{K_e} = \text{Peclet number} \quad (31)$$

$$St = \frac{2h}{\bar{R}(\rho C_v)_e v_z} = \text{Stanton number} \quad (32)$$

Then, Equation (29) can be written as

$$\frac{\partial \bar{T}}{\partial \bar{t}} + R_a \frac{\partial \bar{T}}{\partial \bar{z}} = \frac{1}{Pe_h} \frac{\partial^2 \bar{T}}{\partial \bar{z}^2} - St (\bar{T} - \bar{T}_b) \quad (33)$$

In Equation (33), \bar{T}_b is the dimensionless temperature for the reactor surface. The thermocouples were inserted for measuring the surface temperature at the midpoint of each heating mantle, hence:

$$\bar{T}_b = \bar{T} \Big|_{\bar{z}=1/6} \quad \text{for } 0 \leq \bar{z} < \frac{1}{3} \quad (34)$$

$$\bar{T}_b = \bar{T} \Big|_{\bar{z}=1/2} \quad \text{for } \frac{1}{3} \leq \bar{z} \leq \frac{2}{3} \quad (35)$$

$$\bar{T}_b = \bar{T} \Big|_{\bar{z}=5/6} \quad \text{for } \frac{2}{3} < \bar{z} \leq 1 \quad (36)$$

Before solving for \bar{T} , \bar{T}_b has to be assigned to Equation (33). However, \bar{T}_b is not known until \bar{T} is calculated. To solve this dilemma, a trailing \bar{T}_b is used. In other words, \bar{T}_b is always one time step behind \bar{T} . If the time increment is small enough, this approximation will not cause serious problems.

The temperature profile is obtained by Crank-Nicolson's method (Ketter and Sherwood 1969). First, Equation (33) has to be expressed in finite difference form. For a forward flow system, the backward difference scheme is recommended for the first order differential terms and the central difference formula is recommended for the second order differential terms. Otherwise, instability occurs.

The initial and boundary conditions required to solve for \bar{T} are:

$$\text{I.C.: at } \bar{t} = 0 \quad \bar{T} = 0 \quad \text{for } 0 \leq \bar{z} \leq 1 \quad (37)$$

$$\text{B.C. 1: at } \bar{z} = 0 \quad \bar{T} = 2.5\bar{t} \quad \text{for } 0 \leq \bar{t} \leq 1 \quad (38a)$$

$$\bar{T} = 1 \quad \text{for } \bar{t} < 1 \quad (38b)$$

$$\text{B.C. 2: at } \bar{z} = 1 \quad \frac{\partial \bar{T}}{\partial \bar{z}} = 0 \quad (39)$$

The values for R_a , Pe_h and St are not directly known. However, they can be determined by data fitting. The simplex procedure (Nelder and Mead 1965) is followed to optimize the set of parameters. For fitting three parameters, four sets of parameters are required to initiate the procedure. By substituting the initial guesses, for R_a , Pe_h , and St into Equation (33), unsteady state temperature profiles can be calculated. Then, points are selected from the profiles with respect to the experimental data in Table 14 to calculate the sum of the residual squares. The sum of the

TABLE 14. UNSTEADY STATE TEMPERATURE PROFILE
RUN NO. 6

<u>t (hr)</u>	<u>T (°C)</u>		
	<u>L/6</u>	<u>L/2</u>	<u>5L/6</u>
0.5	60	25	25
1.0	180	60	30
1.5	330	220	110
2.0	360	280	220
2.5	390	390	340

residual squares is the criterion of deleting the set of the initial four. The set with the maximum sum of squares is deleted and a new set of parameters is determined following the reflection, contraction and expansion rules in the simplex method. The procedure is repeated until a set of parameters with the desirable sum of squares is obtained.

The simplex method requires no derivatives of the objective function. Hence, it can be easily applied to data fitting of a partial differential equation.

Since little was known about the physical properties of the solvent (creosote oil) and lignite and the reaction temperature. The initial set of parameters (R_a , Pe_h and St) are estimated from other materials. The properties of light oil at 422K were used to substitute for that of the solvent. The lignite properties were estimated by dry limestone. These values along with the others are shown in Table 15. By substituting the values in Table 15 into Equations (30), (31), (32), the initial set of parameters are calculated to be $R_a = 1.08$, $Pe_h = 536$, $St = 0.062$.

These parameters are to be modified with the experimental temperatures (Table 14) following the simplex procedure. After several trials (Table 16), the initial set was found to be the local optimum. Hence, we conclude that the properties of a light oil and a dry limestone can be used to substitute for that of creosote oil and lignite.

TABLE 15. PHYSICAL PROPERTIES FOR THE ESTIMATION OF PARAMETERS^c

<u>Light Oil^a</u>	<u>Lime Stone^b</u>	<u>Reactor</u>
$\rho = 0.83 \text{ g/cm}^3$	$\rho_s = 1.68 \text{ g/cm}^3$	$R = 2.54 \text{ cm}$
$C = 2.26 \text{ J/g k}$	$C_{vs} = 0.92 \text{ J/g k}$	$L = 78.75 \text{ cm}$
$K = 4.54 \text{ J/cm hr k}$	$K_s = 24.91 \text{ J/cm hr k}$	$v_z = 49 \text{ cm/hr}$
		$\epsilon = 0.6$

a. At 422K, see Kreith (1973)

b. At 294K, see Kreith (1973)

c. The data from Kreith has been converted into S.I. unit.

TABLE 16. RESULT OF SIMPLEX OPTIMIZATION PROCEDURE

<u>Trial No.</u>	<u>R_a</u>	<u>P_e_h</u>	<u>S_t</u>	<u>s*</u>
1	1.08	536	0.062	21
2	1.40	482	0.056	55
3	0.97	697	0.056	23
4	0.97	482	0.081	23
5	0.60	616	0.072	95
6	0.97	482	0.056	51

* standard deviation = $\left(\left(\sum_{i=1}^N (\hat{T}_i - T_i)^2 / N \right)^{1/2} \right)$

BIBLIOTECA

FACULTAD DE CIENCIAS
EN CIENCIAS DE LA TIERRA

The calculated temperature profile with the best set of parameters are shown in Figure 40. The standard deviation for the 15 experimental point is $\pm 21\text{K}$, which is reasonably small at about 5%.

Tubular Reactor Concentration Profile

The concentration of the lignite derived liquid, the lignite conversion, and the gas production rate are estimated. The mathematical model for the estimation uses the rate equation developed with minibatch data, the energy equation and the continuity equation. Both the rate equation and the energy equation have been presented. The continuity equation for the lignite-derived liquid can be expressed as

$$\epsilon \frac{\partial c}{\partial t} + v_z \frac{\partial c}{\partial z} = De \frac{\partial^2 c}{\partial z^2} + W_0 \left(\frac{dx_l}{dt} - \frac{dx_g}{dt} \right) \quad (40)$$

Where, W_0 is the initial weight of lignite per unit reactor volume. The last term of Equation (40) is the generation term and can be expressed as follows:

$$\frac{dX}{dt} = k (X_e - X) \quad (11)$$

$$X_e = X_{e0} \exp \left[\frac{-\Delta V}{R_1 T_0} (P - P_0) - \frac{\Delta h}{R_2} \left(\frac{1}{T} - \frac{1}{T_0} \right) \right] \quad (10)$$

The parameters for Equation (11) and Equation (10) are shown in Table 11.

Equation (40) is to be solved by defining the

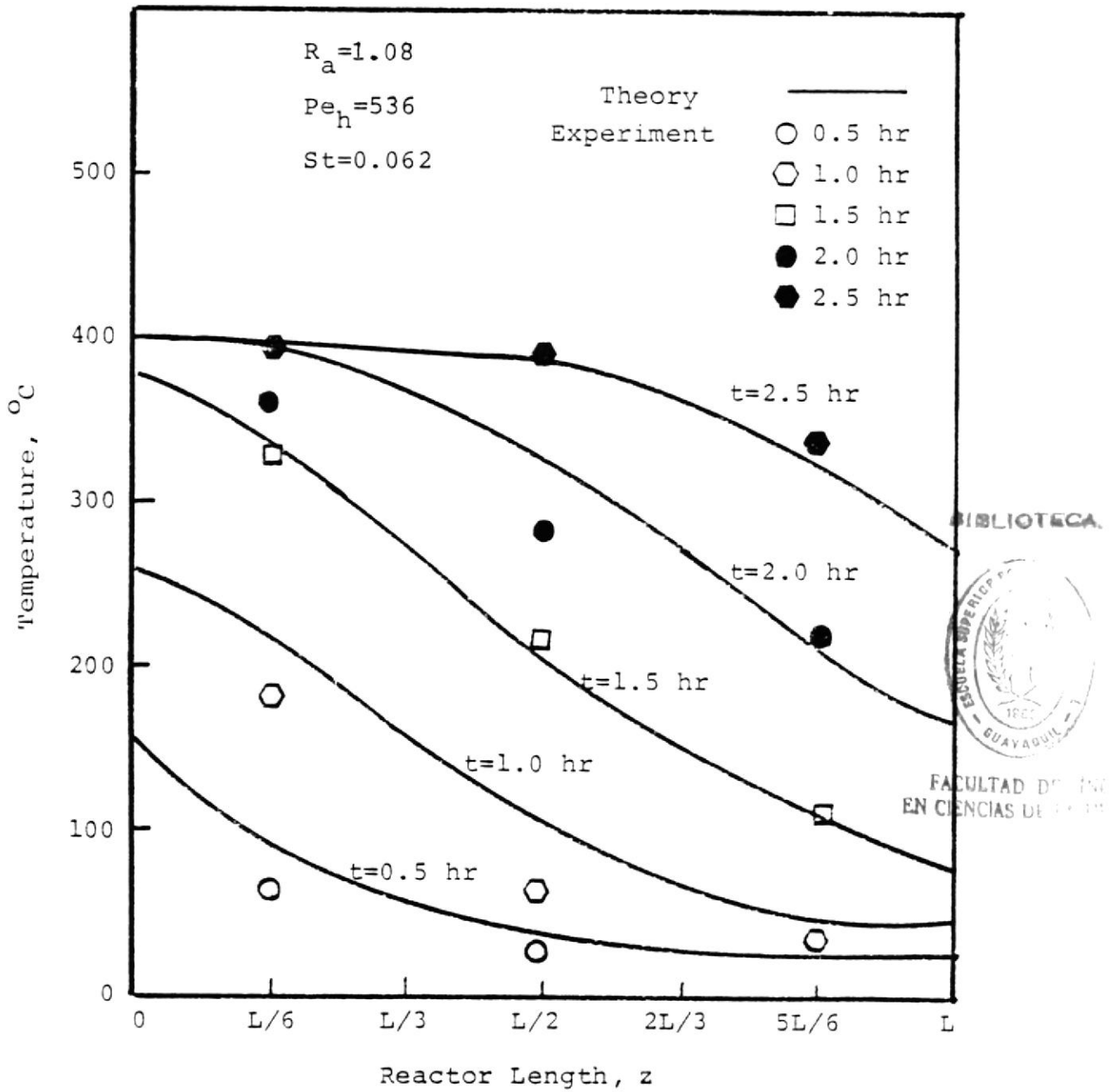


Figure 40. Tubular Reactor Temperature Profile.

dimensionless variables:

$$\bar{t} = \frac{v_z}{L} t \quad (27)$$

$$\bar{z} = \frac{z}{L} \quad (26)$$

$$\bar{c} = \frac{c}{c_0} \quad (41)$$

$$\bar{W} = \frac{W_0}{c_0} \quad (42)$$

$$\bar{T} = \frac{T - T_\infty}{T_m - T_\infty} \quad (25)$$

$$\bar{P} = \frac{P}{P_0} \quad (43)$$

Then, Equations (40), (11), and (10) become:

$$\epsilon \frac{\partial \bar{c}}{\partial \bar{t}} + \frac{\partial \bar{c}}{\partial \bar{t}} = \frac{1}{Pe} \frac{\partial \bar{c}}{\partial \bar{z}^2} + F \quad 0 \leq \bar{z} \leq 1 \quad (44)$$

$$\frac{dX}{d\bar{t}} = \bar{k} (X_e - X) \quad (45)$$

$$X_e = X_{e0} \exp \left[-u_1 (\bar{P}-1) - u_2 \left(\frac{1}{u_2 \bar{T} + u_4} - 1 \right) \right] \quad (46)$$

where: $Pe = \frac{Lv_z}{De} = \text{Peclet Number} \quad (47)$

$$u_1 = \frac{P_0 \Delta v}{R_1 T_0} \quad (48)$$

$$u_2 = \frac{\Delta h}{R_2 T_0} \quad (49)$$

$$u_3 = \frac{T_m - T_\infty}{T_0} \quad (50)$$

$$u_4 = \frac{T_\infty}{T_0} \quad (51)$$

$$\bar{k} = \frac{L}{v_z} k \quad (52)$$

$$F = \bar{W} \left(\frac{dX}{d\bar{t}} - \frac{dX}{d\bar{t}} \right) \quad (52a)$$

Equation (44) is to be solved with its initial and boundary conditions. The boundary conditions for a continuous flow reactor with dispersion have been widely discussed (Danckwerts 1953, Wehner and Wilhelm 1956, Aris and Amundson 1957, Pearson 1959, Fan and Bailie 1960, DeMaria et al. 1961, Bischoff 1961a) They reached the conclusion that the entrance and the exit boundary conditions for a continuous flow system with dispersion were:

$$\bar{c}(-\infty) = \bar{c}(0+) - \frac{1}{Pe} \frac{d\bar{c}(0+)}{d\bar{z}} \quad (53)$$

$$\frac{d\bar{c}(1^-)}{d\bar{z}} = 0 \quad (54)$$

However, all previously mentioned studies dealt with a steady state system and no consideration was given to the important dynamic behavior of such systems. Later Van Cauwenberghe (1966) showed that the above boundary conditions were valid for a dynamic system if and only if the diffusivities were equal to zero for both the entrance and exit sections. The sections are illustrated in Figure 41. For a real system, diffusivities are not equal to zero and are expected in all sections. Therefore, the use of Equation (53) and Equation (54) as boundary conditions for a flow system is strictly limited.

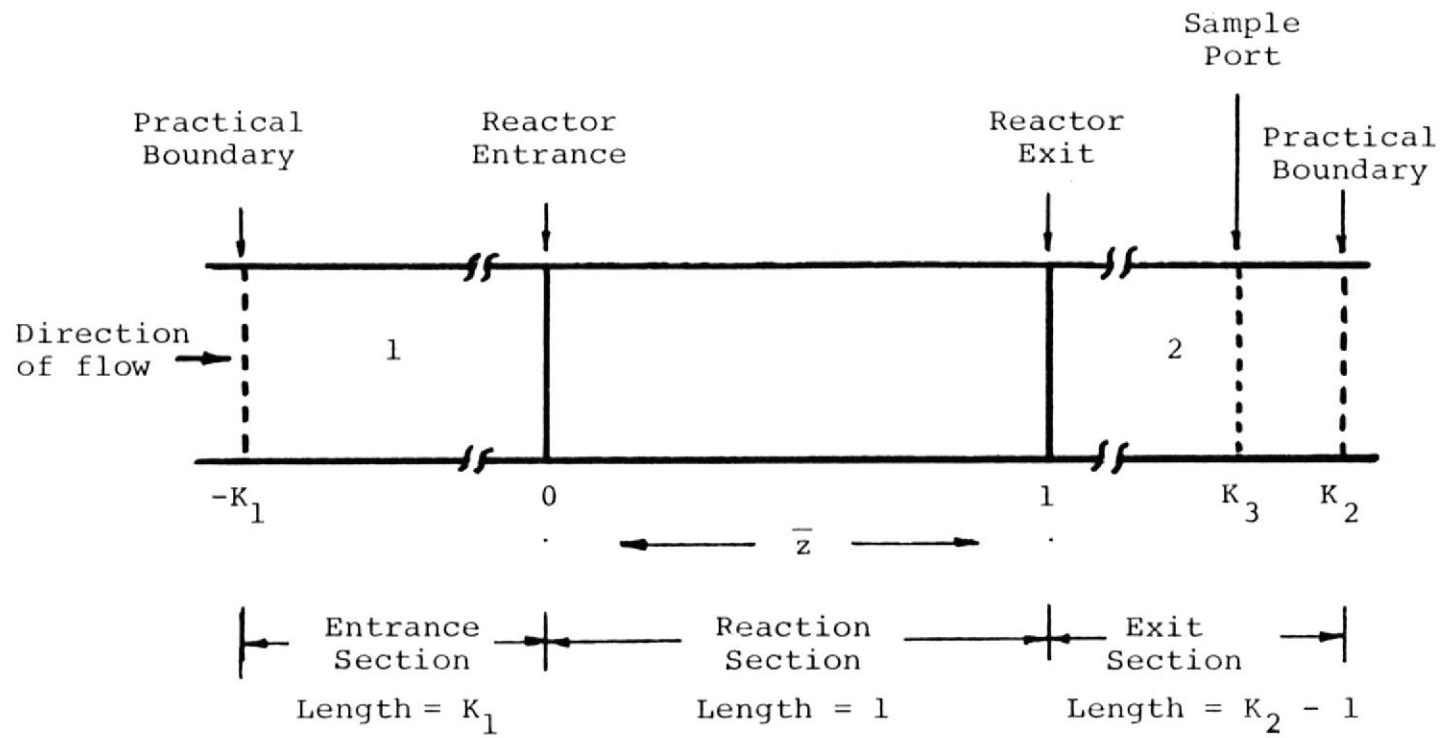


Figure 41. Sections of a Continuous Flow Reactor

To develop a general solution for an unsteady state flow reactor, all sections in Figure 41 are considered. The differential equations for the three sections are:

$$\frac{\partial \bar{c}}{\partial t} + \frac{\partial \bar{c}}{\partial \bar{z}} = \frac{1}{Pe_1} \frac{\partial^2 \bar{c}}{\partial \bar{z}^2} \quad \bar{z} \leq 0 \quad (55)$$

$$\frac{\partial \bar{c}}{\partial t} + \frac{\partial \bar{c}}{\partial \bar{z}} = \frac{1}{Pe} \frac{\partial^2 \bar{c}}{\partial \bar{z}^2} + F \quad 0 \leq \bar{z} \leq 1 \quad (56)$$

$$\frac{\partial \bar{c}}{\partial t} + \frac{\partial \bar{c}}{\partial \bar{z}} = \frac{1}{Pe_2} \frac{\partial^2 \bar{c}}{\partial \bar{z}^2} \quad \bar{z} \geq 1 \quad (57)$$

The Pe group may differ between sections for reasons of velocity, presence of particles and the like.

The six required boundary conditions are:

$$\bar{c}(-\infty) = 0 \quad (58)$$

$$\bar{c}(0^-) - \frac{1}{Pe_1} \frac{d\bar{c}(0^-)}{d\bar{z}} = \bar{c}(0^+) - \frac{1}{Pe} \frac{d\bar{c}(0^+)}{d\bar{z}} \quad (59)$$

$$\bar{c}(0^-) = \bar{c}(0^+) \quad (60)$$

$$\bar{c}(1^-) - \frac{1}{Pe} \frac{d\bar{c}(1^-)}{d\bar{z}} = \bar{c}(1^+) - \frac{1}{Pe_2} \frac{d\bar{c}(1^+)}{d\bar{z}} \quad (61)$$

$$\bar{c}(1^-) = \bar{c}(1^+) \quad (62)$$

$$\bar{c}(+\infty) = \text{finite} \quad \text{or} \quad \frac{\partial \bar{c}(+\infty)}{\partial \bar{z}} = 0 \quad (63)$$

Equation (58) and Equation (63) are readily understood. Equation (59) and Equation (61) result from mass conservation. The mass flux through the boundary is represented by either side of the equation. Equation (60) and Equation (62) arise from the argument that the concentration should

be continuous.

Equation (55) through (63) are to be solved numerically. For practical purposes, Equation (58) is replaced by:

$$\bar{c}(-K_1) = 0 \quad (64)$$

Where K_1 is a finite number which should be large enough so that the replacement can cause little error to the solution. On the other hand, K_1 should be small enough to avoid using long computing times. The error involved in this replacement is expressed by

$$\sigma = \int_0^{\infty} \bar{c}_M(\bar{z}=K_3) \cdot d\bar{t} - \int_0^{\infty} \bar{c}(\bar{z}=K_3) d\bar{t} \quad (65)$$

In Equation (65), $\bar{c}_M(\bar{z}=K_3)$ is the true dimensionless concentration at the sample part ($\bar{z}=K_3$). $\bar{c}_M(\bar{z}=K_3)$ is obtained by taking $K_1 = \infty$. The approximate dimensionless concentration, $\bar{c}(\bar{z}=K_3)$ is obtained by taking K_1 to be a finite number. The relationship between σ and K_1 is illustrated in Figure 42. The error is always a positive number. For a given error, there exists the relationship:

$$K_1 \propto \frac{1}{Pe_1} \quad (66)$$

Equation (66) indicates that for a small Pe_1 , a large K_1 is needed to confine the approximate error to a tolerable range.

Similarly, Equation (63) is also replaced with a finite number and becomes:

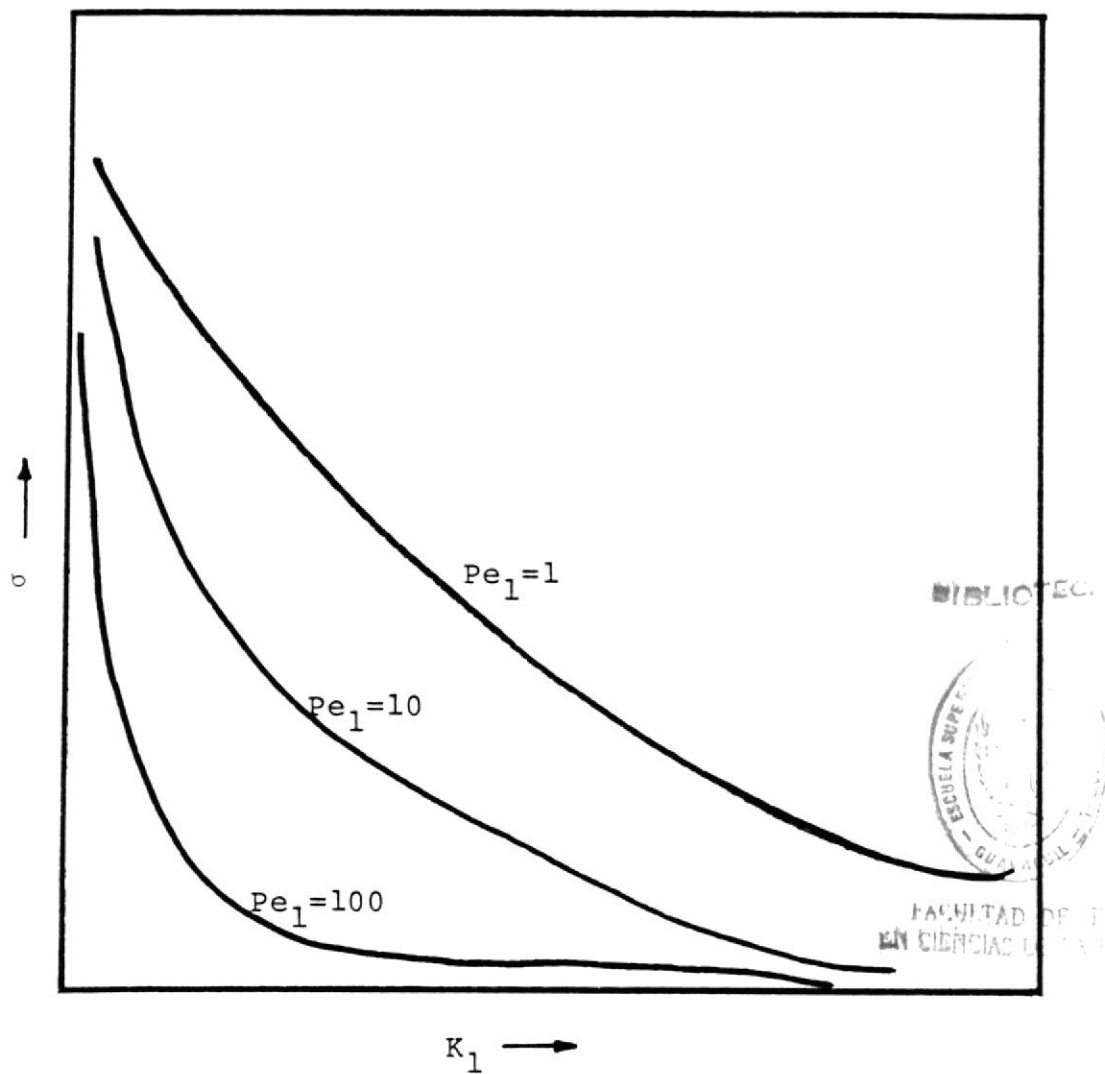


Figure 42. Error Caused by Boundary Condition Approximation.

$$\frac{\partial \bar{c}(K_2)}{\partial \bar{z}} = 0 \quad (67)$$

The initial condition is taken to be:

$$\bar{c} = 0 \quad \text{at } t = 0 \quad (68)$$

Then Equations (55) through (57) can be solved numerically with the initial and boundary conditions. In Equation (56), the generation term, F , can be calculated from Equation (45) and Equation (46). Using Equation (46) to calculate the equilibrium conversion, X_e requires the temperature and pressure distribution to be known. The computer program for calculating the unsteady state temperature distribution has already been developed. Assume the pressure is constant, then X_e can be calculated.

The constants required to calculate the concentration distribution are listed in Table 17. These constants are used to model tubular reactor Run No. 6. For other runs changes should be made accordingly.

For Run No. 6, the system pressure was held at 21.4 atm. Therefore, this pressure is used in modeling Run No. 6.

The reference pressure and temperature are taken to be 32 atm and 673K respectively. These values were used previously to estimate the parameters of the rate equation. In the current model, these parameters are used. Hence the reference state should remain the same.

TABLE 17. CONSTANTS FOR CALCULATING
LIGNITE-DERIVED LIQUID CONCENTRATION

$P = 20 \text{ atm}$	<u>For X_l (see Table 28)</u>
$P_o = 32 \text{ atm}$	$k = 11.8 \text{ hr}^{-1}$
$T_o = 673 \text{ K}$	$X_{eo} = 0.345$
$T_m = 673 \text{ K}$	$\Delta v = 0.265 \text{ l/mol}$
$T_\infty = 298 \text{ K}$	$\Delta h = 32.2 \text{ KJ/mol}$
$R_1 = 0.082 \text{ l atm/mol K}$	
$R_2 = 8.314 \times 10^{-3} \text{ KJ/mol K}$	<u>For X_g (see Table 28)</u>
$\epsilon = 0.6$	$k = 4.5 \text{ hr}^{-1}$
$L = 78.74 \text{ cm}$	$X_{eo} = 0.0857$
$v_z = 49.3 \text{ cm/hr}$	$\Delta v = -0.0348 \text{ l/mol}$
$c_o = 0.1 \text{ g/cm}^3$	$\Delta h = 19.9 \text{ KJ/mol}$
$W_o = 0.37 \text{ g/cm}^3 \text{ (MAF)}$	
$K_1 = 1$	
$K_2 = 2$	
$K_3 = \text{adjustable}$	
$Pe = Pe_1 = Pe_2 = \text{adjustable}$	

The values of the T_m and T_∞ are taken to be 673K and 298K respectively for the purpose of defining the dimensionless temperature. Because of the different units used in the model, the gas constant should change accordingly. The porosity is taken to be a constant ($\epsilon = 0.6$) despite the fact that ϵ should be a function of the conversion. As a matter of fact $\epsilon = 0.6$ is roughly the average porosity during the experiment. The reactor length, L , is the actual length measured. The solvent velocity is calculated from the pump capacity (1,000 ml/hr) and the reactor radius ($R = 2.54$ cm). The reference concentration, c_o , is arbitrarily taken to be 0.1 g/cm^3 . No special reason is involved in making the choice except that c_o is in the same order of magnitude of the concentration of the lignite derived liquid. The initial lignite density, W_o , is obtained by dividing the initially charged lignite ($= 604$ g MAF for Run No. 6) with the reactor volume ($= 1596$ ml). The rate equation parameters for the calculation of the conversions are also shown in Table 17. These values are taken from Table 11 for the case of creosote oil.

The entrance section is given a length equal to that of the reactor. In other words, K_1 is given a value of 1. Earlier discussion has shown that the determination

K_1 is a battle of computing time and accuracy. A long entrance section (large K_1) is a better approximation of the true model ($K_1 = \infty$). However, large K_1 represents long computing time in solving the partial differential equation (Equation (55)). Whether the selected length ($K_1 = 1$) is long enough or not will be judged later.

The exit section is also given a length equal to that of the reactor. Hence, K_2 equals to 2. Like K_1 , K_2 should be large enough to approximate the true case ($K_2 = \infty$). K_2 should also be small enough to avoid using long computer times K_2 should also be greater than the length between the reactor entrance and the sample port, K_3 . With $K_2 > K_3 > 1$, the sample port is located in the exit section and the sample concentration can be calculated.

It should be emphasized the K_3 is not the physical length between the reactor entrance and the sample port. Rather, it is an equivalent length between those locations. This is because the model assumes a geometry quite different from the actual situation. The model assumes the same size for the entrance section, reactor section and the exit section. However, they are different in reality. Hence the model length, K_3 , cannot be determined by direct measurement. The directly measured length between the reactor entrance and the sample port can be used as the first guess of K_3 . Then, K_3 is refined by the measured sample concentrations.

BIBLIOTECA



FACULTAD DE CIENCIAS EXACTAS Y NATURALES

The Peclet numbers for the sections are different because of the differences among the sections in their solvent flow pattern and geometry. To simplify the problem, these three numbers are assumed to be equal and are adjusted to obtain the experimental result. Whether the simplification is justifiable or not remains to be proved.

There are now two adjustable parameters, K_3 and Pe . By substituting these parameters into the model, the concentrations at the sample port can be calculated for different times. Results are shown in Figure 43. In Figure 43, the curve is bell-shaped. K_3 and Pe affect the curve in different ways. K_3 shifts the curves in the time scale and Pe changes the slopes. The curve shifts to the right with increasing K_3 and the bell is taller with large Pe (even though the area under it is unchanged). The determination of K_3 and Pe is a matter of trial and error until the curve generated matches the experimental results (Table 10).

The trial and error starts with calculating the unsteady state concentration profile of each section. The following steps illustrate the calculation procedure:

1. Enter the constants and parameters.
2. Set $\bar{t} = 0$ and $X = 0$, then enter the initial and boundary conditions for \bar{T} and \bar{c} .
3. Advance the time: $\bar{t} = \bar{t} + \Delta\bar{t}$
4. Update the time dependent boundary condition, $\bar{T}(\bar{z}=0)$

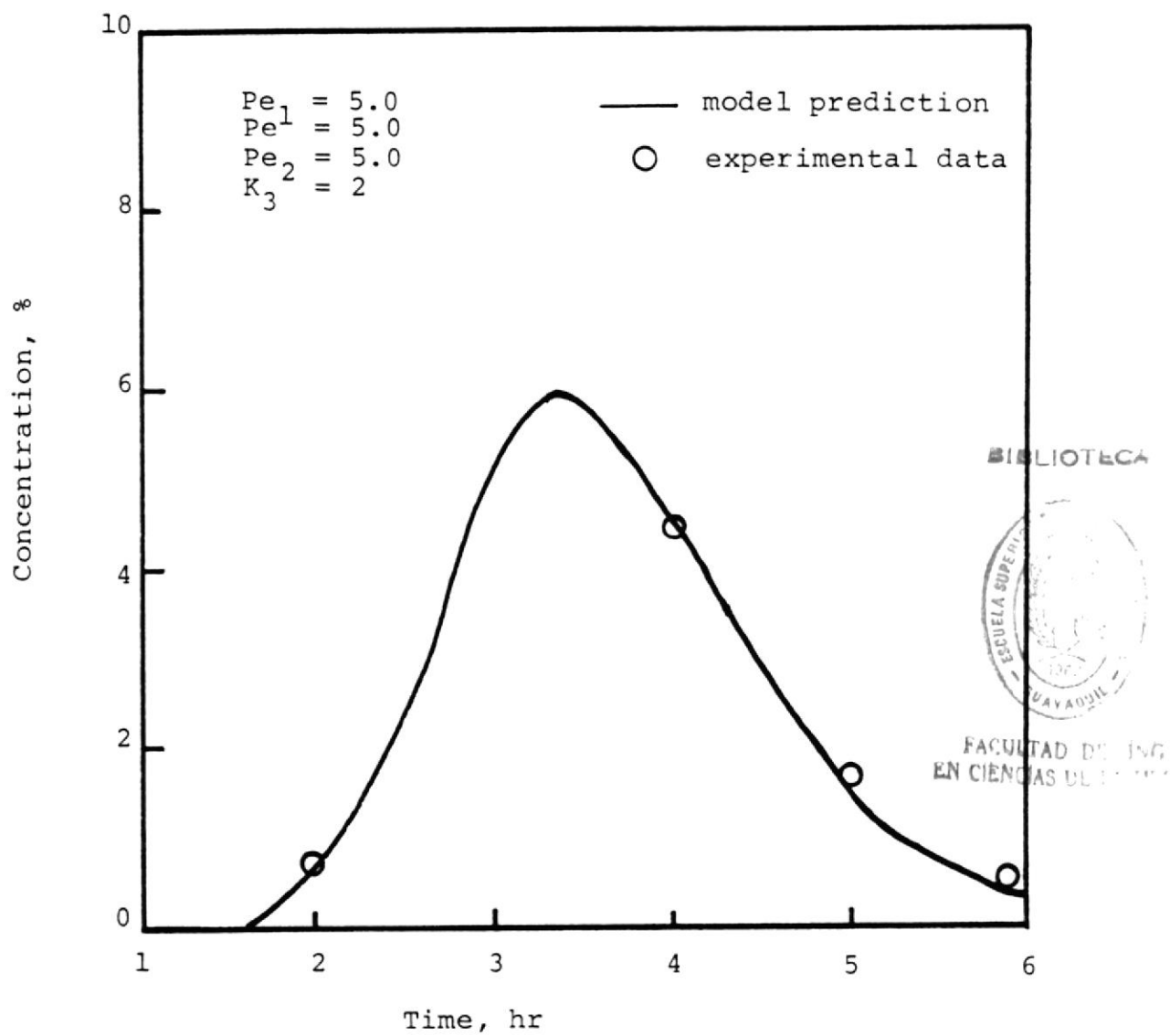


Figure 43: Liquid Product Concentration at the Sample Port ($z=2L$)

5. Calculate the temperatures along \bar{z} .
6. Use the temperatures to calculate the equilibrium conversion, X_e .
7. Calculate the conversion rate $\Delta X/\Delta \bar{t} = \bar{k}(X_e - X)$.
8. Calculate the generation term, $F = \bar{W}(\Delta X_\ell/\Delta \bar{t} - \Delta X_g/\Delta t)$
9. Use Crank-Nicolson's method to calculate the concentration distribution.
10. Update the conversion, $X = X + \Delta X$. ΔX is obtained by integrating Equation (45). Runge Kutta method is recommended for the integration.
11. Repeat steps 3 through 10 until the desired reaction time is reached.

The above procedure involves the calculations of \bar{T} , X_e , $\Delta X/\Delta \bar{t}$, F , \bar{c} and ΔX . These variables are of course functions of \bar{z} and \bar{t} . No reaction is assumed to occur at a temperature below 250° C. In steps 6, 7, 8, and 10, $F = 0$ and $\Delta X = 0$ for $T < 250^\circ \text{C}$.

The calculated concentration profiles are shown in Figure 44. The curves show trends as expected. The curve skews to the left at the early stage of the reaction. Then the curve gradually grows into one which skews to the right. This is the result of the maximum reaction rate which travels from the left to the right because of the temperature and the reactable lignite. The concentration increases as a result of the increasing temperatures which cause an increase in the conversion. The solvent flow rate

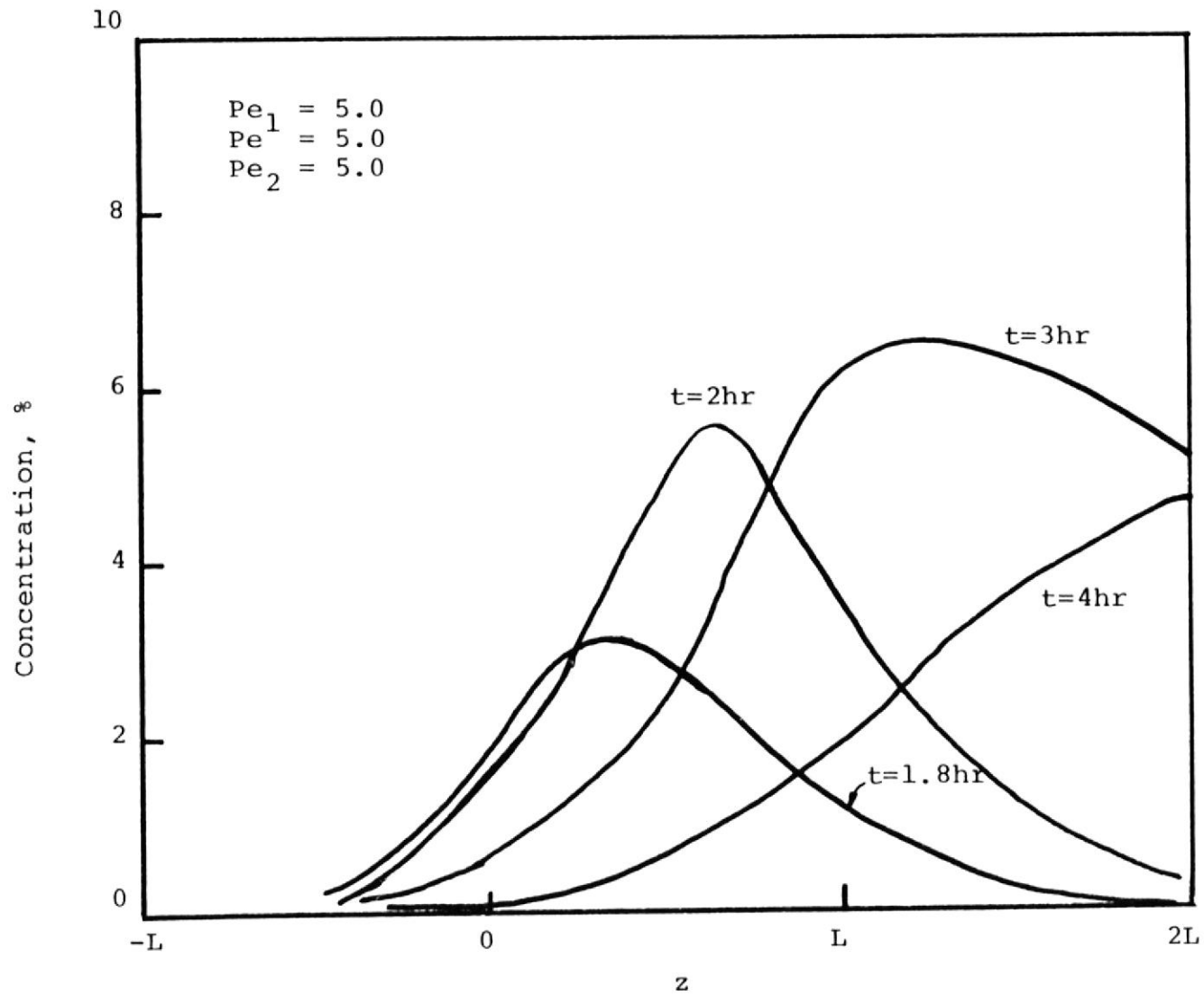


Figure 44: Concentration Distribution

shifts the curve to the right.

The shape of the concentration distribution in the reactor shown in Figure 44 is a function of the Peclet number, Pe . By plotting the calculated concentrations at $\bar{z} = K_3$, a curve similar to that in Figure 43 is obtained. By repeating the procedure with different Pe and K_3 , the concentration curve at the sample port (Figure 43) will be reasonably close to the experimental data (Table 10).

The best set of parameters were found to be $Pe = 5.0$ and $K_3 = 2$. Figures 43 and 44 were obtained with these numbers.

The curves in Figures 43 smoothly approach zero at $\bar{z} = -L$ (or $\bar{z} = K_1 = -1$) is an indication that the selection of $K_1 = 1$ is large enough. Since Figure 43 shows that the calculated curve matches the experimental data amazingly well, the assumption $Pe = Pe_1 = Pe_2$ and the approximation $K_2 = 2$ are considered to be acceptable.

The Peclet number defined in Equation (45) may be rearranged as follows:

$$Pe = \frac{Lv_z}{De} + \frac{1}{(D\varepsilon/v_z d_p)} \frac{\varepsilon L}{d_p} \quad (69)$$

Where d_p is the initial lignite particle size (=0.5 cm), ε is porosity (=0.6) and L is the reactor length (=78.74 cm).

Bischoff (1961 b) measured the dimensionless group, $D\varepsilon/v_z d_p$ by passing fluid through a packed bed at various Reynolds numbers. For liquid of laminar flow, the group was found to be about 1.7. Since our experiment was also in laminar flow region, this number was used. By substituting all the numbers into Equation (69), the Pe was calculated to be 56 which is substantially greater than the result (Pe = 5) used herein. The gas generated during extraction probably has a mixing effect which enlarges the diffusivity term in Equation (69) therefore decreasing the Peclet number.

The calculated lignite conversion and equilibrium conversion are shown in Figure 45. Equilibrium conversion are obtained after 4 hours of operation.

The gas production rate is defined as

$$\left(\frac{dX_g}{dt}\right)_p = \frac{\int_0^L \left(\frac{dX_g}{dt}\right) dz}{L} \quad (70)$$

The calculated result is shown in Figure 46. The multiplication of $(dX_g/dt)_p$ by the weight of lignite charged results in the absolute value of the gas production. The percent of lignite recovered at various time is expressed as follows

$$Y_g = \frac{\int_0^t [c(z=K_3L)] (v_z) (\pi R^2) dt}{\text{wt. of lignite (MAF) charged}} \times 100 \quad (71)$$

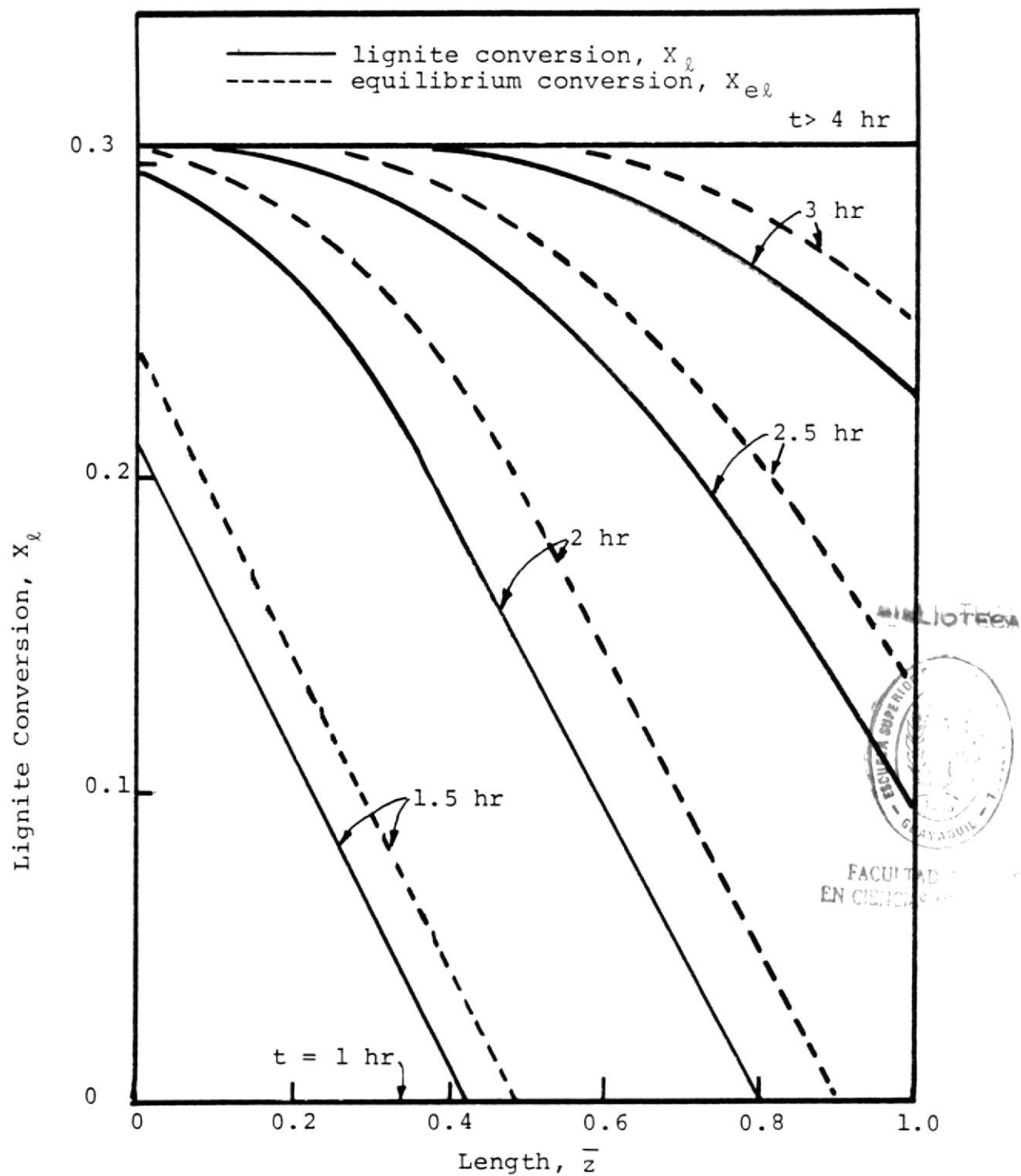


Figure 45. Tubular Reactor Conversion Profile.

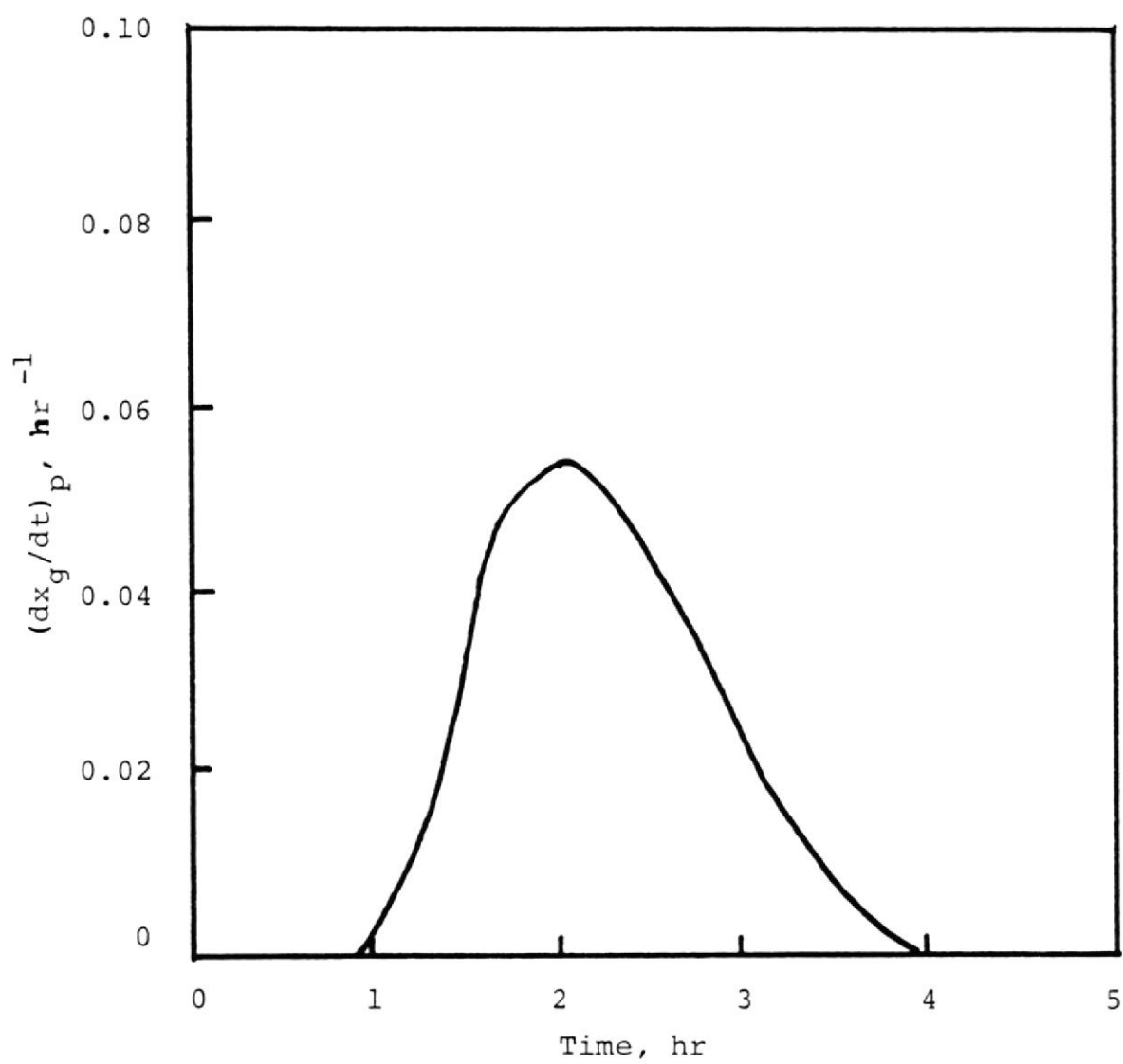


Figure 46. Tubular Reactor Gas Production Rate.

The concentration of lignite-derived liquid is shown in Figure 43. Y_l is the percent of lignite recovered as liquid product. The following equation gives the percent of the lignite recovered as the gas product.

$$Y_g = \left[\int_0^t \left(\frac{dx_g}{dt} \right)_p dt \right] \times 100 \quad (72)$$

The results of Y_l and Y_g are plotted in Figure 47. Both curves approach the equilibrium conversion.

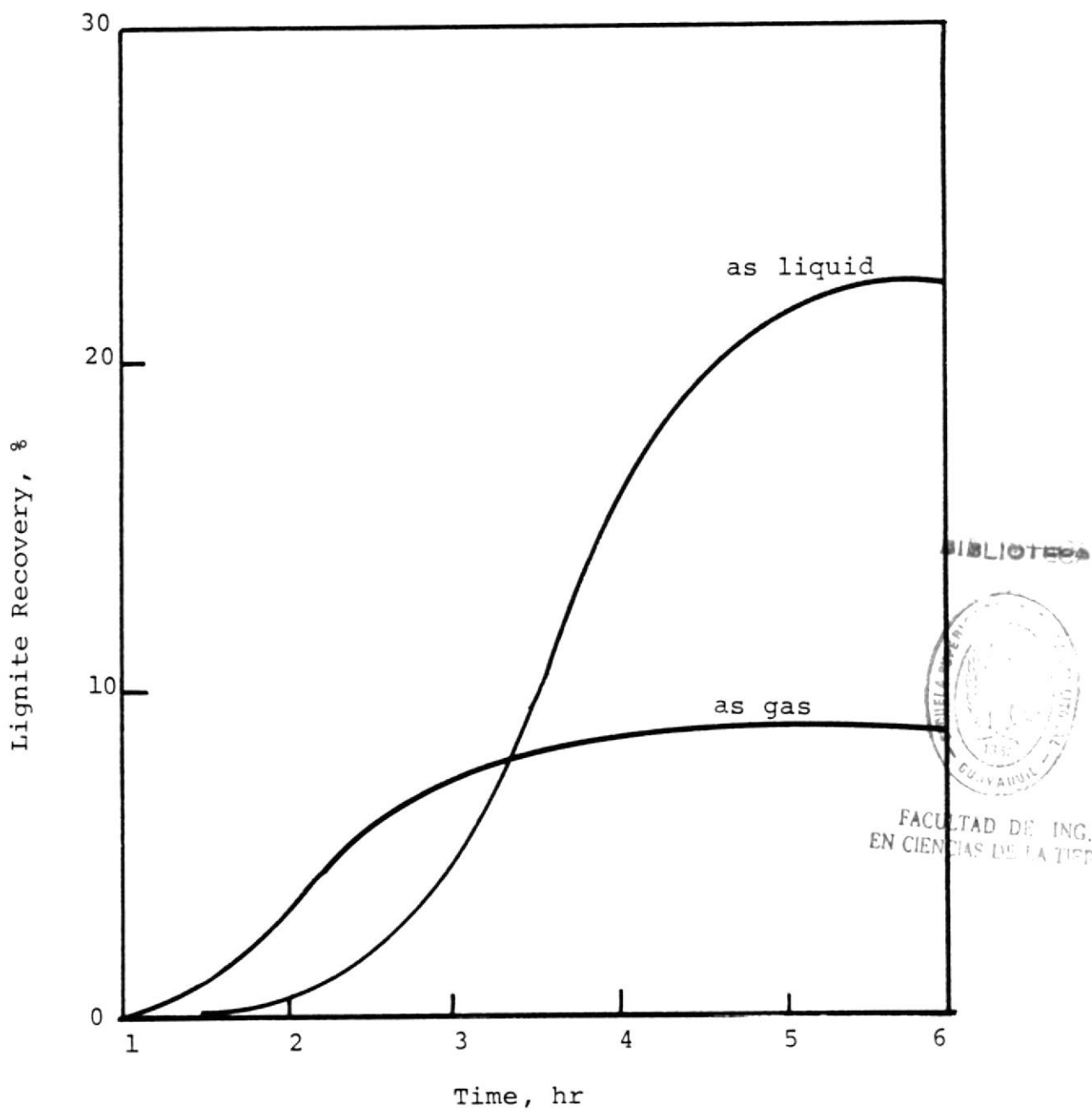


Figure 47. Lignite Recovery.

CHAPTER VIII

MATHEMATICAL SIMULATION OF
UNDERGROUND LIQUEFACTION

At this point, the proposed calculational procedure is successful in predicting the performance of a laboratory simulation system. A similar approach is applied to the simulation of a field test. Several adjustments are required to meet the new situation. First, the heat loss through the surrounding formations, even though it may be small, may not be neglected. The heat loss affects the temperature distribution. The high sensitivity of lignite conversion on temperature makes the heat loss an important factor to determine the amount of lignite that is recoverable. Second, the underground liquefaction will be conducted on a large scale, hence a one dimensional model may not be adequate. A two dimensional model will be used.

Only the temperature distribution will be studied in this chapter, because it is the key factor in determining the success of a underground liquefaction process. Other considerations, such as the amount of lignite that can be recovered, the quality of the products, etc., can be estimated following the same treatments as that used for the laboratory simulation system previously discussed.

Model Description

Assume that the lignite to be liquefied is located

between the two boreholes and is in a cylindrical shape as shown in Figure 48. The center core represents the lignite to be recovered. The hot solvent is injected into the lignite seam at $z = 0$. The slurry is recovered at the production bore-hole ($z = L$).

The lignite seam is divided into two sections: the solvent-contacted section (section A), and the section not contacted by the solvent (section B). The boundary between sections A and B is moving in the direction of the solvent flow as the solvent is continuously injected.

The field of computation also includes the surrounding formations (section C). The thickness of section C is arbitrarily chosen to be R to demonstrate the effect of the heat loss and the temperature distribution in the formation.

Mathematical Formulation

As a result of the hot solvent injection, the lignite seam is gradually heated. The hot solvent in section A reacts with the lignite and generates gases, volatile material and steam. The gases, volatiles and steam along with solvent vapor move to the cooler section B where condensation occurs.

The underground liquefaction is an extremely complicated process which involves reaction, evaporation, condensation and multiple phase flow. To model this process, some degree of simplification must be made. First of all,

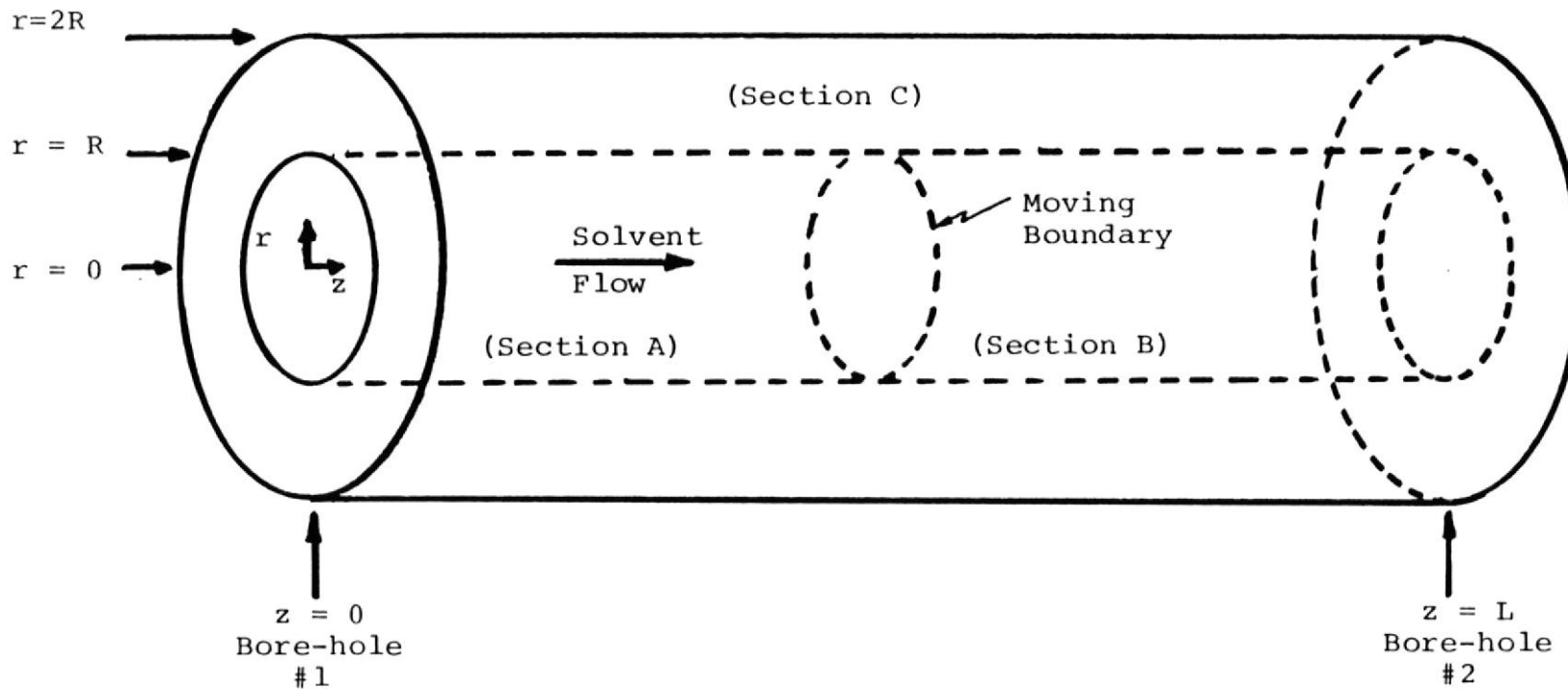


Figure 48. Model for Underground Liquefaction



the heats of reaction, evaporation, condensation and the gas produced are neglected in the modeling. The effects of these phenomena are lumped in other parameters which are determined empirically. After simplification, the modeling of the underground liquefaction is similar to that of a packed reactor.

The heat balance for the solvent in section A can be expressed as

$$\rho_a C_{va} \left(\epsilon_a \frac{\partial T}{\partial t} + v_z \frac{\partial T}{\partial z} \right) = K_{ea} \left[\frac{1}{r} \frac{\partial T}{\partial r} + \frac{\partial^2 T}{\partial r^2} + \frac{\partial^2 T}{\partial z^2} \right] - (1 - \epsilon_a) \rho_l C_{vl} \frac{\partial T}{\partial t} \quad (73)$$

The last term in Equation (73) represents the heat loss of the solvent to the lignite. The lignite is assumed to be at a uniform temperature which is the same as that of the surrounding solvent. ρ_a and C_{va} are the solvent properties. v_z is the superficial velocity of the solvent flow. K_{ea} is the effective conductivity. K_{ea} is a function of the solvent and the lignite. K_{ea} is estimated with the relation:

$$K_{ea} = \epsilon_a K_a + (1 - \epsilon_a) K_l \quad (74)$$

Similarly, in Section B, the heat balance and K_{eb} are expressed as

$$\rho_b C_{vb} \left(\epsilon_b \frac{\partial T}{\partial t} + v_z \frac{\partial T}{\partial z} \right) = K_{eb} \left[\frac{1}{r} \frac{\partial T}{\partial r} + \frac{\partial^2 T}{\partial r^2} + \frac{\partial^2 T}{\partial z^2} \right] - (1 - \epsilon_b) \rho_l C_{vl} \frac{\partial T}{\partial t} \quad (75)$$

$$K_{eb} = \epsilon_b k_b + (1 - \epsilon_b) K_l \quad (76)$$

ρ_b , C_{vb} and K_b are water properties because the solvent untouched lignite is considered to be water saturated. As a result of material conservation, the velocity in section B is the same as in section A.

No convection is assumed for section C, therefore, the energy equation is written as:

$$\rho_c C_{vc} \frac{\partial T}{\partial t} = K_{ec} \left[\frac{1}{r} \frac{\partial T}{\partial r} + \frac{\partial^2 T}{\partial r^2} + \frac{\partial^2 T}{\partial z^2} \right] \quad (77)$$

where ρ_c , C_{vc} and K_{ec} are the properties of the surrounding formations. Equations (73), (75), and (77) neglect the viscous heat dissipation, the temperature gradients in the angular directions and the convective flow in the radial direction.

The above equations can be expressed in dimensionless form by defining:

$$\bar{T} = \frac{T - T_\infty}{T_m - T_\infty} \quad (25)$$

$$\bar{z} = \frac{z}{L} \quad (26)$$

$$\bar{t} = \frac{v_z}{L} t \quad (27)$$

$$\bar{r} = \frac{r}{R} \quad (78)$$

Then, the equations become

$$\frac{\partial \bar{T}}{\partial t} + f_a \frac{\partial \bar{T}}{\partial z} = \frac{1}{Pe_a} \left[g \left(\frac{1}{r} \frac{\partial \bar{T}}{\partial r} + \frac{\partial^2 \bar{T}}{\partial r^2} \right) + \frac{\partial^2 \bar{T}}{\partial z^2} \right] \quad (79)$$

$$\frac{\partial \bar{T}}{\partial t} + f_b \frac{\partial \bar{T}}{\partial z} = \frac{1}{Pe_b} \left[g \left(\frac{1}{r} \frac{\partial \bar{T}}{\partial r} + \frac{\partial^2 \bar{T}}{\partial r^2} \right) + \frac{\partial^2 \bar{T}}{\partial z^2} \right] \quad (80)$$

$$\frac{\partial \bar{T}}{\partial t} = \frac{1}{Pe_c} \left[g \left(\frac{1}{r} \frac{\partial \bar{T}}{\partial r} + \frac{\partial^2 \bar{T}}{\partial r^2} \right) + \frac{\partial^2 \bar{T}}{\partial z^2} \right] \quad (81)$$

where

$$f_a = \frac{\rho_a C_{va}}{[\epsilon_a \rho_a C_{va} + (1 - \epsilon_a) \rho_l C_{vl}]} \quad (82)$$

$$f_b = \frac{\rho_b C_{vb}}{[\epsilon_b \rho_b C_{vb} + (1 - \epsilon_b) \rho_l C_{vl}]} \quad (83)$$

$$Pe_a = \frac{[\epsilon_a \rho_a C_{va} + (1 - \epsilon_a) \rho_l C_{vl}] v_z L}{K_{ea}} \quad (84)$$

$$Pe_b = \frac{[\epsilon_b \rho_b C_{vb} + (1 - \epsilon_b) \rho_l C_{vl}] v_z L}{K_{eb}} \quad (85)$$

$$Pe_c = \frac{[\rho_c C_{vc}] v_z L}{K_{ec}} \quad (86)$$

$$g = \frac{L^2}{R^2} \quad (87)$$

The values required for the calculation of Equation (82)

through (87) are as follows:

$$\rho_a = 0.83 \text{ g/cm}^3 \quad (88)$$

$$C_{va} = 2.26 \text{ J/g}\cdot\text{k} \quad (89)$$

$$K_a = 4.54 \text{ J/cm}\cdot\text{hr}\cdot\text{k} \quad (90)$$

$$\rho_b = 1.00 \text{ g/cm}^3 \quad (91)$$

$$C_{vb} = 4.23 \text{ J/g}\cdot\text{k} \quad (92)$$

$$K_b = 19.87 \text{ j/cm}\cdot\text{hr}\cdot\text{k} \quad (93)$$

$$\rho_c = 1.68 \text{ g/cm}^3 \quad (94)$$

$$C_{vc} = 0.92 \text{ J/g}\cdot\text{k} \quad (95)$$

$$K_{ec} = 24.91 \text{ J/cm}\cdot\text{hr}\cdot\text{k} \quad (96)$$

$$\rho_l = 1.68 \text{ g/cm}^3 \quad (97)$$

$$C_{vl} = 0.92 \text{ J/g}\cdot\text{k} \quad (98)$$

$$K_l = 24.91 \text{ J/cm}\cdot\text{hr}\cdot\text{k} \quad (99)$$

$$\epsilon_a = 0.3 \quad (100)$$

$$\epsilon_b = 0.1 \quad (101)$$

$$L = 2.5 \times 10^3 \text{ cm} \quad (102)$$

$$R = 100 \text{ cm} \quad (103)$$

$$v_z = 50 \text{ cm/hr} \quad (104)$$

BIBLIOTECA

FACULTAD DE INGENIERIA
EN CIENCIAS DE LA TIERRA

ρ_a , C_{va} and K_a are the solvent properties and are approximated by the properties of a light oil at 422K. The temperature is considered to be the average temperature during the reaction in section A.

ρ_b , C_{vb} , and K_b are the water properties and are estimated at 298K. In using this temperature, we assumed that the water in section B is basically at 298K.

ρ_c , C_{vc} , and K_{ec} are the surrounding formation properties. ρ_l , C_{vl} , and K_l are the lignite properties. We assumed the surrounding formation and the lignite can be approximated by dry limestone at 294K.

All the values are reported by Kreith (1973). The reason for making all these approximations is the lack of information on lignite and solvent. The approximations have been successful in determining the parameters of the tubular reactor model, and are, therefore, applied for the underground simulation.

The porosity in Section A is assumed to be 0.3. This value is considered as the average porosity of section A during the reaction. In section B, there is no reaction and the porosity is assumed to be 0.1. We arbitrarily chose $L = 2.5 \times 10^3$ cm and $v_z = 5 \times 10^2$ cm. R is restricted by the seam thickness and is assumed to be one meter.

K_{ea} in Equation (84) can be calculated from Equation (74). K_{eb} in Equation (85) can be calculated from Equation (76). Then, Equation (82) through (87) can be solved and the results are as follows:

$$K_{ea} = 18.80 \text{ J/cm}\cdot\text{hr}\cdot\text{K} \quad (105)$$

$$K_{eb} = 24.41 \text{ J/cm}\cdot\text{hr}\cdot\text{K} \quad (106)$$

$$f_a = 1.14 \quad (107)$$

$$f_b = 2.33 \quad (108)$$

$$Pe_a = 1.09 \times 10^4 \quad (109)$$

$$Pe_b = 9.29 \times 10^3 \quad (110)$$

$$Pe_c = 7.76 \times 10^3 \quad (111)$$

$$g = 625 \quad (112)$$

The initial and boundary conditions used for these equations are:

$$\text{I.C.: at } \bar{t} = 0 \quad \bar{T} = 0 \quad (113)$$

Boundary conditions for $\bar{t} \geq 0$

$$\text{B.C.1 : at } \bar{z} = 0 \quad T = 1 \text{ for } 0 \leq \bar{r} \leq 1 \quad (114)$$

$$\frac{\partial \bar{T}}{\partial \bar{z}} = 0 \text{ for } 1 < \bar{r} \leq 2 \quad (115)$$

$$\text{B.C.2 : at } \bar{z} = 1 \quad \frac{\partial \bar{T}}{\partial \bar{z}} = 0 \quad (116)$$

$$\text{B.C.3: at } \bar{r} = 0 \quad \frac{\partial \bar{T}}{\partial \bar{r}} = 0 \quad (117)$$

$$\text{B.C. 4: at } \bar{r} = 2 \quad \frac{\partial \bar{T}}{\partial \bar{t}} = 0 \quad (118)$$

The intersectional boundary conditions are neglected. We assume the temperatures are smooth and continuous at the intersectional boundaries.

Following L'Hospital's rule, the term $(1/\bar{r}) (\partial \bar{T} / \partial \bar{r})$, in Equation (79) and (80) becomes $(\partial^2 \bar{T} / \partial \bar{r}^2)$ at $\bar{r} = 0$. Hence, at $\bar{r} = 0$, these equations become:

$$\frac{\partial \bar{T}}{\partial \bar{t}} + f_a \frac{\partial \bar{T}}{\partial \bar{z}} = \frac{1}{Pe_a} \left[2g \frac{\partial^2 \bar{T}}{\partial \bar{r}^2} + \frac{\partial^2 \bar{T}}{\partial \bar{z}^2} \right] \quad (119)$$

$$\frac{\partial \bar{T}}{\partial \bar{t}} + f_b \frac{\partial \bar{T}}{\partial \bar{z}} = \frac{1}{Pe_b} \left[2g \frac{\partial^2 \bar{T}}{\partial \bar{r}^2} + \frac{\partial^2 \bar{T}}{\partial \bar{z}^2} \right] \quad (120)$$

The boundary between section A and section B is moving toward the production borehole as the solvent is continuously injected into the lignite seam. The boundary moving velocity is calculated from the following equation:

$$v_b = v_z / \epsilon_b \quad (121)$$

Both v_z and ϵ_b are constants, therefore, v_b is also a constant.

Numerical Method

The computation field of underground liquefaction is shown in Figure 49. The ranges are $0 \leq \bar{r} \leq 2$ and $0 \leq \bar{z} \leq 1$. The axial center of the lignite is represented by $\bar{r} = 0$.

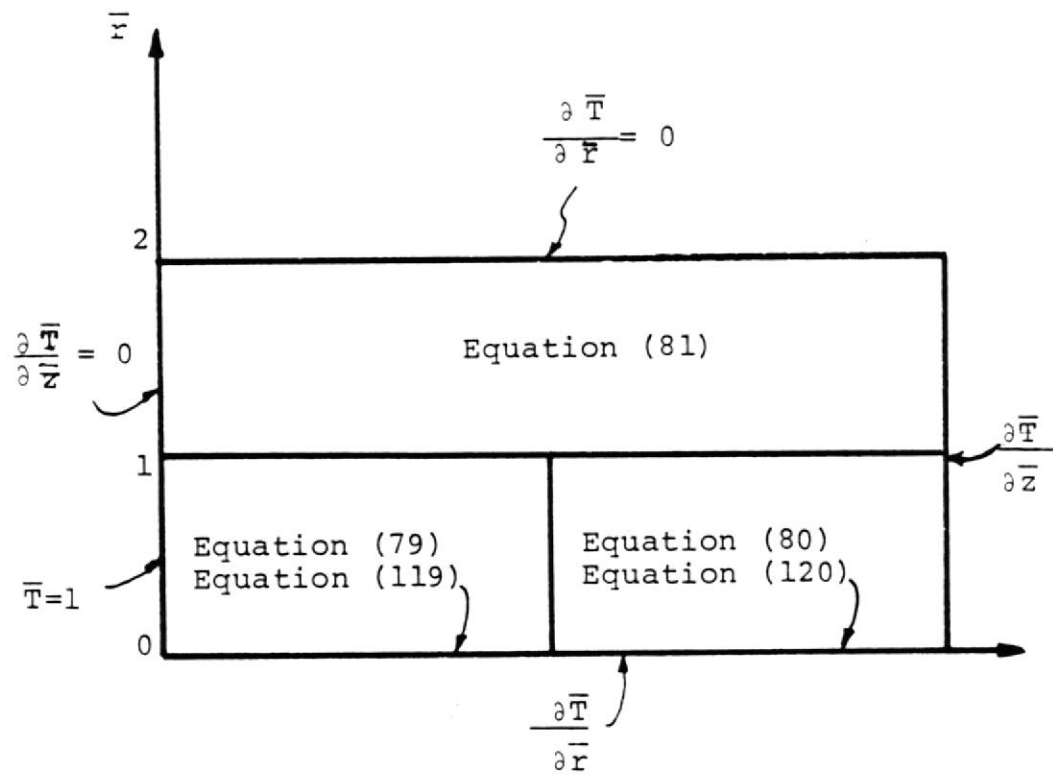


Figure 49. Computation Field of Underground Liquefaction.

Because we assumed that there was no temperature difference in the angular direction, the field represents the whole model shown in Figure 48.

The boundary conditions and the equations required for the calculation are also shown in Figure 49. Equation (119) and Equation (120) are used at $\bar{r} = 0$.

The field of computation (Figure 49) was transferred into grid coordinates (Figure 50). In Figure 50, the actual field is represented by the solid lines. The dashed lines were used to take care of the derivative boundary conditions.

The computation field in \bar{r} direction is divided into $M-2$ increments. The length of each increment, hence, is:

$$\Delta \bar{r} = 2 / (M-2) \quad (122)$$

Similarly, the increment in the z direction is:

$$\Delta \bar{z} = 1 / (N-2) \quad (123)$$

The boundary between the lignite seam and the surrounding formation is represented by the line at $i = M_b$. In this case, M_b can be calculated from M .

$$M_b = \frac{M - 2}{2} + 2 \quad (124)$$

The moving boundary between section A and section B is located at $j = N_b$. N_b increases with time until $N_b = N$. N_b was calculated from the following equations:

$$N_b = \left(\frac{v_b t}{L} \right) (N-2) + 2 \quad (125)$$

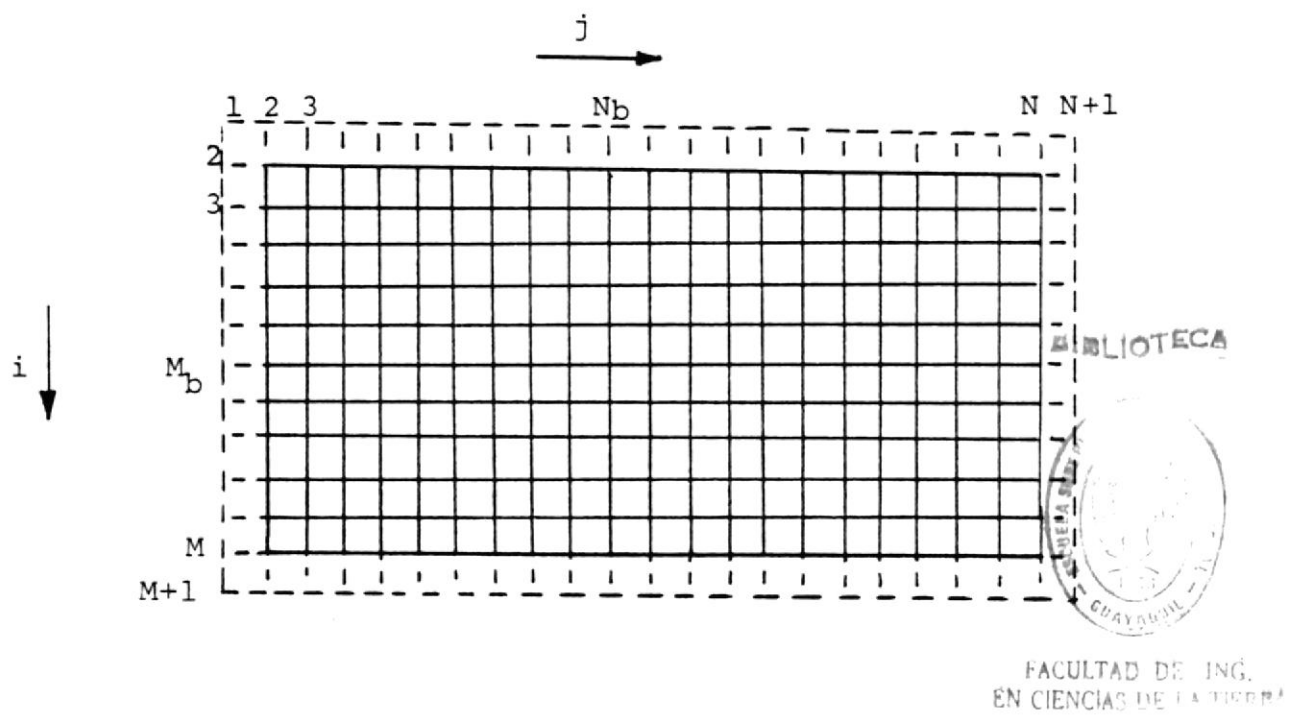


Figure 50. Computation Field of Underground Liquefaction in Grid Coordinates.

where v_b is the velocity of the moving boundary and is defined in Equation (121). Equation (125) can be expressed in dimensionless form.

$$N_b = \left[\frac{\left(\frac{v_b}{\epsilon_b}\right) \left(\frac{L}{v_b} \bar{t}\right)}{L} \right] (N-2) + 2 = \frac{\bar{t}}{\epsilon_b} (N-2) + 2 \quad (126)$$

Alternate direction implicit (A.D.I.) method (Mitchell 1969) was used to solve Equation (79), (80), and (81). In this method the time increment is divided into steps. Each step takes only half of the time increment and only one of the two space increments is considered in the step. The procedure will be illustrated in the formulation of the matrix.

A.D.I. method starts with writing the differential equations in finite difference form. For the first half time step, Equation (79) becomes (For simplicity, the overbar "-" which denote the dimensionless variables is omitted for the rest of this section):

$$\begin{aligned} & \frac{T_{i,j}^{t+\Delta t/2} - T_{i,j}^t}{\Delta t/2} + f_a \left(\frac{T_{i,j}^{t+\Delta t/2} - T_{i,j-1}^{t+\Delta t/2}}{\Delta z} \right) = \\ & \frac{g}{Pe_a} \frac{1}{(M-i) \Delta r} \left(\frac{T_{i,j}^t - T_{i+1,j}^t}{\Delta r} \right) + \\ & \frac{g}{Pe_a} \left(\frac{T_{i-1,j}^t - 2T_{i,j}^t + T_{i+1,j}^t}{\Delta r^2} \right) + \\ & \frac{1}{Pe_a} \left(\frac{T_{i,j-1}^{t+\Delta t/2} - 2T_{i,j}^{t+\Delta t/2} + T_{i,j+1}^{t+\Delta t/2}}{\Delta z^2} \right) \end{aligned} \quad (127)$$

The backward difference formula is used for the first derivative terms and the central difference formula for the second derivative terms. An unstable solution occurred when using central difference formula for the first order derivative. A general rule is that for a forward flow system, the use of backward difference formula is encouraged.

In Equation (127), the temperatures at time level $t+\Delta t/2$ represent the unknown values. Of the 2 space dimensions, only the derivatives with respect to z are advanced to $t+\Delta t/2$ in the first half time step. Equation (127) can be rearranged to become:

$$[a_1 T_{i,j-1} + a_2 T_{i,j} + a_3 T_{i,j+1}]^{t+\Delta t/2} = [\text{RHSA}_{i,j}]^t \quad (128)$$

where

$$a_1 = \frac{-f_a}{\Delta z} + \frac{1}{\text{Pe}_a} \frac{-1}{\Delta z^2} \quad (129)$$

$$a_2 = \frac{2}{\Delta t} + \frac{f_a}{\Delta z} + \frac{1}{\text{Pe}_a} \frac{2}{\Delta z^2} \quad (130)$$

$$a_3 = \frac{1}{\text{Pe}_a} \frac{-1}{\Delta z^2} \quad (131)$$

$$\begin{aligned} \text{RHSA}_{i,j} = & \left(\frac{g}{\text{Pe}_a} \frac{1}{\Delta r^2} \right) T_{i-1,j}^t + \\ & \left(\frac{2}{\Delta t} + \frac{g}{\text{Pe}_a} \frac{1}{(M-i)\Delta r} \frac{1}{\Delta r} + \frac{g}{\text{Pe}_a} \frac{-2}{\Delta r^2} \right) T_{i,j}^t + \\ & \left(\frac{g}{\text{Pe}_a} \frac{1}{(M-i)\Delta r} \frac{-1}{\Delta r} + \frac{g}{\text{Pe}_a} \frac{1}{\Delta r^2} \right) T_{i+1,j}^t \quad (132) \end{aligned}$$

At $i=M$, Equation (132) has to be reformed following L'Hospital's rule to become:

$$\begin{aligned} \text{RHSA}_{M,j} = & \left(\frac{2g}{\text{Pe}_a} \frac{1}{\Delta r^2} \right) T_{i-1,j}^t + \left(\frac{2}{\Delta t} + \frac{2g}{\text{Pe}_a} \frac{-2}{\Delta r^2} \right) T_{i,j}^t \\ & + \left(\frac{2g}{\text{Pe}_a} \frac{1}{\Delta r^2} \right) T_{i+1,j}^t \end{aligned} \quad (133)$$

Similarly, for Equation (80), we obtain:

$$\left[b_1 T_{i,j-1} + b_2 T_{i,j} + b_3 T_{i,j+1} \right]^t + \frac{\Delta t}{2} = [\text{RHSB}_{i,j}]^t \quad (134)$$

where

$$b_1 = \frac{-f_b}{\Delta z} + \frac{1}{\text{Pe}_b} \frac{-1}{\Delta z^2} \quad (135)$$

$$b_2 = \frac{2}{\Delta t} + \frac{f_b}{\Delta z} + \frac{1}{\text{Pe}_b} \frac{2}{\Delta z^2} \quad (136)$$

$$b_3 = \frac{1}{\text{Pe}_b} \frac{-1}{\Delta z^2} \quad (137)$$

$$\begin{aligned} \text{RHSB}_{i,j} = & \left(\frac{g}{\text{Pe}_b} \frac{1}{\Delta r^2} \right) T_{i-1,j}^t \\ & + \left(\frac{2}{\Delta t} + \frac{g}{\text{Pe}_b} \frac{1}{(M-i)\Delta r} \frac{1}{\Delta r} + \frac{g}{\text{Pe}_b} \frac{-2}{\Delta r^2} \right) T_{i,j}^t \\ & + \left(\frac{g}{\text{Pe}_b} \frac{1}{(M-i)\Delta r} \frac{-1}{\Delta r} + \frac{g}{\text{Pe}_b} \frac{1}{\Delta r^2} \right) T_{i+1,j}^t \end{aligned} \quad (138)$$

At $i=M$, Equation (138) has to be reformed following

L'Hospital's rule to become

$$\begin{aligned} \text{RHSB}_{M,j} = & \left(\frac{2g}{\text{Pe}_b} \frac{1}{\Delta r^2} \right) T_{i-1,j}^t + \left(\frac{2}{\Delta t} + \frac{2g}{\text{Pe}_b} \frac{-2}{\Delta r^2} \right) T_{i,j}^t \\ & + \left(\frac{2g}{\text{Pe}_b} \frac{1}{\Delta r^2} \right) T_{i+1,j}^t \end{aligned} \quad (139)$$

Again, for Equation (81), the difference form is

$$[c_1 T_{i,j-1} + c_2 T_{i,j} + c_3 T_{i,j+1}]^{t+\Delta t} = [\text{RHSC}_{i,j}]^t \quad (140)$$

where

$$c_1 = \frac{1}{\text{Pe}_c} \frac{-1}{\Delta z^2} \quad (141)$$

$$c_2 = \frac{2}{\Delta t} + \frac{1}{\text{Pe}_c} \frac{2}{\Delta z^2} \quad (142)$$

$$c_3 = \frac{1}{\text{Pe}_c} \frac{-1}{\Delta z^2} \quad (143)$$

$$\begin{aligned} \text{RHSC}_{i,j} = & \left(\frac{g}{\text{Pe}_c} + \frac{1}{\Delta r^2} \right) T_{i-1,j}^t \\ & + \left(\frac{2}{\Delta t} + \frac{g}{\text{Pe}_c} \frac{1}{(M-i)\Delta r} \frac{1}{\Delta r} + \frac{g}{\text{Pe}_c} \frac{-2}{\Delta r^2} \right) T_{i,j}^t \\ & + \left(\frac{g}{\text{Pe}_c} \frac{1}{(M-i)\Delta r} \frac{-1}{\Delta r} + \frac{g}{\text{Pe}_c} \frac{1}{\Delta r^2} \right) T_{i+1,j}^t \end{aligned} \quad (144)$$

The boundary conditions for the first half time step are:

$$T_{i,1} = T_{i,3} \quad \text{for } i = 2, M_b - 1 \quad (145)$$

$$T_{i,2} = 1 \quad \text{for } i = M_b, M \quad (146)$$

$$T_{i,N+1} = T_{i,N-1} \quad \text{for } i = 2, M \quad (147)$$

Then, the temperature field at $t + \Delta t / 2$ is calculated as:

$$\text{For } i = 2, M_b - 1$$

$$\begin{bmatrix} c_2 & 2c_3 & & 0 \\ c_1 & c_2 & c_3 & \\ & \vdots & \vdots & \vdots \\ & & c_1 & c_2 & c_3 \\ 0 & & & 2c_1 & c_2 \end{bmatrix} \begin{bmatrix} T_{i,2} \\ T_{i,3} \\ \vdots \\ T_{i,N-1} \\ T_{i,N} \end{bmatrix} = \begin{bmatrix} \text{RHSC}_{i,2} \\ \text{RHSC}_{i,3} \\ \vdots \\ \text{RHSC}_{i,N-1} \\ \text{RHSC}_{i,N} \end{bmatrix} \quad (148)$$

For $i=M_b, M-1$

$$\begin{bmatrix} a_2 & a_3 & & 0 \\ a_1 & a_2 & a_3 & \\ & \vdots & \vdots & \vdots \\ & & a_1 & a_2 & a_3 \\ & & & b_1 & b_2 & b_3 \\ 0 & & & & 2b_1 & b_2 \end{bmatrix} \begin{bmatrix} T_{i,3} \\ T_{i,4} \\ \vdots \\ T_{i,N_b} \\ T_{i,N_b+1} \\ \vdots \\ T_{i,N-1} \\ T_{i,N} \end{bmatrix} = \begin{bmatrix} \text{RHSA}_{i,3} - a_1 T_{i,2} \\ \text{RHSA}_{i,4} \\ \vdots \\ \text{RHSA}_{i,N_b} \\ \text{RHSB}_{i,N_b+1} \\ \vdots \\ \text{RHSB}_{i,N-1} \\ \text{RHSB}_{i,N} \end{bmatrix} \quad (149)$$

The above matrix is also used for $i=M$. However, Equation (133) must be used to calculate the right hand side instead of Equation (132). A subroutine to solve the tridiagonal matrix (Carnahan et al. 1969) can be used to obtain the solution.

The location of the moving boundary, N_b , has to be calculated at every time step according to Equation (126). Thus, the temperatures at $t+\Delta t/2$ are obtained and the boundary conditions at $i=1, i=M+1, j=1$ and $j=N+1$ have to be updated before moving to the second half time step.

The second-half time step moves the time from $t+\Delta t/2$ to $t+\Delta t$. This time, the derivatives with respect to r are at $t+\Delta t$. The finite difference form of Equation (79) in the second step is:

$$\begin{aligned}
& \frac{T_{i,j}^{t+\Delta t} - T_{i,j}^{t+\Delta t/2}}{\Delta t/2} + f_a \left(\frac{T_{i,j} - T_{i,j-1}}{\Delta z} \right)^{t+\Delta t/2} \\
& = \frac{g}{Pe_a} \frac{1}{(M-i)\Delta r} \left(\frac{T_{i,j} - T_{i+1,j}}{\Delta r} \right)^{t+\Delta t} \\
& + \frac{g}{Pe_a} \left(\frac{T_{i-1,j} - 2T_{i,j} + T_{i+1,j}}{\Delta r^2} \right)^{t+\Delta t} \\
& + \frac{1}{Pe_a} \left(\frac{T_{i,j-1} - 2T_{i,j} + T_{i,j+1}}{\Delta z^2} \right)^{t+\Delta t/2} \quad (150)
\end{aligned}$$

By rearranging Equation (150), the following equation is obtained.

$$\left[a_4 T_{i-1,j} + a_5 T_{i,j} + a_6 T_{i+1,j} \right]^{t+\Delta t} = [RHS A_{i,j}]^{t+\Delta t/2} \quad (151)$$

where

$$a_4 = \frac{g}{Pe_a} \frac{1}{\Delta r^2} \quad (152)$$

$$a_5 = -\frac{2}{\Delta t} + \frac{g}{Pe_a} \frac{1}{(M-i)\Delta r} \frac{1}{\Delta r} + \frac{g}{Pe_a} \frac{-2}{\Delta r^2} \quad (153)$$

$$a_6 = \frac{g}{Pe_a} \frac{1}{(M-i)\Delta r} \frac{-1}{\Delta r} + \frac{g}{Pe_a} \frac{1}{\Delta r^2} \quad (154)$$

$$\begin{aligned}
\text{RHSA}_{i,j} &= \left(\frac{-f_a}{\Delta z} + \frac{1}{\text{Pe}_a} \frac{-1}{\Delta z^2} \right) T_{i,j-1}^{t+\Delta t/2} \\
&+ \left(-\frac{2}{\Delta t} + \frac{f_a}{\Delta z} + \frac{1}{\text{Pe}_a} \frac{-2}{\Delta z^2} \right) T_{i,j}^{t+\Delta t/2} \\
&+ \left(\frac{1}{\text{Pe}_a} \frac{-1}{\Delta z^2} \right) T_{i,j+1}^{t+\Delta t/2}
\end{aligned} \tag{155}$$

At $i = M$, a_5 and a_6 are replaced by

$$a_7 = \frac{2g}{\text{Pe}_a} \frac{1}{\Delta r^2} \tag{156}$$

$$a_8 = -\frac{2}{\Delta t} + \frac{2g}{\text{Pe}_a} \frac{-2}{\Delta r} \tag{157}$$

$$a_9 = \frac{2g}{\text{Pe}_a} \frac{1}{\Delta r^2} = a_7 \tag{158}$$

Similarly, Equation (80) yields

$$\begin{aligned}
[b_4 T_{i-1,j} + b_5 T_{i,j} + b_6 T_{i+1,j}]^{t+\Delta t} = \\
[\text{RHSB}_{i,j}]^{t+\Delta t/2}
\end{aligned} \tag{159}$$

where

$$b_4 = \frac{g}{\text{Pe}_b} \frac{1}{\Delta r^2}$$

$$b_5 = -\frac{2}{\Delta t} + \frac{g}{\text{Pe}_b} \frac{1}{(M-i)\Delta r} \frac{1}{\Delta r} + \frac{g}{\text{Pe}_b} \frac{-2}{\Delta r} \tag{161}$$

$$b_6 = \frac{g}{\text{Pe}_b} \frac{1}{(M-i)\Delta r} \frac{-1}{\Delta r} + \frac{g}{\text{Pe}_b} \frac{-2}{\Delta r^2} \tag{162}$$

BIBLIOTECA



FACULTAD DE ING.
EN CIENCIAS DE LA TIERRA

$$\begin{aligned}
\text{RHSB}_{i,j} = & \left(\frac{-f_a}{\Delta z} + \frac{1}{\text{Pe}_b} \frac{-1}{\Delta z^2} \right) T_{i,j-1}^{t+\Delta t/2} \\
& + \left(-\frac{2}{\Delta t} + \frac{f_b}{\Delta z} + \frac{1}{\text{Pe}_b} \frac{2}{\Delta z^2} \right) T_{i,j}^{t+\Delta t/2} \\
& + \left(\frac{1}{\text{Pe}_b} \frac{-1}{\Delta z^2} \right) T_{i,j+1}^{t+\Delta t/2}
\end{aligned} \tag{163}$$

At $i = M$, b_5 and b_6 are replaced by

$$b_7 = \frac{2g}{\text{Pe}_b} \frac{1}{\Delta r^2} \tag{164}$$

$$b_8 = -\frac{2}{\Delta t} + \frac{2g}{\text{Pe}_b} \frac{-2}{\Delta r} \tag{165}$$

$$b_9 = \frac{2g}{\text{Pe}_b} \frac{1}{\Delta r^2} = b_7 \tag{166}$$

Again, for Equation (81), the difference form is

$$\begin{aligned}
& [c_4 T_{i-1,j} + c_5 T_{i,j} + c_6 T_{i+1,j}]^{t+\Delta t} = \\
& [\text{RHSC}_{i,j}]^{t+\Delta t/2}
\end{aligned} \tag{167}$$

where

$$c_4 = \frac{g}{\text{Pe}_c} + \frac{1}{\Delta r^2} \tag{168}$$

$$c_5 = -\frac{2}{\Delta t} + \frac{g}{\text{Pe}_c} \frac{1}{(M-i)\Delta r} \frac{1}{\Delta r} + \frac{g}{\text{Pe}_c} \frac{-2}{\Delta r^2} \tag{169}$$

$$c_6 = \frac{g}{\text{Pe}_c} \frac{1}{(M-i)\Delta r} \frac{-1}{\Delta r} + \frac{g}{\text{Pe}_c} \frac{1}{\Delta r^2} \tag{170}$$

$$\begin{aligned}
 \text{RHSC}_{i,j} = & \left(\frac{1}{\text{Pe}_c} \frac{-1}{\Delta z^2} \right) T_{i,j-1}^{t+\Delta t/2} \\
 & + \left(\frac{-2}{\Delta t} + \frac{1}{\text{Pe}_c} \frac{2}{\Delta z^2} \right) T_{i,j}^{t+\Delta t/2} \\
 & + \left(\frac{1}{\text{Pe}_c} \frac{-1}{\Delta z^2} \right) T_{i,j+1}
 \end{aligned} \tag{171}$$

The boundary conditions for the second half time stop are:

$$T_{1,j} = T_{3,j} \quad j = 2, N \tag{172}$$

$$T_{M_b,j} = 1 \quad j = 2 \tag{173}$$

$$T_{M+1,j} = T_{M-1,j} \quad j = 3, N \tag{174}$$

Then, the temperatures at $t+\Delta t$ can be calculated from the following matrices:

For $j = 2$

$$\begin{bmatrix}
 c_5 & 2c_6 & & 0 \\
 c_4 & c_5 & c_6 & \\
 & c_4 & c_5 & c_6 \\
 & & c_4 & c_5
 \end{bmatrix}
 \begin{bmatrix}
 T_{2,2} \\
 T_{3,2} \\
 \vdots \\
 T_{M_b-2,2} \\
 T_{M_b-1,2}
 \end{bmatrix}
 =
 \begin{bmatrix}
 \text{RHSC}_{2,2} \\
 \text{RHSC}_{3,2} \\
 \vdots \\
 \text{RHSC}_{M_b-2,2} \\
 \text{RHSC}_{M_b-1,2} \quad -c_6 T_{M_b,2}
 \end{bmatrix}
 \tag{175}$$

BIBLIOTECA



FACULTAD DE ING.
EN CIENCIAS DE LA TIERRA

The computer time depends on the size of the space and the number of time increments. In other words, it depends on N , M , and K_t . N and M are the number of grid points shown in Figure 50. K_t is the number of time increments and is calculated according to

$$K_t = \frac{\text{total reaction time}}{\text{time increment}} \quad ((178))$$

The total reaction time in the above equation is predetermined. By choosing $N = 14$, $M = 8$, and $K_t = 60$, the program requires 1.56 seconds computer time on an Amdahl 470V/6 computer.

The overall procedure may be summarized as follows:

1. Input constants: f_a , f_b , Pe_a , Pe_b , Pe_c , g , M , N , K_t , Δt , t_b , and v_z .
2. Calculate Δr , Δz , M_b , v_z .
3. Input initial and boundary conditions.
4. Advance time $t = t + \Delta t$.
5. Calculate N_b by Equation (126). N_b is the location of the moving boundary and is a function of time. The range, $2 \leq N_b \leq N$, should be observed.
6. For first half time step:
 - a) Calculate new temperatures for section C as follows:

- (i) Calculate c_1 , c_2 , and c_3 using Equations (141) through (143).
 - (ii) Calculate $RHSC_{i,j}$ (Equation 144) for $j=2, N$
 - (iii) Form matrix (148) and then solve it.
 - (iv) Repeat (ii) through (iii) for $i = 2, M_b - 1$.
- (b) Calculate new temperatures for sections A and B (not including $i=M$) as follows:
- (i) Calculate a_1 , a_2 , and a_3 (Equations (129), (130) and (131)).
 - (ii) Calculate b_1 , b_2 and b_3 (Equations (135) (136) and (137)).
 - (iii) Calculate $RHSA_{1,j}$ (Equation (132)) repeat for $j=2, N_b$.
 - (iv) Calculate $RHSB_{1,j}$ (Equation (138)) repeat for $j = N_b + 1, N$
 - (v) Form Matrix (149), then solve it.
 - (vi) Repeat (iii) to (v) for $i=M_b, M-1$
- (c) Calculate new temperatures for $i = M$
- (i) Calculate $RHSA_{i,j}$ (Equation (133)) for $j=2, N_b$.
 - (ii) Calculate $RHSB_{M,j}$ (Equation (134)) for $j = N_b + 1, N$.
 - (iii) Form Matrix (149) then solve.
- (d) Update the boundary conditions (Equations (145), (146), and (147)).

BIBLIOTECA

FACULTAD DE ING.
EN CIENCIAS DE LA TIERRA

7. For second half time step (use the calculated new temperatures of the first half step as the known values).

(a) For $j = 2$

(i) Calculate c_4 , c_5 , and c_6 (Equations (168), (169) and (170)).

(ii) Calculate $RHSC_{i,j}$ (Equation (171)) for $i=1, M_b-1$.

(iii) Form Matrix (175) then solve.

(b) For $j=3, N_b$.

(i) Calculate a_4 , a_5 , a_6 , a_7 , a_8 , and a_9 , by Equations (152), (153), (154), (156), (157), and (158).

(ii) Calculate $RHSC_{i,j}$ (Equation (171)) repeat for $i=2, M_b-1$.

(iii) Calculate $RHSA_{i,j}$ (Equation (155)) repeat for $i=M_b, M$

(iv) Form Matrix (176) then solve.

(v) Repeat (iii) to (iv) for $j=3, N_b$.

(c) For $j=N_b+1, N$

(i) Calculate b_4 , b_5 , b_6 , b_7 , b_8 , and b_9 by Equations (160), (161), (162), (164), (165), and (166).

(ii) Calculate $RHSC_{i,j}$ (Equation (171)) repeat for $i=2, M_b-1$.

alstiotera



FACULTAD DE ING.
EN CIENCIAS DE LA TIERRA

- (iii) Calculate $RHSB_{1,j}$ (Equation (163)) repeat for $i = M_b, M$.
 - (iv) Form Matrix (177) then solve.
 - (v) Repeat (ii) to (iv) for $j = N_b+1, N$.
 - (d) Update boundary conditions (Equations (172), (173) and (174)).
8. Repeat steps (4) through (7) until the predetermined time of advance K_t is reached.

Results and Discussion

The calculated temperatures were plotted in three ways shown in Figures 51 through 53. These curves are strongly dependent on the parameters: f_a , f_b , Pe_a , Pe_b , Pe_c , and g . Even though these parameters were carefully estimated, a field test is required to refine them.

Figure 51 shows the temperature profile at the center of the lignite seam. The profile covers only 8.4 m of the 35 m seam. The temperature distribution of the rest of the seam is an extension of those curves.

Figure 52 shows a sharp drop in temperatures at the boundary between the lignite seam and the surrounding formation. The sudden drop in temperature is the result of low conductivity of the surrounding formation. Hence, the figure indicates that the surrounding formation is an excellent insulator.

With the calculated temperature profile, the heat loss can be estimated from the equation:

$$\text{Heat Loss} = \int_0^L \left(\frac{\partial T}{\partial r} \right)_{r=R^+} K_{ec} 2\pi R dz \quad (179)$$

Since $\left(\frac{\partial T}{\partial r} \right)_{r=R^+}$ is a function of time, the heat loss is also a function of time.

The temperature profiles at three different locations are shown in Figure 53. The curves show the same trend as those measured in the tabular reactor experiments.

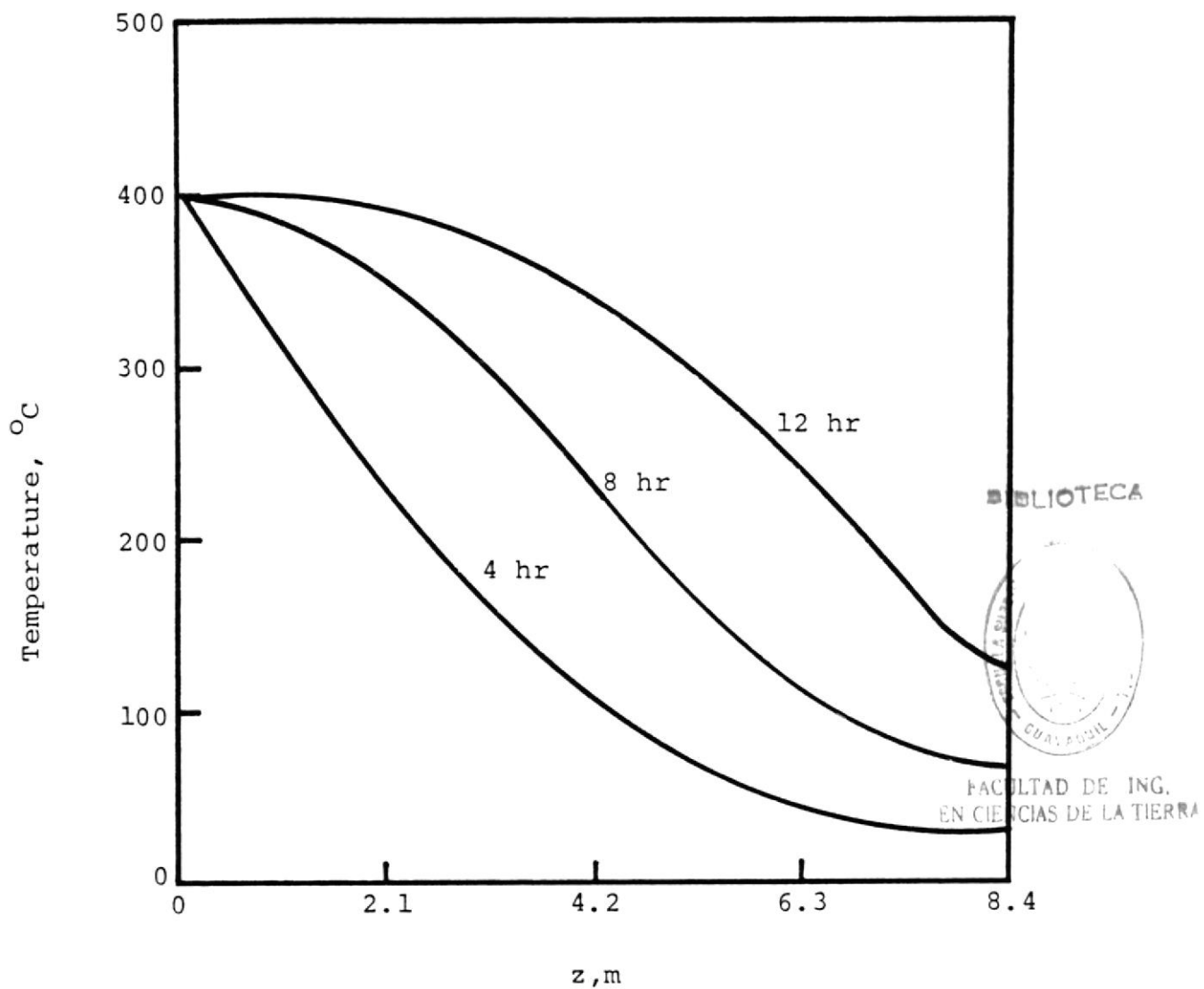


Figure 51. Temperature Profile of the Lignite Seam at $r = 0$ for a Solvent Feed Temperature of 400°C .

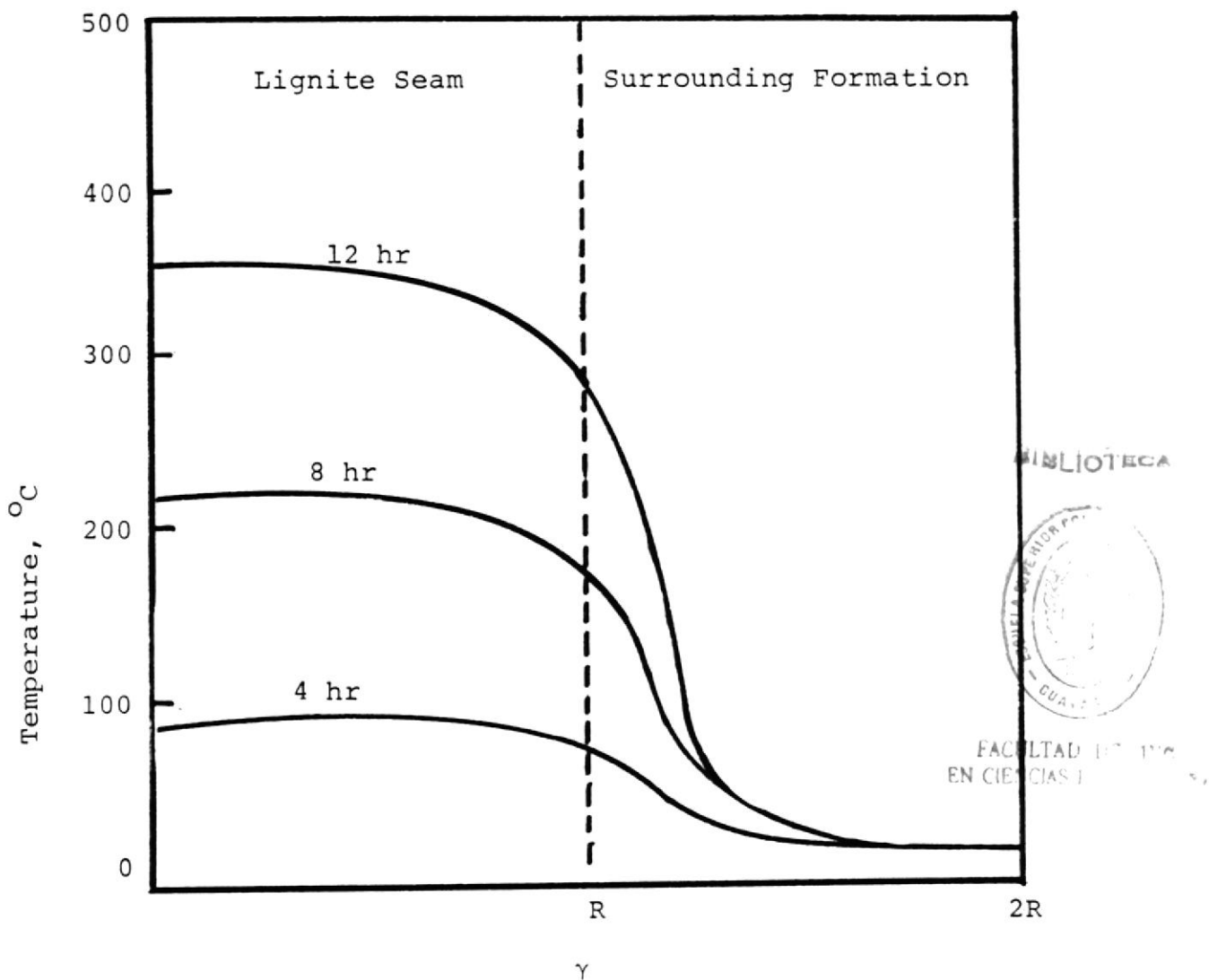


Figure 52. Temperature Profile in the Radial Direction, $z = L/6$ (i.e., 4.2 m from the injection borehole).

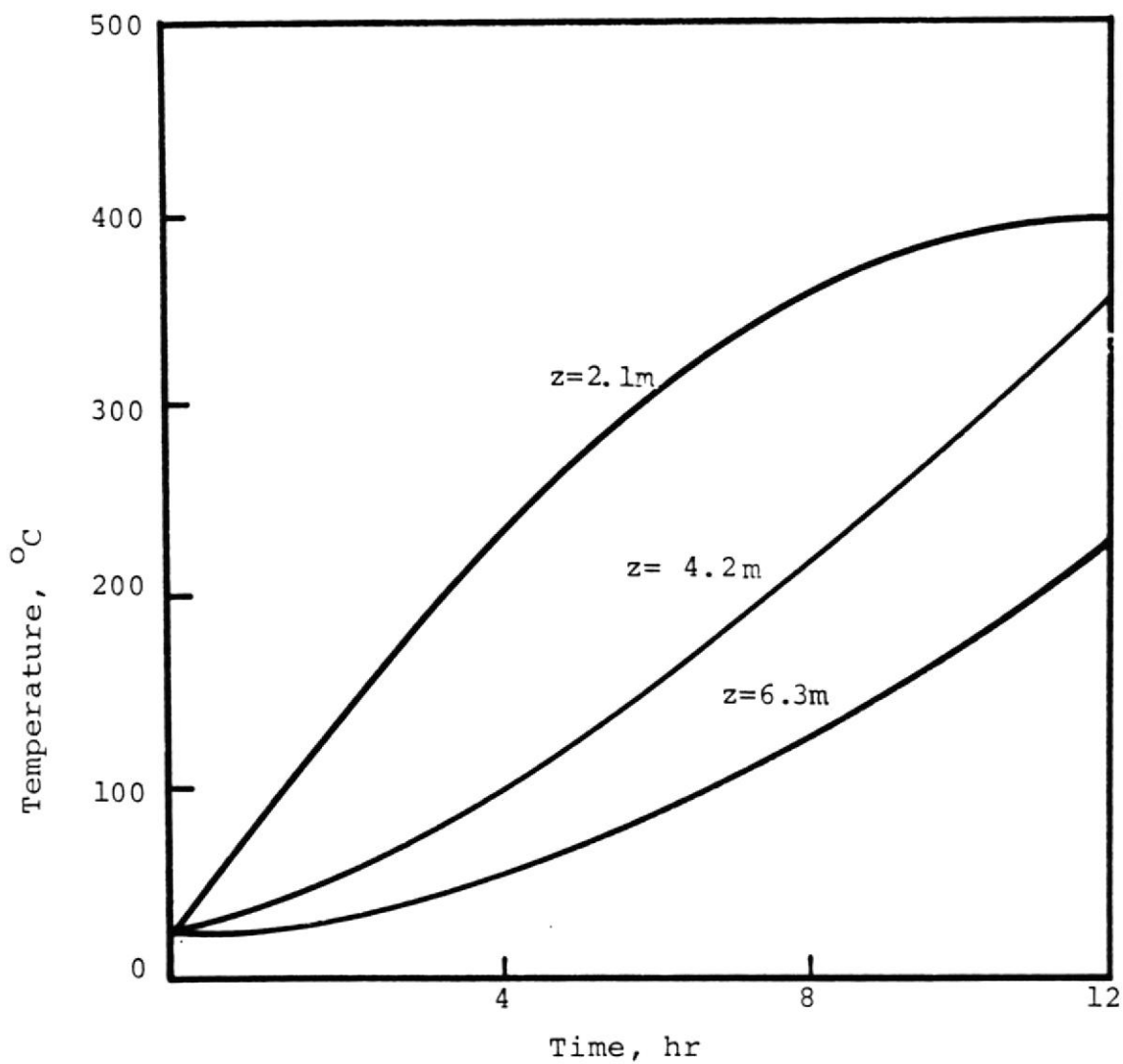


Figure 53: Temperature Profile at $r = 0$
(i.e., at center of seam).

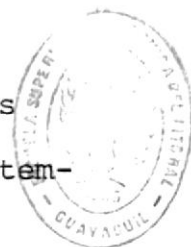
CHAPTER IX

CONCLUSION AND RECOMMENDATIONS

In this research, Texas lignite was used throughout the work. Tetralin, SRC recycled solvent, creosote oil, kolineum, and steam were studied for their effectiveness in dissolving Texas lignite. Data were collected at temperatures of 375°C, 400°C and 425°C. The pressure for these experiments ranged from 20 atm to 70 atm. Kinetic data were obtained using tetralin, SRC recycled solvent and creosote oil by using a 60 ml mini-reactor and a fluidized sand bath. A reaction model based on the thermodynamic equilibrium concept and the kinetic theory was developed. BIBLIOTEC.

This model suggest that:

1. The lignite liquefaction for 5 mm particles is a mass transfer controlling reaction and that temperature has no effect on the reaction rate constant.
2. Temperature and pressure affect only the equilibrium conversion.
3. Increasing temperatures and pressures increases the lignite conversion.
4. Increasing temperatures increases the gas production. However, increasing pressures increase the gas production only when tetralin is used



FACULTAD DE ING.
EN CIENCIAS DE LA TIERRA

as a solvent. For the other two solvents, increasing the pressure has a negative effect on the gas production. With creosote, the lignite conversions were approximately the same as obtained for devolatilization experiments.

A technique for determining the concentration of lignite derived liquid in a solvent was developed by using gel permeation chromatography (GPC). This technique was used to monitor the lignite extraction rate from the tubular reactor experiment and should be applicable in a field test.

Underground liquefaction was simulated by a laboratory apparatus that consisted of a tubular reactor packed with lignite and was treated as the lignite seam. Solvent was continuously pumped through the reactor. The performance of the reactor was successfully predicted by a mathematical model which calculated the temperature profile then coupled the results with the reaction model to predict the quality of the product.

Finally, a two dimensional model was used to predict the actual underground operation. The temperature profiles were shown in various ways.

This research does not exhaust all the efforts toward underground liquefaction. Recommendations for further research are:

1. Search for a better solvent: A good solvent is

measured by both economics and effectiveness on the lignite conversion. For the large scale underground liquefaction the price of the solvent becomes an important factor in determining the cost of lignite-derived product. Special emphasis should be placed on the lignite-derived liquid itself. If the self-generated solvent is proved to be effective, then only small amounts of "start-up" solvent will be necessary.

2. Continue to improve the analytical technique: This is an effort to determine quantitatively the components of the lignite-derived liquid. The detailed analytical work not only indicates the quality of the product but also reveals the basic chemical structure of the lignite. Furthermore, it serves as a powerful tool for identifying the most effective components in the solvent. Hence, an improved solvent can be obtained.

3. Use catalyst: Cobalt molybdenum catalysts are widely used to improve the conversion of the above-ground coal liquefaction. The zinc chloridewas also reported to be effective to increase the conversion. Both can be further studied for underground use.

4. Understand the geological factors: the mechanical strength of the formation determines the pressure applicable. The enhancement of the lignite seam permeability needs to be studied. Information on the physical properties



SOCIETAD DE INGENIEROS
EN CIENCIAS DE GUAYAQUIL

such as the conductivity of the formations is also needed.

5. Avoid the environmental problems: Possible environmental problems such as polluting the underground water and ground subsidence should be studied in advance.

Underground liquefaction is a promising technique to recover the energy in deep basin lignite. This research served as the first step toward the final goal of solution mining of lignite.

BIBLIOTECA



FACULTAD DE ING.
EN CIENCIAS DE LA TIERRA

LITERATURE CITED

- Anthony, R.G., "In Situ Comminution or Liquefaction of Texas Lignite," Texas Engineering Experiment Station Technical Bulletin, 3, 4 (1976).
- Anthony, R.G., C.V. Philip, T.C. Liu, S.K. Haley and D.A. Shumbera, "Liquefaction of Lignite," Texas A&M University Lignite Symposium Proceeding, April 17-18 (1980), In Press.
- Aris, R. and N.R. Amundson, "Some Remarks on Longitudinal Mixing or Diffusion in Fixed Beds," A.I.Ch.E. J., 3,2, 280 (1957).
- Benjamin, B.M., E.W. Hagaman, V.F. Raaen and C.J. Collins, "Pyrolysis of Tetralin," Fuel, Vol. 58, No. 5, 386 (1979).
- Bird, R.B., W.E. Stewart and E.N. Lightfoot, Transport Phenomena, John Wiley and Sons, Inc. New York, p. 138 (1960).
- Bischoff, K.B., "A Note on Boundary Conditions for Flow Reactors," Chem. Eng. Sci., 16, 1, 131 (1961).
- Bischoff, K.B., Fluid Dispersion Generalization and Comparison of Mathematical Model, Ph.D. Thesis, Illinois Institute of Technology (1961a).
- Brunson, R.J., "Kinetics of Donor-vehicle Coal Liquefaction in a Flow Reactor," Fuel, Vol. 58, 203, March (1979).
- Carnahan, B., H.A. Luther and J.O. Wilkes, Applied Numerical Methods, John Wiley and Sons, Inc. New York, p. 446 (1969).
- Curran, G.P., R.T. Struck and E. Gorin, "Mechanism of the Hydrogen-Transfer Process to Coal and Coal Extract," Ind. Eng. Chem. Process Des. Dev., Vol. 6, No. 2, 166, April (1967).
- Danckwerts, P.V., "Continuous Flow System Distribution of Residence Time," Chem. Eng. Sci., 2, 1 (1953).
- Davies, G.O., F.J. Derbyshire and R. Price, "An Investigation of Coal Solubility in Anthracene Oils," J. of the Inst. of Fuel, Vol. 1, Sept. (1977).

- DeMaria, F., J.L. Longfield and G. Butler, "Catalytic Reactor Design," *Ind. Eng. Chem.*, 53, 4, 259 (1961).
- Denbigh, K.G., The Principles of Chemical Equilibrium, p. 3, Cambridge University Press, 3rd ed. (1971).
- Ellington, R.T., Liquid Fuels from Coal, p. 8, Academic Press New York (1977).
- Fan, L.T. and R.C. Bailie, "Axial Diffusion in Isothermal Tubular Flow Reactors," *Chem. Eng. Sci.*, 13, 63 (1960).
- Francis, W., Coal - Its Formation and Decomposition, Edward Arnold Ltd., London (1961).
- Friedel, R.A. and J.A. Queiser, "Ultra-violet - Visible Spectrum and the Aromaticity of Coal," *Fuel*, 38, 369 (1959).
- Given, P.H., "The Distribution of Hydrogen in Coals and Its Relation to Coal Structure," *Fuel*, 31, 147 (1960).
- Given, P.H. and M.E. Peover, "Polarographic and Electrolytic Reduction of the Aromatic System in Solvent Extracts or Coals," *Fuel*, 39, 463 (1960).
- Given, P.H., J. Bimer, and S. Raj, "Oxidative Study of the Structure of Vitrinites," Presented at the Fuel Division Chicago ACS Meeting. August (1977).
- Gregg, D.W. and T.F. Edger, "Underground Coal Gasification," *A.I.Ch.E. J.*, 24, 753 (1978).
- Gun, S.R., J.K. Sama, P.B. Chowdhury, S.K. Mukherjee and D.K. Mukherjee, "A Mechanistic Study of Hydrogenation of Coal," *Fuel*, 58, 171 (1979).
- Han, K.W., V.B. Dixit, and C.Y. Wen, "Analysis and Scale-Up Consideration of Bituminous Coal Liquefaction Rate Processes," *Ind. Eng. Chem. Process Des. Dev.*, Vol. 17, No. 1 (1978).
- Han, K.W. and C.Y. Wen, "Initial Stage (Short Residence Time) Coal Dissolution," *Fuel*, 58, 779 (1979).
- Hill, G.R., H. Harivi, R.I. Reed and L.L. Anderson, "Coal Science," *Adv. in Chem. Series*, No. 55, ACS, Washington D.C., 427 (1966).

- Himmelblau, D.M., Process Analysis by Statistical Method, John Wiley & Sons, Inc. p. 135, (1970).
- Holland, C.D. and R.G. Anthony, Fundamentals of Chemical Reaction Engineering, Prentice-Hall Inc. New Jersey (1979).
- Hooper, R.J., H.A.J. Battaerd and D.G. Evans, "Thermal Dissociation of Tetralin Between 300 and 400°C," *Fuel*, Vol. 58, No. 2, 132 (1979).
- Juettner, G., R.C. Smith and H.C. Howard, "Oxidation of a Pittsburgh Seam Bituminous Coal and Low Temperature Coke by Alkaline Permanganate," *Journal of ACS*, 59, 236 (1937).
- Kamiya, Y., "Formation of Aromatic Polycarboxylic Acid From Bituminous Coal by Oxygen-oxidation in Alkaline Medium," *Fuel*, 40, 149 (1961).
- Ketter, R.L. and P.O. Sherwood Jr., Modern Methods of Engineering Computation, McGraw-Hill Book Co. New York, p. 397 (1969).
- Kreith, F., Principle of Heat Transfer, 3rd ed. Intex Press Inc. New York, p. 633 (1973).
- Lee, M.H., J.A. Guin, A.R. Tarrer, "A Dispersion Model for the Solvent Refined Coal Process," *Ind. Eng. Chem. Process Des. Dev.*, Vol. 17, No. 2, 127 (1978).
- Max Nestler, F.H., "Characterization of Wood-Preservation Coal-Tar Creosote by Gas-Liquid Chromatography," *Analytical Chemistry*, Vol. 46, No. 1, January (1974).
- Mitchell, A.R., Computational Methods in Partial Differential Equations, John Wiley and Sons, New York, p. 50 (1969).
- Nelder, J.A. and R. Mead, "A Simplex Method for Function Minimization," *The Computer Journal*, Vol. 7, 4, 308 (1965).
- Pearson, J.R.A., "A Note on the "Danckwerts" Boundary Conditions for Continuous Flow Reactor," *Chem. Eng. Sci.*, 10, 281 (1959).
- Philip, C.V. and R.G. Anthony, "Chemistry of Texas Lignite Liquefaction in Hydrogen-Donor Solvent System," *ACS Div. Fuel Chem. Preprints*, Vol. 24, No. 4, 196 (1978).
- Philip, C.V., and R.G. Anthony, "Separation of Coal-derived Liquid by Gel Permeation Chromatograph," *ACS Div. Fuel Chem. Preprints*, Vol. 24, No. 3, 204 (1979).

- Roylance, T.F., L.L. Anderson, W.G. Pariseau and L.H. Lattman, "Simulated Solution Mining of a Utah Bituminous Coal," Bulletin No. 144 of the Utah Engineering Experiment Station, University of Utah, August (1977).
- Ruof, C.H., T.R. Savich and H.C. Howard, "Nuclear Structure of the Water-soluble Polycarboxylic Acid from Oxidation of Bituminous Coal," J. of ACS, 73, 3873 (1951).
- Skidmore, D.R., "In-Situ Coal Liquefaction," Abstract, Fifth Annual DOE/Fossil Energy Conference on University Coal Research, Sponsored by U.S. Department of Energy Program, G. Fumich, Program Director, Conducted by University of Kentucky, T. Schrodtt, Conference chairman, August, (1978).
- Skidmore, D.R., and C.J. Konya, "Liquefaction Study of Several Coal and a Concept for Underground Liquefaction," 165th National Meeting of ACS, Division of Fuel, Vol. 18, No. 2, 86, Dallas, Texas, April (1973).
- Smith, R.C., R.C. Tomarelli and H.C. Howard, "Oxidation of Carbonaceous Materials to Organic Acid by Oxygen at Elevated Pressures," J. of ACS, 61, 2398 (1939).
- Van Cauwenberghe, A.R., "Further Note on Dankewerts Boundary Conditions for Flow Reactors," Chem. Eng. Sci., 21, 203 (1966).
- Wehner, J.F. and R.H. Wilhelm, "Boundary Conditions of Flow Reactor," Chem. Eng. Sci., 6, 89 (1956).
- Wen, C.Y. and K.W. Han, "Kinetics of Coal Liquefaction," ACS Div. of Fuel Chem., Preprints, 20, 1, 216 (1975).
- Whitehurst, D.D., "Chemistry and Constitution of Coal," Organic Chemistry of Coal, ACS Symposium Series 71, Fuel Div., 174th meeting of the ACS, Chicago, Illinois, Aug. 29 - Sep. 1, editor J.W. Larsen (1977).
- Wise, D.L. and D.C. Augenstein, "Engineering Analysis of In Situ Liquefaction of Coal," In Situ, Vol. 2, No. 3, 173 (1978).
- Wiser, W., Fuel Div. ACS Meeting, Preprints, 20(2), 122 (1975).

APPENDIX A
NOMENCLATURE

a_i	= matrix coefficient
A_1	= chromatographic area of lignite-derived liquid
A_2	= chromatographic area of the creosote oil
ΔA	= differential area of the reactor
b_i	= matrix coefficient
c_i	= matrix coefficient
c	= concentration, g of lignite-derived liquid/solvent, ml.
c_{A0}	= concentration of solvent
\bar{c}	= dimensionless concentration = c/c_0
c_M	= concentration at $\bar{z} = K_3$
\bar{c}_M	= c_M/c_0
c_0	= reference concentration, arbitrarily taken to be 0.1 g/cm^3
C_v	= heat capacity
d_p	= partical size
D_e	= Effective diffusivity
D_1	= diffusivity in the entrance section
D_2	= diffusivity in the exit section
E	= activation energy
f_a	= $\rho_a C_{va} / [\epsilon_a \rho_a C_{va} + (1-\epsilon_a) \rho_l C_{vl}]$
f_b	= $\rho_b C_{vb} / [\epsilon_b \rho_b C_{vb} + (1-\epsilon_b) \rho_l C_{vl}]$

BIBLIOTECA



FACULTAD DE ING.
EN CIENCIAS DE LA TIERRA

F	= generation of the lignite-derived liquid = $\bar{W}_O (dx_\ell/d\bar{t} - dx_g/d\bar{t})$
g	= $(L/R)^2$
G	= weight of the gas generated (g)
h	= heat transfer coefficient
Δh	= a characteristic difference in the enthalpy of the product and of the reactants
k	= rate constant or mass transfer coefficient
\bar{k}	= dimensionless = Lk/v_z
k_o	= Arrhenius constant
K	= solvent conductivity
K_e	= effective conductivity
K_ℓ	= lignite conductivity
K_t	= number of time advances
K_1	= length of the entrance section, dimensionless
K_2	= length of the reaction section plus exit section
K_3	= sample port location, dimensionless
L	= reactor length
M	= number of grid point in r direction
M_i	= molecular weight of component i
\bar{M}	= average molecular weight
MAF	= moisture and ash free basis
MFB	= moisture free basis
N	= number of grid points in z direction
P	= pressure

P_1	= upstream pressure
P_2	= downstream pressure
\bar{P}	= dimensionless pressure = P/P_0
P_0	= reference pressure = 32 atm
Pe_h	= Peclet number for heat transfer = $L (\rho C_v)_e v_z / K_e$
Pe_a	= Peclet number in section a = $[\epsilon_a \rho_a C_{va} + (1-\epsilon_a) \rho_l C_{vl}] v_z L / K_{ea}$
Pe_b	= Peclet number in section b = $[\epsilon_b \rho_b C_{vb} + (1-\epsilon_b) \rho_l C_{vl}] v_z L / K_{eb}$
Pe_c	= Peclet number in section c = $[\rho_c C_{vc}] v_z L / K_{ec}$
Pe	= Peclet number for mass transfer = $L v_z / D_e$
Q_1	= heat transfer to lignite
Q_2	= heat loss through the reactor surface
r	= radius, distance
\bar{r}	= r/R , dimensionless
R	= radius of the reactor
\bar{R}	= R/L , dimensionless
R_a	= $\rho C_v / (\rho C_v)_e$, dimensionless group
R_1	= gas constant = 0.082 l-atm/g-mole K
R_2	= gas constant = 8.314×10^{-3} KJ/g-mole K
$RHSA_{ij}$	= right hand side, section A
$RHSB_{ij}$	= right hand side, section B
$RHSC_{ij}$	= right hand side, section B
St	= Stanton number = $2h / \bar{R} (\rho C_v)_e v_z$

t	=	time
\bar{t}	=	$v_z t/L$ = dimensionless time
T	=	temperature
\bar{T}	=	$(T-T_\infty)/(T_m-T_\infty)$ dimensionless temperature
T_o	=	reference temperature = 673°K
T_b	=	reactor surface temperature
\bar{T}_b	=	$(T_b-T_\infty)/(T_m-T_\infty)$ = dimensionless T_b
T_m	=	entrance solvent temperature = 673°K
T_∞	=	environmental temperature = 298°K
u_1	=	dimensionless group = $(P_o \Delta v / R_1 T_o)$
u_2	=	dimensionless group = $(\Delta h / R_2 T_o)$
u_3	=	dimensionless group = $(T_m - T_\infty) / T_o$
u_4	=	dimensionless group = T_∞ / T_o
v_b	=	moving boundary velocity
v_z	=	superficial velocity of fluid flow
Δv	=	characteristic difference in volumes of the products and of the reactant
V	=	volume of the product gas
ΔV	=	differential volume of the reactor
W_l	=	weight of lignite (MFB)
W_g	=	weight of the gas product
W_r	=	weight of residue (MFB)
W_o	=	weight of lignite (MAF)/reactor volume = 0.36 g/ml (measured)
\bar{W}	=	dimensionless = W_o / c_o

BIBLIOTECA

FACULTAD DE ING.
EN CIENCIAS DE LA TIERRA

X	= conversion
X_a	= ash content = 0.15
X_e	= equilibrium conversion
X_g	= conversion of lignite to gas
X_l	= conversion of lignite
\hat{X}_g	= predicted conversion of lignite to gas
\hat{X}_l	= predicted conversion of lignite
X_{eo}	= equilibrium conversion at 673°K and 32 atm
X_{el}	= intermediate equilibrium
Y_i	= molar fraction of component i
Y_l	= lignite recovered as liquid product, %
Y_g	= lignite recovered as gas product, %
z	= z coordinate
\bar{z}	= dimensionless = z/L

Greek Letters

ρ	= density
ϵ	= porosity
ξ_i	= percentage error
σ	= error caused by approximation
Δ	= increment

BIBLIOTECA


 FACULTAD DE ING.
 EN CIENCIAS DE LA TIERRA

Subscript s

l = lignite

g = gas

1 = section 1 = entrance section

2 = section 2 = exit section

e = effective or equivalent

a = section contacted by solvent

b = section not contacted by solvent

c = surrounding formation

APPENDIX B

TUBULAR REACTOR CONTINUOUS EXTRACTION EXPERIMENTS

There were 9 runs conducted using the tubular reactor which had been packed with 5 mm particles of wet lignite. Successful runs and failures are reported because some useful information was obtained from runs which were classified as failures. For the first four runs, the reactor was not externally heated. Insulation was used to reduce heat losses. The temperatures were continuously monitored with a multi-point recorder. The feeds to the preheater were water, tetralin, kolineum and creosote oil. The reactor was operated as a downflow reactor for eight runs. Upflow was then used for the ninth run.

Run No. 1:

The experiment was stopped at $t = 3.75$ hours due to a material failure. Temperature profiles indicate vaporization of water at 200°C . The gas production was recorded to be 52 liters.

Run No. 2:

The temperature profile (Figure 22) shows that the heat loss was so large that the reactor never reached the desired reaction temperature. The gas production was recorded to be 18.2 liters.

Run No. 3:

More insulation materials were wrapped around the reactor and the section between the preheater and the reactor. The lignite was unchanged from Run No. 2. The temperature profile is shown in Figure 23. Like the previous two runs, the horizontal sections of the profiles at about 200° C represent the phase change where water in the lignite as well as vaporization of steam which had been condensed in the heating of the lignite is being vaporized. The temperature differences of the three thermocouples at the steady state indicate a heat loss (heating mantles were not used until Run No. 5).

Run No. 4:

Tetralin was used for this run. Unlike that of using water as the solvent, the temperature profile (Figure 24) does not show signs of phase change because water within the lignite had been removed in Runs 2 and 3. At steady state, the reactor does not have a uniformed temperature which indicates that significant heat losses still exist. Because the lignite in the reactor was initially charged prior to Run No. 2 and not removed for Runs 3 and 4, a low CO₂ concentration occurs.

Run No. 5:

The heating mantles were used for this experiment. The temperature (Figure 25) at $z = \frac{5}{6} L$ is questionable,

because it is higher than the entrance solvent temperature. It could be a bad thermocouple or local overheating because of the heating mantle.

A solvent called Kolineum (supplied by Koppers Co. in Chicago) was used. The composition of Kolineum is unknown. Kolineum is a black liquid with a viscosity greater than water and tetralin.

This experiment has been tried twice. The first trial was stopped at $t=2.2$ hours due to a sudden increase of the reactor temperature. The volume of gas produced for the first trial was 81 liters at $t = 2.2$ hours. At $t = 2.1$ hours, the volume was recorded to be 24 liters.

The second trial was on the same lignite as the first trial. Furnance was turned on and off to avoid overheating the preheater surface. However, this effort did not prevent the carbonization of Kolineum. The system was plugged at $t = 4.8$ hours. The back pressure regulator requires adjustment as well. The setting of the back pressure regulator was done on nitrogen gas. However, for operating on liquid, the same setting resulted in a higher back pressure.

Because the lignite had been heat treated one time, the second trial showed low CO_2 concentration.

Run No. 6:

This run is different from the others in that the

reactor was flushed with runs by steam and cooled with water flowing through it. Water was fed to the system at $t = 6.23$ hour. At this time, the furnace and the heating mantles remained on. Thus, the feed water was vaporized in the preheater. The steam was then passed through the lignite residue. After 15 minutes, the heaters were turned off. The feed water was then serving as a quenching medium.

At $t = 6.25$ hrs., there was a surge in reactor pressure when water was fed.

Run No. 7:

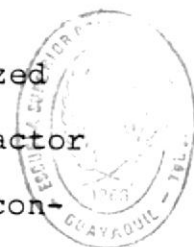
The preheater was plugged during the run. The reason could be the low solvent flow rate (500 ml/hr). Also, the carbon deposit which caused the plugging problem in the preheater, could have accumulated from previous runs.

The compositions of the product gases were normalized and do not include nitrogen that was present in the reactor at the beginning of the run. The sample at $t = 1$ hr. contains 97% nitrogen due to the small volume of gas produced. The normalization, therefore, is expected to cause errors.

Run No 8:

The carbon deposit in the preheater was scraped clean and then Run No 8 was started. This experiment was the most troublesome one, because of mistakes of packing the

BIBLIOTECA



FACULTAD DE ING.
EN CIENCIAS DE LA TIERRA

preheater with steel wool (Trial No. 1) and ceramic beads (Trial No. 2). Both packing materials caused serious coking problem which quickly plugged the preheater.

Trial No. 1 lasted for 1.6 hours. The nitrogen pressure (14.6 atm.) used to set the back pressure regulator was not released for this trial. The effect of this initial pressure will result in higher gas production readings than without the pressure. The reactor volume is about 1.5 liters. The porosity is about 0.5. Therefore, with the initial pressure of 14.6 atm., the reading is about $1.5 \times 0.5 \times (14.6 - 1.0) = 102$ liters higher than without the initial pressure.

The second trial was performed two days later. The preheater was packed with ceramic beads. The preheater was plugged in one hour. It was so serious that a new preheater had to be made.

It took another seven days before the third trial could be performed. The preheater was not packed. However at $t = 2$ hours, the pump had failed.

Two days were spent to fix the pump. The 4th trial failed due to a leaky preheater. The 4th trail lasted only 0.5 hours.

The fifth trial was finally a successful one.

Run No. 9:

Run No. 9 was different from the other runs in two

BIBLIOTECA



FACULTAD DE ING.
EN CIENCIAS DE LA TIERRA

places. First, the hot solvent was introduced to the reactor from the bottom. Second, a relief valve was used instead of a back pressure regulator. The use of a relief valve enables us to obtain more stable pressure than the back pressure regulator. However, the relief valve has a viton gasket which can not stand our operation temperature. The regulator was still in line, therefore the experiment was only temporarily interrupted.

The composition of the tubular reactor gas products are shown in Table B1. Run No. 8, Trial No. 1, was with an initial nitrogen pressure of 14.6 atm. The reactor volume is about 1.5 liters and with 0.5 porosity. Therefore, the initial pressure causes $(1.5)(0.5)(14.6 - 1) = 10.2$ liters extra volume reading on the wet test meter. Similarly, for Trial No. 5 (run no. 8), the extra volume is 36 liters (initial pressure = 5.8 atm). The cumulative volumes for these two trials reported in Table A2 have already been corrected. Hence, all the cumulative values are on 1 atm initial pressure basis.

BIBLIOTECA

FACULTAD DE ING.
CIENCIAS DE LA TIERRA

TABLE B1. COMPOSITION OF TUBULAR REACTOR GAS PRODUCT, % MOLE

t (hr)	H ₂	CO ₂	C ₂ H ₄	C ₂ H ₆	CH ₄	CO	C ₃ H ₈	C ₃ H ₆	i-C ₄ ^e	H ₂ S	n-C ₄ ^f	vol. ^g
		(Run No. 3)										
5.0	4.5	27.5	1.6	5.3	29.7	11.2	18.4	1.8	--	--	--	--
7.0	16.0	23.1	1.3	5.8	27.2	9.6	15.6	1.5	--	--	--	--
		(Run No. 4)										
2.0	49.1	8.7	0.4	2.5	32.4	4.7	1.5	0.4	--	--	--	11.13
3.0	42.4	19.6	0.4	2.7	29.1	5.5	0.4	0.1	--	--	--	12.29
4.0	53.6	17.0	0.5	2.9	22.7	2.9	0.4	0.1	--	--	--	16.51
5.0	69.7	8.2	0.4	2.1	17.2	1.9	0.4	0.1	--	--	--	21.94
6.0	78.7	3.9	0.1	1.9	13.7	1.2	0.1	0.0	--	--	--	26.73
		(Run No. 5, Trial No. 2) ^b										
2.0	46.9	3.4	0.4	9.1	33.5	4.4	1.8	0.5	--	--	--	16.14
3.5	36.9	2.0	1.2	9.9	41.8	5.5	1.8	1.0	--	--	--	51.54
4.7	34.2	1.8	1.5	9.8	43.4	5.8	2.2	1.4	--	--	--	82.68
		(Run No. 6)										
2.0	7.4	49.3	4.1	8.5	18.7	3.3	3.8	3.3	0.3	0.7	0.7	10.00
3.0	2.6	55.4	0.8	6.7	17.5	4.6	4.5	1.1	0.5	2.2	0.6	35.10
4.0	6.2	42.8	0.8	10.9	24.7	5.0	4.9	1.2	0.5	2.4	0.7	46.27
5.0	13.2	28.5	1.5	13.0	31.7	4.9	3.8	1.0	0.3	1.6	0.5	51.25
6.0	18.7	20.6	0.8	14.8	34.1	4.3	3.6	0.8	0.4	1.2	0.5	55.05
		(Run N. 7)										
1.0	0.0	36.7	0.0	10.0	20.0	0.0	13.3	3.3	0.0	0.0	3.3	0.26
2.0	9.1	3.3	7.5	19.2	43.0	0.3	8.1	7.8	0.5	0.0	1.0	18.34
2.6	4.5	7.5	8.8	21.4	28.4	0.3	12.9	12.8	1.0	0.0	2.2	26.05
		(Run No. 8, Trial No. 1) ^c										
0.6	31.0	2.7	4.0	7.1	48.9	3.3	0.8	2.3	0.0	0.0	0.0	2.15
1.1	23.8	0.9	2.8	10.6	59.1	1.4	0.6	1.2	0.0	0.0	0.0	11.12

 FACULTAD DE ING.
 EN CIENCIAS DE LA TIERRA


ANILLO OFICIAL

TABLE B1. (CONTINUED)

<u>t (hr)</u>	<u>H₂</u>	<u>CO₂</u>	<u>C₂H₄</u>	<u>C₂H₆</u>	<u>CH₄</u>	<u>CO</u>	<u>C₃H₈</u>	<u>C₃H₆</u>	<u>i-C₄^e</u>	<u>H₂S</u>	<u>n-C₄^f</u>	<u>vol^g</u>
		(Run No. 8, Trial No. 5)										
1.5	0.0	0.0	0.0	0.0	0.0	0.0	0.0	0.0	0.0	0.0	0.0	0.0
2.0	0.0	74.2	0.0	1.8	5.6	3.8	1.3	0.9	0.2	0.9	0.4	6.25
2.5	0.2	74.2	0.4	2.8	9.5	5.7	1.7	0.9	0.1	3.7	0.5	15.09
3.0	1.0	62.2	0.4	5.3	15.9	6.4	2.9	0.9	0.3	4.1	0.8	29.53
4.0	5.7	33.8	0.4	12.9	30.0	3.1	7.1	1.1	0.9	3.0	1.9	41.71
4.5	6.0	30.6	0.3	14.2	31.4	2.6	7.8	1.1	1.0	2.9	1.9	43.69
5.0	7.2	29.2	0.3	14.1	34.9	2.4	6.5	0.8	0.8	2.6	1.3	45.10
6.0	9.1	21.9	0.3	15.5	37.3	1.6	8.0	0.9	1.0	2.7	1.6	53.32
		(Run No. 9)										
2.0	0.2	98.9	0.3	0.1	1.9	3.8	0.2	0.1	0.7	2.0	0.0	4.25
2.5	4.5	41.5	0.7	4.5	23.3	8.6	5.1	1.3	0.5	3.6	1.2	31.15
3.0	5.1	39.1	0.4	11.9	26.5	3.5	7.3	1.0	0.8	2.9	1.5	37.66
4.0	16.9	18.2	0.5	14.4	32.3	3.8	7.9	1.3	1.0	1.9	2.0	46.44
4.5	--	--	--	--	--	--	--	--	--	--	--	51.54
5.0	23.3	8.9	0.5	14.8	35.5	2.6	8.2	1.3	1.2	1.6	2.3	59.75
5.5	28.9	8.7	0.4	11.2	41.7	2.2	4.1	0.6	0.5	0.8	0.8	62.30
6.0	32.6	9.6	0.3	11.2	37.4	2.3	4.2	0.5	0.5	0.8	0.7	64.24
6.5	35.0	10.0	0.6	11.2	32.7	2.6	4.6	0.8	0.5	1.1	0.8	65.84

- a. Gas composition is not cumulative value.
 b. Run No. 5, Trial No. 1, produces 24 liters at 5=2.1 hours and 81 litera t 5=2.2 hours.
 c. The effect of initial pressure on the cumulative volume has been corrected.
 d. Measured at 298 K and 1 atm.
 e. iso-butane
 f. n-butane
 g. Cumulative volume (in liters)



BIBLIOTECA

APPENDIX C

The correlation of lignite-derived liquid concentration and the area A_1 (see Figure 37) were obtained by injecting 5 samples into the GPC. The first sample was the liquid product from the mini-reactor Run No. C15. Since the concentration of the lignite-derived liquid in the liquid product is not directly known, a concentration index of 1 is given to the first sample. The second sample was prepared by mixing 3 parts by weight of C15 liquid with 1 part of creosote oil. The concentration index, hence, is 0.75. Samples No. 3 and No. 4 were prepared in a similar way. Sample No. 5 was creosote oil. The results are shown in Table C1. Table C1 is then plotted to obtain Figure 37.

TABLE C1. CORRELATION OF LIGNITE DERIVED LIQUID CONCENTRATION AND THE GPC AREA A_1

Sample No.	Concentration index	A_1 (cm ²)	$\frac{A_1}{A_1 \text{ (highest)}}$
1	1.00	1.60	1.00
2	0.75	0.96	0.69
3	0.50	0.67	0.42
4	0.25	0.34	0.21
5	0.00	0.00	0.00

BIBLIOTECA

FACULTAD DE ING.
CIENCIAS DE LA TIERRA

APPENDIX D. ESTIMATED PARAMETERS AND
STATISTICAL ANALYSIS
(4 Parameters)

A. Lignite Conversion - Tetralin

Non-Linear Least Squares Summary Statistics

Source	DF	Sum of Squares	Mean Square
Regression	4	6.04883	1.51221
Residual	13	0.01125	0.00087
Uncorrected Total	17	6.06009	
(Corrected Total)	16	0.31225	

Parameter	Estimate	Asymptotic Std. Error	Asymptotic 95% Confidence Interval	
			Lower	Upper
X_{eo}	0.651	0.014	0.621	0.681
Δh	37.810	2.674	32.033	43.587
Δv	-0.145	0.023	-0.195	-0.095
k	4.474	0.394	3.621	5.325

Asymptotic Correlation Matrix of the Parameters

	X_{eo}	Δh	Δv	k
X_{eo}	1.00	0.28	-0.56	-0.77
Δh	0.28	1.00	-0.14	-0.33
Δv	-0.56	-0.14	1.00	0.36
k	-0.77	-0.33	0.36	1.00



BIBLIOTECA
FACULTAD DE ING.
CIENCIAS DE LA TIERRA

APPENDIX D. (CONTINUED)

A. Lignite Conversion - SRC Recycled Solvent

Non-Linear Least Squares Summary Statistics

Source	DF	Sum of Squares	Mean Square
Regression	4	2.46171	0.61543
Residual	6	0.00076	0.00013
Uncorrected Total	10	2.46247	
(Corrected Total)	9	0.05559	

Parameter	Estimate	Asymptotic Std. Error	Asymptotic 95% Confidence Interval	
			Lower	Upper
X_{eo}	0.549	0.008	0.531	0.568
Δh	28.875	1.983	24.021	33.729
Δv	-0.124	0.034	-0.197	-0.051
k	6.176	0.317	5.401	6.952

Asymptotic Correlation Matrix of the Parameters

	X_{eo}	Δh	Δv	k
X_{eo}	1.00	0.54	-0.71	-0.74
Δh	0.54	1.00	-0.38	-0.42
Δv	-0.71	-0.38	1.00	0.49
k	-0.74	-0.42	0.49	1.00

APPENDIX D. (CONTINUED)

A. Lignite Conversion - Creosote Oil

Non-Linear Least Squares Summary Statistics

Source	DF	Sum of Squares	Mean Square
Regression	4	1.78648	0.44662
Residual	10	0.00579	0.00058
Uncorrected Total	14	1.79227	
(Corrected Total)	13	0.06746	

Parameter	Estimate	Asymptotic Std. Error	Asymptotic 95% Confidence Interval	
			Lower	Upper
X_{eo}	0.345	0.009	0.325	0.365
Δh	32.154	3.546	24.253	40.056
Δv	-0.265	0.090	-0.459	-0.071
k	11.769	3.274	4.474	19.063

Asymptotic Correlation Matrix of the Parameters

	X_{eo}	Δh	Δv	k
X_{eo}	1.00	-0.38	-0.47	-0.57
Δh	-0.38	1.00	0.17	0.19
Δv	-0.47	0.17	1.00	0.23
k	-0.57	0.19	0.23	1.00

APPENDIX D. (CONTINUED)

B. Conversion of Lignite to Gas - Tetralin

Non-Linear Least Squares Summary Statistics

Source	DF	Sum of Squares	Mean Square
Regression	4	0.05102	0.01275
Residual	10	0.00098	0.00010
Uncorrected Total	14	0.05200	
(Corrected Total)	13	0.00220	

Parameter	Estimate	Asymptotic Std. Error	Asymptotic 95% Confidence Interval	
			Lower	Upper
X_{eo}	0.070	0.006	0.056	0.084
Δh	23.775	12.411	-3.878	51.429
Δv	-0.029	0.090	-0.223	0.165
k	4.280	1.263	1.465	7.094

Asymptotic Correlation Matrix of the Parameters

	X_{eo}	Δh	Δv	k
X_{eo}	1.00	0.65	-0.61	-0.73
Δh	0.65	1.00	-0.39	-0.38
Δv	-0.61	-0.39	1.00	0.38
k	-0.73	-0.38	0.38	1.00

APPENDIX D. (CONTINUED)

B. Conversion of Lignite to Gas-SRC Recycled Solvent

Non-Linear Least Squares Summary Statistics

Source	DF	Sum of Squares	Mean Square
Regression	4	0.08482	0.02120
Residual	8	0.00040	0.00005
Uncorrected Total	12	0.08523	
(Corrected Total)	11	0.00633	

Parameter	Estimate	Asymptotic Std. Error	Asymptotic 95% Confidence Interval	
			Lower	Upper
X_{eo}	0.096	0.004	0.085	0.105
Δh	47.498	6.078	33.481	61.514
Δv	0.238	0.118	-0.017	0.493
k	3.516	0.596	2.142	4.890

Asymptotic Correlation Matrix of the Parameters

	X_{eo}	Δh	Δv	k
X_{eo}	1.00	-0.25	-0.36	-0.81
Δh	-0.26	1.00	0.12	0.09
Δv	-0.36	0.11	1.00	0.20
k	-0.81	0.09	0.20	1.00



FACULTAD DE ING.
EN CIENCIAS DE LA TIERRA

APPENDIX D. (CONTINUED)

B. Conversion of Lignite to Gas - Creosote Oil

Non-Linear Least Squares Summary Statistics

Source	DF	Sum of Squares	Mean Square
Regression	4	0.04546	0.01136
Residual	5	0.00011	0.00002
Uncorrected Total	9	0.04557	
(Corrected Total)	8	0.00260	

Parameter	Estimate	Asymptotic Std. Error	Asymptotic 95% Confidence Interval	
			Lower	Upper
X_{eo}	0.085	0.004	0.076	0.095
Δh	19.942	7.359	1.023	38.861
Δv	0.035	0.100	-0.181	0.251
k	4.510	0.631	2.889	6.133

Asymptotic Correlation Matrix of the Parameters

	X_{eo}	Δh	Δv	k
X_{eo}	1.00	0.26	-0.62	-0.65
Δh	0.26	1.00	-0.15	0.28
Δv	-0.63	-0.15	1.00	0.37
k	-0.65	0.28	0.37	1.00

APPENDIX E. ESTIMATED PARAMETERS AND
STATISTICAL ANALYSIS
(5 parameters)

A. Lignite Conversion - Tetralin

Non-Linear Least Squares Summary Statistics

Source	DF	Sum of Squares	Mean Square
Regression	5	6.0495	1.20991
Residual	12	0.0106	0.00088
Uncorrected Total	17	6.0601	
(Corrected Total)	16	0.3122	

Parameter	Estimate	Asymptotic Std. Error	Asymptotic 95% Confidence Interval	
			Lower	Upper
X_{eo}	0.649	0.014	0.620	0.680
Δh	35.164	4.118	26.191	44.137
Δv	-0.146	0.022	-0.194	-0.098
k_o	58.879	177.345	-327.523	445.281
E	14.479	16.886	-22.312	51.270

Asymptotic Correlation Matrix of the Parameters

	X_{eo}	Δh	Δv	k_o	E
X_{eo}	1.00	0.18	-0.55	-0.10	-0.08
Δh	0.18	1.00	-0.09	-0.78	-0.78
Δv	-0.55	-0.09	1.00	0.06	0.05
k_o	-0.10	-0.78	0.05	1.00	1.00
E	-0.08	-0.78	0.05	1.00	1.00



APPENDIX E. (Continued)

A. Lignite Conversion - SRC Recycled Solvent

Non-Linear Least Squares Summary Statistics

Source	DF	Sum of Squares	Mean Square
Regression	5	2.46180	0.49236
Residual	5	0.00067	0.00013
Uncorrected Total	10	2.46247	
(Corrected Total)	9	0.05559	

Parameter	Estimate	Asymptotic Std. Error	Asymptotic 95% Confidence Interval	
			Lower	Upper
X_{eo}	0.546	0.009	0.523	0.569
Δh	26.382	3.592	17.148	35.616
Δv	-0.135	0.038	-0.217	-0.053
k_o	37.219	80.183	-168.895	243.332
E	9.997	11.964	-20.757	40.751

Asymptotic Correlation Matrix of the Parameters

	X_{eo}	Δh	Δv	k_o	E
X_{eo}	1.00	0.56	-0.75	-0.51	-0.50
Δh	0.66	1.00	-0.50	-0.84	-0.83
Δv	-0.75	-0.50	1.00	0.39	0.38
k_o	-0.52	-0.84	0.39	1.00	1.00
E	-0.50	-0.83	0.38	1.00	1.00

APPENDIX E. (CONTINUED)

A. Lignite Conversion - Creosote Oil

Non-Linear Least Squares Summary Statistics

Source	DF	Sum of Squares	Mean Square
Regression	5	1.78713	0.35743
Residual	9	0.00515	0.00057
Uncorrected Total	14	1.79228	
(Corrected Total)	13	0.06746	

Parameter	Estimate	Asymptotic Std. Error	Asymptotic 95% Confidence Interval	
			Lower	Upper
X_{eo}	0.347	0.009	0.327	0.368
Δh	29.711	4.203	20.204	39.218
Δv	-0.259	0.090	-0.453	-0.065
k_o	91000.000	1041655.560	-2265408.636	2447408.636
E	49.851	62.350	-91.194	190.898

Asymptotic Correlation Matrix of the Parameters

	X_{eo}	Δh	Δv	k_o	E
X_{eo}	1.00	-0.46	-0.48	-0.12	-0.10
Δh	-0.46	1.00	0.19	-0.33	-0.34
Δv	-0.48	0.19	1.00	0.10	0.09
k_o	-0.12	-0.33	0.10	1.00	1.00
E	-0.10	-0.34	0.09	1.00	1.00



FACULTAD DE ING.
CIENCIAS DE LA TIERRA

APPENDIX E. (CONTINUED)

B. Conversion of Lignite to Gas - Tetralin

Non-Linear Least Squares Summary Statistics

Source	DF	Sum of Squares	Mean Square
Regression	5	0.05102	0.01020
Residual	9	0.00098	0.00011
Uncorrected Total	14	0.05200	
(Corrected Total)	13	0.00220	

Parameter	Estimate	Asymptotic Std. Error	Asymptotic 95% Confidence Interval	
			Lower	Upper
X_{eo}	0.070	0.007	0.054	0.087
Δh	23.775	19.559	-20.471	68.022
Δv	-0.029	0.098	-0.240	0.183
k_o	4.280	45.116	-97.781	106.340
E	0.000	58.687	-132.760	132.760

Asymptotic Correlation Matrix of the Parameters

	X_{eo}	Δh	Δv	k_o	E
X_{eo}	1.00	0.69	-0.64	-0.41	-0.39
Δh	0.69	1.00	-0.43	-0.75	-0.73
Δv	-0.64	-0.43	1.00	0.25	0.24
k_o	-0.41	-0.75	0.25	1.00	1.00
E	-0.39	-0.74	0.24	1.00	1.00

VITA

Tuan-chi Liu, the second of his parents four sons, was born in March, 1951, in Taiwan, The Republic of China.

He came to the U.S.A. in August, 1974, attending Texas A&M University. In December, 1975, he obtained his M.E. degree in Chemical Engineering.

His permanent mailing address is:

No. 2, 3rd District
Chu-E New Village
Sung-Wu, Chung-Li
Taiwan 320, R.O.C.

The typists for this dissertation were the staff at
ON THE DOUBLE, 331 University Drive, College Station, TX.